INFORMATION TO USERS

This manuscript has been reproduced from the microfilm master. UMI films the text directly from the original or copy submitted. Thus, some thesis and dissertation copies are in typewriter face, while others may be from any type of computer printer.

The quality of this reproduction is dependent upon the quality of the copy submitted. Broken or indistinct print, colored or poor quality illustrations and photographs, print bleedthrough, substandard margins, and improper alignment can adversely affect reproduction.

In the unlikely event that the author did not send UMI a complete manuscript and there are missing pages, these will be noted. Also, if unauthorized copyright material had to be removed, a note will indicate the deletion.

Oversize materials (e.g., maps, drawings, charts) are reproduced by sectioning the original, beginning at the upper left-hand corner and continuing from left to right in equal sections with small overlaps. Each original is also photographed in one exposure and is included in reduced form at the back of the book.

Photographs included in the original manuscript have been reproduced xerographically in this copy. Higher quality 6" x 9" black and white photographic prints are available for any photographs or illustrations appearing in this copy for an additional charge. Contact UMI directly to order.

UMI

A Bell & Howell Information Company
300 North Zeeb Road, Ann Arbor MI 48106-1346 USA
313/761-4700 800/521-0600

Université d'Ottawa • University of Ottawa

STRUCTURE, TIMING, AND MODEL OF EMPLACEMENT OF THE ROSE BLANCHE GRANITES, SOUTHWESTERN NEWFOUNDLAND.

by

Mikhail B. Genkin

A thesis submitted to the School of Graduate Studies and Research in partial fulfillment of the requirements for the degree of M. Sc. in Earth Sciences

OTTAWA-CARLETON GEOSCIENCE CENTRE

AND

UNIVERSITY OF OTTAWA

OTTAWA, CANADA

Abstract.

The Rose Blanche Granites are a suite of two-mica granites emplaced within amphibolite-grade metasediments of the Harbour Le Cou Group (Exploits subzone of the Dunnage Zone, Central Mobile Belt), in the Appalachians of SW Newfoundland. Regional D_2 is a result of oblique collision of the St. Lawrence and Cabot promontories, while D_3 is a result of orogen-parallel transpression. Bedding and bedding sub-parallel S_1 in the Harbour Le Cou wall rocks has been transposed and overprinted by S_2 - the dominant regional fabric which contains a well-developed stretching lineation L_2. D_2 fabrics are folded by steeply-inclined southeast-verging periclinal F_3 folds. The Rose Blanche Granite suite consists of a multitude of cm- to km-scale sheets and dykes, which are both concordant with, and cut across S_2, and include xenoliths with S_2 fabrics. Some of the larger plutons are demonstrably laccoliths, and often occur in association with anatectic migmatites. The RBG sheets and dykes are folded by F_3. Anisotropy of Magnetic Susceptibility analysis was carried out for 34 sites collected from three large-scale intrusions. Dominantly low values of magnetic susceptibility ($K_m \leq 200$ SI) indicate

that in the majority of samples it is dominated by biotite, although in some, accessory amounts of ilmenite and late magnetite make a contribution. In the majority of samples the Anisotropy of Magnetic Susceptibility fabric represents an indirect estimation of biotite shape preferred orientation. Magnetic lineations (K_1) are tightly grouped and coaxial with the main concentrations of L_2, while poles to magnetic foliations (K_3) are coaxial with the poles to S_2. Microstructures observed in the Rose Blanche Granites are indicative of solid-state, amphibolite-grade deformation. The data support the interpretation that the suite was intruded syn-D_2, during peak metamorphic conditions. The Rose Blanche Granite suite was most likely generated by anatexis of the HLCG metasediments. The melt was extracted via fluid overpressure-driven fracturing, transported in dykes and emplaced as sills and laccoliths, whose shape and locations were controlled by the presence of strong planar mechanical anisotropy and possibly migmatite zones in the wall rocks, consistent with the model of Clements and Mawer (1992).

Acknowledgments.

This work was in part financed by the NSERC operating grant to Dr. K. Benn (University of Ottawa). During the 1993 field season the author was in the employ of the Geological Survey of Canada, and working under the direction of Dr. Cees van Staal, who is thanked for valuable guidance in the field. During the 1994 field season the same GSC crew contributed accommodations and meals. I would like to thank my field assistants Helena Karam (1993 field season) and Brad Jonhson (1994 field season) whose voluntary help was very much appreciated. I would also like to thank Drs. Cees van Staal and Keith Benn for thorough manuscript reviews which helped to substantially improve the quality of the thesis. I gratefully acknowledge the contribution of Universal Systems Ltd., who provided CARIS GIS software and GEMM (Geological Mapping Module) which was used in the preparation of structural maps.

Statement of Original Contribution.

All of the structural, microstructural and Anisotropy of Magnetic Susceptibility data collected in the course of the thesis are given in Chapters 4 and 5. All of the structural mapping, sampling and microstructural observations presented in Chapter 4 were performed by the author. Portions of these data were generalized and incorporated into regional geologic maps (van Staal et al., 1996). In Chapter 5, fifteen Anisotropy of Magnetic Susceptibility sites located in the Rose Blanche-Harbour Le Cou sector were sampled when the author was employed as a field assistant by Dr. K. Benn during the 1992 field season. These data were published in Benn et al. (1993) during the course of the thesis. The author assisted with the collection of these AMS samples, and performed the magnetic fabric measurements and microstructural analyses of them.

Table of Contents.

List of Tables.

List of Illustrations.

Figures.

Plates.

CHAPTER 1 - INTRODUCTION

Pluton emplacement has generated many debates in scientific literature since the turn of the century. Emplacement studies conducted in multi-deformed terrains are complicated by the need to separate intrusion-related structures from those produced by regional deformation. Establishing the timing of emplacement becomes an integral component of the study, because pre- syn- and post-deformational emplacement scenarios can lead to similar end-result structures (Guglielmo, 1993). A notable feature of Newfoundland Appalachian geology is the fact that a large proportion of the currently exposed crustal levels is underlain by granitoid plutons (Fig. 1, Williams, 1978). This study is a structural investigation which focuses on the timing and mode of emplacement of one of these suites.

The thesis area (part of NTS-11 O/11) is situated on the southwest coast of Newfoundland. This is a geologically important region of the orogen, where the vestiges of the

important region of the orogen, where the vestiges of the ancient Iapetus Ocean have been nearly completely pinched out by the collision of the Cabot and St. Lawrence promontories of Laurentian and Gondwanan continental blocks.

The study area is underlain by multi-deformed, amphibolite-grade metasedimentary and metavolcanic rocks collectively known as the Harbour Le Cou Group (van Staal et al., 1992). The Harbour Le Cou Group rocks are intruded by a multitude of garnetiferous, two-mica, granite to granodiorite dykes, sills and sheets collectively referred to as the Rose Blanche Granites (RBG, Brown, 1974). The portion of the suite examined in the course of this study crops out between the villages of Burnt Islands and Rose Blanche, as well as further inland, to the northeast of the latter locality.

Brown (1974, 1976), the first worker to map in detail in the vicinity of Rose Blanche, concentrated on what he perceived as basement-cover relationships apparent in the country rocks. He viewed this region as a suture zone, which preserved evidence for the complete closure of the Iapetus ocean. His mapping did not show detailed internal structure

of the granite sheets and in many places the boundaries of the suite were not accurately mapped.

A preliminary structural, microstructural, and anisotropy of magnetic susceptibility study of an RBG pluton cropping out near the village of Rose Blanche revealed possible discrepancies with previously held interpretations (Benn, 1993; Genkin, 1994). It became evident that a more extensive study of the suite would contribute significantly to the understanding of the geology of this area, as well as provide a valuable example of granite emplacement at mid-crustal levels.

Pluton emplacement is a difficult topic which can be studied from several perspectives and employing a variety of techniques such as structural mapping, geochronology, petrology, isotope geochemistry, geophysics (e.g. Tobisch et al., 1993; Vigneresse, 1995; Olivier and Archanjo, 1994). This study offers a structural perspective into the emplacement of the RBG. The following combination of field and laboratory methods were used:

1. Detailed structural mapping (1:10,000 scale) of selected portions of the suite.
2. Microstructural analysis of (57) thin sections cut from the RBG and wall rock (HLCG) samples.
3. Anisotropy of Magnetic Susceptibility (AMS) analysis of samples collected from selected intrusions of the RBG suite.

Published findings of other workers, many of whom began studying metamorphism, geochronology, structure, and geochemstry of the rocks of southwestern Newfoundland around the same time this project was conceived, will be used to supplement and support discussions presented below.

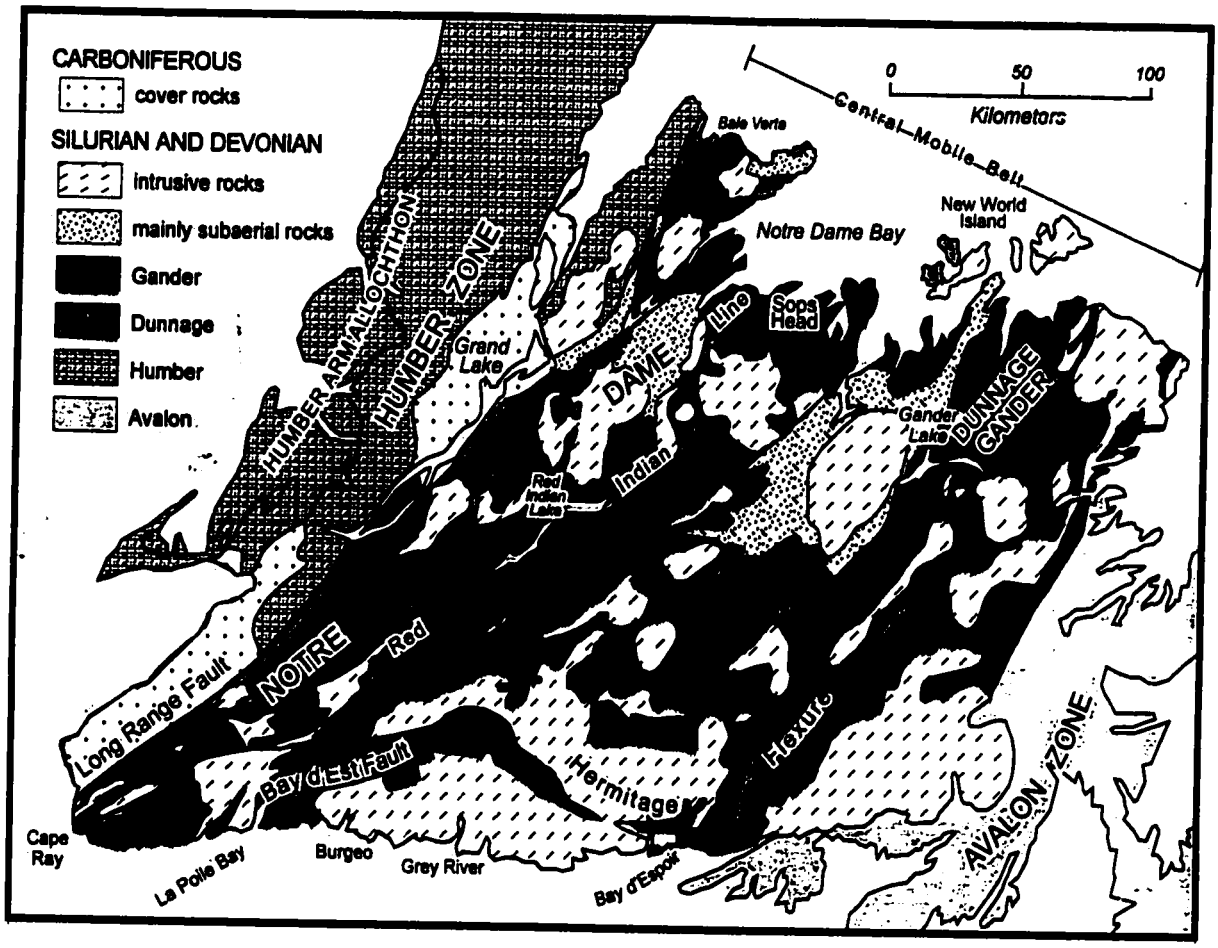

Fig. 1. Teconic stratigraphy of the Northern Appalachian orogen, and the distribution of plutonism in Newfoundland.Adapted from Williams et al., 1988.

CHAPTER 2 – Regional Geology of the Southwest Coast.

2.1 Tectonics of the Northern Appalachians.

Following the advent of plate tectonic theory, it has been suggested that the geological history of the Appalachian orogen records the formation, growth, and closure of the late Precambrian - Early Paleozoic Iapetus ocean, and, possibly, some smaller related basins (Wilson, J. T., 1966). Since then several subdivision schemes have been proposed for the northern Appalachians, with most following a basic large scale subdivision of the orogen into two continental blocks separated by a Central Mobile Belt within which deformation and Paleozoic plutonism are concentrated (Fig. 1).

Williams (1979) organized geology of the northern Appalachians into five zones based on stratigraphic and structural contrasts between Cambrian-Ordovician and older rocks. This framework remains the most widely accepted one to this day. From west to east these are the Humber, Dunnage, Gander, Avalon and Meguma Zones (Fig. 1). The first four are

exposed in Newfoundland, while rocks of the Meguma Zone crop out only in Nova Scotia.

Sedimentary rocks of the Humber Zone, the western block, are underlain by Grenvillian crystalline basement (Williams, 1979), and have been interpreted to represent the ancient continental margin of eastern North America. The Avalon Zone, the eastern block, is considered to be a fragment of Gondwana[*] It is underlain by relatively unmetamorphosed late Proterozoic sedimentary and volcanic rocks which are thought to have been formed as part of the Pan-African orogenic cycle (Williams, 1978, Fryer et Al., 1992). This is not so in New Brunswick, where structural and stratigraphic evidence preserved in the Brunswick subduction complex records a history of westward-dircted underthrusting of the Tetagouche back arc basin sequence by continental rocks of the Gander margin of Avalon (van Staal, 1994). Underthrusting of the oceanic rocks of the Dunnage by Avalonian margin rocks is becoming recognized in Newfoundland, and is supported by seismic evidence (Quinlan et al., 1992).

The geology of the Dunnage and Gander Zones, which together constitute the Central Mobile Belt, is more complicated. The

* reference (are you sure of this?).

Dunnage Zone represents the vestiges of the ancient Iapetus Ocean (Williams et al., 1988). Based on contrasting stratigraphy, structural style, faunas, and plutonism it has been subdivided into two subzones - Notre Dame to the southeast and Exploits to the southwest. The Red Indian Line, a fault zone of major tectonic significance, separates the two subzones. Rocks assigned to the Dunnage Zone are multi-deformed and metamorphosed marine sediments mixed with volcanic rocks of marine origin.

The Gander Zone of the Central Mobile Belt includes multi-deformed and metamorphosed clastic sedimentary rocks which lack appreciable volcanic component (Williams, 1988). Like the Dunnage Zone this zone has been further subdivided into three subzones (see Fig. 1): 1 - the Gander Lake subzone (type locality); 2 - the Mount Cormack subzone; 3 - the Meelpaeg subzones. The Mount Cormack subzone is everywhere surrounded by rocks of the Exploits subzone. Structural relations indicate that it is a tectonic window through the Dunnage (Colman-Sadd and Swinden, 1984). Structural relations of the Meelpaeg Subzone appear to be similar (Williams H., Colman-Sadd S. P., et al. 1988).

Due to extensive magmatism (Fig. 1) and structural overprinting assigning tectono-stratigraphic boundaries in central Newfoundland, and particularly on the south coast, has been very difficult. Colman-Sadd and Swinden (1984) propose that the complex relationships between rocks of the Dunnage and Gander Zones can be explained by ccnsidering the former to be an allochthonous terrain, which has been thrust and transported over the continental margin rocks of the latter. Gander Zone rocks crop out within tectonic windows through the Dunnage. How do the rocks hosting the RBG fit into this complex tectonic picture? In the next section we will discuss the regional geology of the southwest coast.

2.2 Regional geology of southwest coast of Newfoundland.

2.2.1 Historical Perspective.

Peter Brown (1973, 1974, 1976, 1977) was the first worker to interpret the geology of the Port Aux Basques - Rose Blanche area within a plate tectonic framework. Prior to 1992, when a new regional mapping effort got under way (van Staal et al, 1992) his data constituted the only solid background information about the RBG and the wall rocks. He recognized that geology of the southwest coast could be described as two gneissic complexes separated by a fault of major tectonic significance - the Cape Ray Fault Zone. To the northeast of the Cape Ray Fault Zone was the Cape Ray Igneous Complex, and to the southwest - geneisses of the Port Aux Basques Complex.

Brown (1974) correlated the Cape Ray Igneous Complex with the Grenvillian Long Range Complex of western Newfoundland and belonging to the western margin of the ancient Iapetus ocean. The Port Aux Basques Complex was viewed as the sialic

basement to the Devonian Bay du Nord Group cover rocks, then assigned to the Gander Zone - the eastern margin of the Iapetus. Based primarily on these perceived basement-cover relationships the Port Aux Basques Gneiss and associated intrusive rocks, including the Rose Blanche Granites, were assigned Precambrian ages. This interpretation meant that the Cape Ray Fault Zone juxtaposed two basement complexes from opposing margins of the Iapetus across a kilometer-wide zone of intense mylonitization. Brown called this fault a "cryptic suture", across which the complete closure of the Iapetus ocean took place (Brown, 1974).

More recent regional work (e.g. van Staal et al., 1992; Burgess et al., 1994; Dube et al., 1995) has produced much more detailed data about the structural geology, geochronology, and metamorphic history of the southwest coast. The understanding of regional tectonic history has been considerably refined. Modern regional geology and tectonic interpretations are summarized in the sections below.

2.2.2 Major Faults and Shear Zones.

Rocks of the southwest coast are segmented by several major shear zones. Available information about the kinematics and the timing of movement along these structures provides a structural framework for the discussion of regional geology and the history of deformation and metamorphism.

The Cape Ray Fault Zone (CRFZ).

Characterized as a several hundred meter wide, 100 km long zone of high strain, the CRFZ contains mylonite zones over 200 m thick, and six generations of structures. There is considerable variation in cross-strike and along-strike metamorphic grade and strain, and evidence for a complicated movement history (Dube et al., 1996, Lin et at., 1994). The CRFZ is a major sinistral reverse-oblique shear which overthrust high-grade Port Aux Basques Gneisses (described in section below) onto the lower-grade Windsor Point Group rocks during late Silurian to early Devonian (Dube et al., 1996, see Fig. 2). Viewed in the context of the tectonic framework of the Northern Appalachians this shear zone is the continuation of the Red Indian Line (van Staal et al., 1994,

Lin et al., 1994, Dube et al., 1996). It is a fault of large displacement and major tectonic significance. Motion along the fault zone has been bracketed between 415 Ma (Dube et al., 1996) and 386 Ma.

Dube et al. (1996) subdivided the CRFZ into two structural segments. The western northeast-oriented segment shows primarily a reverse-oblique sense of motion, whereas the northern east-northeast-oriented segment records primarily dextral strike-slip kinematics (Dube et al., 1996). The latter segment represents a tear fault accommodating the differential displacement between the CRFZ and correlative fault systems in central Newfoundland. Estimated total displacement along the northeast-oriented segment is 40 km (Dube et al., 1996). Along the east-northeast-oriented segment amphibolite-grade rocks are juxtaposed against greenschist-grade rocks, suggesting a considerable component of vertical displacement (Dube et al., 1996).

Both the HLCG wall rocks and the northern-most portions of the Rose Blance Granite suite (outside of the thesis field area) are sheared by the east-northeast-oriented segment of

the CRFZ (Dube et al., 1996) to produce mylonites, which are retrogressed to greenschist-grade conditions.

The Isle Aux Morts Fault Zone (IAMFZ).

The IAMFZ (Fig. 2) is a steeply northwest-dipping shear zone which has a complicated movement history and shows evidence of both sinistral and dextral shearing (van Staal et al., 1992).

The Bay Le Moine Shear Zone (BLMSZ).

To the east, the thesis field area is bounded by the Bay Le Moine Shear Zone (Fig. 2). This feature has not been assigned the same level of tectonic significance as the CRFZ. Nevertheless, it is a large scale structure which extents over 15 km inland from Bay Le Moine. The BLMSZ records a complicated movement history involving both brittle and ductile deformation Lin et al. (1993). The major movement is oblique dextral shear. The main zone of dextral shearing is more than 1 km wide. The BLMSZ juxtaposes amphibolite-grade rocks with their greenschist-grade equivalents (Lin et al., 1993) and, therefore, must have a significant component of vertical displacement.

2.2.3 Lithologies of the Southwest Coast.

The Grand Bay Complex (GBC).

The Grand Bay Complex (GBC) is bounded to the northwest by the Cape Ray Fault Zone. The dominant lithologies are gt-st-ky schists. Thin bedded shale-siltstone rhythmites with occational sandstone beds formed the protolith for these units. Interlayered with the metasediments are also sheets of amphibolites, ultramafic and granitoid rocks. The latter are mylonitic near the tectonic boundaries of this unit - the CRFZ and the Grand Bay Fault Zone (GBFZ, Fig. 2) to the east. Stretching lineations in the mylonites plunge steeply to the south-southeast and kinematic indicators show tectonic transport to the northwest (Burgess et al., 1995). The GBC has been assigned to the Exploits Subzone of the Dunnage Zone.

The Port Aux Basques Complex (PaBC).

The Port Aux Basques Complex is bounded by the GBFZ to the west and by the Isle Aux Morts Fault Zone (IAMFZ) to the east (Fig. 2). It consists primarily of a succession of migmatitic, psammite-plite rhythmites metamorphosed to upper

amphibolite facies (van Staal et al., 1996). Amphibolites, intricately interlayered with the metasediments comprise 20-25% of the complex. The metamorphic grade increases from ky-st-gt near GBFZ to sil-gt and then to sil-kspar-migmatite to the southeast (Burgess et al., 1995). The metasedimentars of the PaBC have been intruded by granitoid and mafic rocks of the Margaree and Kolby Cove orthogneisses, and the leucocratic Port Aux Basques Granite (van Staal et al., 1996). The PaBC has been assigned to the Gander Zone (van Staal et al., 1996). It separates the Exploits Subzone along the Southwest coast into eastern and western parts.

The Harbour Le Cou Group (HLCG).

The Harbour Le Cou Group is bounded to the east by the Isle Aux Morts Fault Zone (IAMFZ, see Fig. 2), which separates it from the PaBC. To the west it is separated from the Bay du Nord Group rocks by the Bay Le Moine Shear Zone. Rocks of HLCG are intruded extensively by the RBG suite. Originally this unit was restricted to two thin lenses cropping out near the village of Rose Blanche (Brown, 1974). However, more recent mapping indicates that this definition should be extended to include the rocks which were earlier viewed as

microstructurally reworked portions of the Port Aux Basques Gneisses (Lin et al., 1993).

The HLCG has been subdivided into two formations: 1 - the Otter Bay Formation consisting primarily of feldspathic psammite with thin beds of rusty pelite; 2 - the Grandy's Bay Formation consisting of a succession of rusty pelitic to semi-pelitic schists. Migmatitic rocks are volumetrically a major component of the HLCG.

Bay Du Nord Group (BDNG).

This group consist of biotite grade, greenschist-facies sedimentary and volcanic rocks, with the dominant lithology being a package of thin-bedded, locally tuffaceous siltstones and mudstones. Rocks of the BDNG have been intruded by the La Poille and Petites granites, which have narrow contact aureoles (van Staal et al., 1996).

Lin et al. (1993) correlated the HLCG with the lower grade rocks of the Bay du Nord Group, and both units have been assigned to the Exploits Subzone of the Dunnage Zone.

2.2.4 History of Deformation and Metamorphysm.

Recent structural, metamorphic and geochronological studies indicate that the lithological units of the Southwest coast share the same history of deformation and metamorphism in both spatial and temporal sense (Burgess et al., 1995, Dube et al., 1996, Lin et al., 1994). Structures and fabrics observed in the rocks can be explained by three major episodes of ductile deformation and a fourth episode of limited spatial extent (Lin et al., 1993; van Staal et al., 1992; Burgess et al., 1995; van Staal et al., 1996). These are summarized below.

The first episode of deformation produced rare recumbent F_1 folds, whose existence is supported mainly by an S_1 foliation which is folded by F_2. The second generation of deformation is characterised by tight to isoclinal F_2 folds, which are recumbent at the hinges of F_3 folds, and have a strong S_2 axial planar cleavage. The third episode of deformation is represented by open to tight F_3 folds, with locally developed axial planar crenulation cleavage. The fourth

generation of deformation is represented by kink folds. These are spatially related to late shear zones.

Burgess et al. (1995) established that the rocks of the southwest coast experienced a history of metamorphism characterized by a clockwise P-T-t path. Prograde metamorphism during D_1 is poorly constrained with the growth of garnet and kyanite. They conclude that peak metamorphic conditions of 650-750°C at 6-9 kbar were reached syn- to late-D_2. Some of their metamorphic and geochronological data, along with data collected from other publications is given in Table 1.

Metamorphism during D_3 was retrogressive, but still in the stability field of sillimanite. It was accompanied by recrystallization of hornblende in amphibolites, and muscovite and biotite in pelitic rocks. No growth of andalusite or cordierite was observed and consequently Burgess et al. (1995) estimated peak metamorphic conditions during D_3 at c. 550°C and 3-5 kbar.

A 416.5 ± 9.8 Ma U-Pb isotopic cooling age of titanite, separated from a sample taken from a calc-silicate pod in the HLCG metasediments, was interpreted to represent the minimum age of peak metamorphism. Data from Burgess et al. (1995) show moderate cooling rates of 8-10 °C/Ma for samples from HLCG. Dubé et al. (1996), however, argue for rapid exhumation of the Port Aux Basques Gneisses and Harbour Le Cou Group rocks.

2.2.5. Regional Tectonic Model.

Deformation and metamorphism are more intense in southwestern Newfoundland than in other parts of the Canadian Appalachians. Lin et al. (1994) propose that this is the result of the collision of two promontories - the St. Lawrence promontory on the Laurentian margin and the Cabot promontory on the Avalonian margin.

Within this context D_1 represents crustal thickening which produced recumbent F_1 folds with an associated axial planar schistosity. D_2 represents northwest-directed thrusting (Burgess et al., 1995). D_2 structures overprinted and

transposed the S_1 foliation. D_1, D_2, and D_3 form a continuous cycle of deformation (van Staal et al., 1994b, Burgess et al., 1995, Dube et al., 1996). Present day northeast trending structural grain of the area is reflective of D_3. This event represents the transition from overthrusting to transpressional deformation during which strain was partitioned into major dextral transcurrent shear zones and tight upright to steeply inclined doubly plunging folds (Burgess et al., 1995). Metamorphism, which accompanied the deformation, is characterized by a clockwise P-T-t path, with upper-amphibolite grade peak conditions being reached during D_2. Metamorphic grade increases eastwards along the southwest coast reaching peak conditions favorable for melt generation in the HLCG (Burgess et al., 1995).

Viewed within the regional structural framework the rocks of the HLCG are located in the center of a large scale thrust sheet bounded to the west and north by the CRFZ and to the east by the Bay D'Est Fault (Fig. 3). The rocks of the southwest coast are further transected by major dextral shear zones which developed to accommodate the geometry of the collision zone imposed by the shape of the Cabot Promontory

(Dube et al., 1996). The geometry of the collision zone is summarized in Fig. 3.

2.3 The Rose Blanche Granites – summary of previous work.

Brown (1976) characterized the RBG as consisting of granite to granodiorite sheets which strike northeast to east-northeast and dip to the northwest at a shallow angle. The average modal mineralogy of the suite was described by the following:

1. - microcline or perthitic microcline - 30-50%;
2. - plagioclase An_{18-35} - 20-30%;
3. - interstitial quartz - up to 40%;
4. - biotite as the mafic phase in granite and hornblende in granodiorite sheets;
5. - muscovite as the dominant mica in late dykes.

The same author recognized that the granite sheets were affected by two phases of deformation (Brown, 1973) and concluded that it must have been emplaced pre- or syn-D_2. Hornfels textures were observed near the more western sheets (Brown, 1976) - an indication that the granites intruded following peak metamorphism.

Some portions of the suite were studied by Van Staal et al. (1992) during a reconnaissance geotraverse through southwestern Newfoundland, and by Lin et al. (1993) during their regional mapping effort in the Burnt Islands - Rose Blanche area. Both authors noted that some of the dykes were folded by both regional F_2 and F_3, and that the fabrics in them were either controlled by F_2 axial planes (Lin et al., 1993) or were oriented consistently with regional D_2 (Van Staal et al., 1992).

The most recent and specific study was carried out on a part of the suite by Benn et al. in the summer of 1992. A significant exposure of the RBG (The Rose Blanche Pluton, Benn et al., 1993) in and around the village of Rose Blanche was mapped and sampled for AMS analysis. Results of the analyses showed that some of the fabrics, in particular the quartz stretching lineations and the maximum principal susceptibility axes (K_1) of the AMS ellipsoids appeared to be consistent with regional D_3 fabrics. This led to a preliminary interpretation that at least some of the suite was emplaced late-D_2 to early-D_3, and possibly during the transition between these two deformational events (Benn et al., 1993).

Recent (Van Staal et al., 1994) geochronological dating of the RBG was carried out on a sample from a location near the village of Rose Blanche. At that locality the granite was clearly affected by two phases of deformation (D_2 and D_3; Van Staal, personal communication), and yielded a U-Pb zircon age of ca. 419 Ma (Van Staal et al., 1994). This age correlates extremely well with isotope ages of peak metamorphism (see Table 1).

Walen et al. (1995), in a recently submitted publication, describe the RBG as a granite with 'S-type' petrographic characteristics, arc-type (VAG) trace element designation, positive ϵ_{Nd} and elevated $\delta^{18}O$. The authors conclude that the geochemistry of the RBG can be attributed to derivation of the magma by partial melting of immature arc volcaniclastic sediments. Rocks of the HLCG, in particular, were viewed as a likely source for the melt (Whalen et al., 1995).

Table 1. Structural and metamorphic history of the rocks southeast of the CRFZ.

DEFORMATION		METAMORPHISM				
EVENT	STRUCTURAL STYLE	MINERAL GROWTH	P-T CONDITIONS	AGE	TECHNIQUE	REFERENCE
D_1	rare recumbent folds; bedding sub-parallel foliation folded by D_2.	garnet; kyanite; chlorite, muscovite, biotite.	Poorly constrained.	470 Ma. Pre- D_1 Margaree Orthogneiss	U-Pb on zircon	Van Stall et al. (1995)
				453 Ma. Syn-D_1 Port Aux Basques Granite.	U-Pb on zircon	Burgess et al. (1995)
D_2	Tight to isoclinal folds, sheath folds; recumbent or reclined at hinges of F_3 folds, verging to the northwest; well developed axial planar schistosity S2 forms the strongest regional fabric.	Kyanite, staurolite and garnet; syn-D_2 sillimanite and garnet; muscovite, biotite, K-feldspar.	peak conditions >700 °C, 8 kbar Presence of anatectic migmatites.	Minimum peak metamorphic age of 415±2 Ma.	U-Pb on titanite	Van Stall et al. (1995)
D_3	Open to tight upright folds which overprint F_2 folds and sometimes exhibit a weakly developed axial planar cleavage; near Bay Le Moine have a "Z" symmetry.	Recrystallized hornblende, chlorite, muscovite, biotite; sillimanite, K-feldspar.	Cooling through 500 °C	405.7±1.3 Ma, 422.2±1.4 Ma	$^{40}Ar/^{39}Ar$ on recrystallized hornblende.	Burgess et al. (1995)
			Cooling through 375 °C	391.1±1.7 Ma	$^{40}Ar/^{39}Ar$ on muscovite.	Burgess et al. (1995)
D_4	Localized, minor-displacement late shear zones with associated kink folds.	Chlorite.				

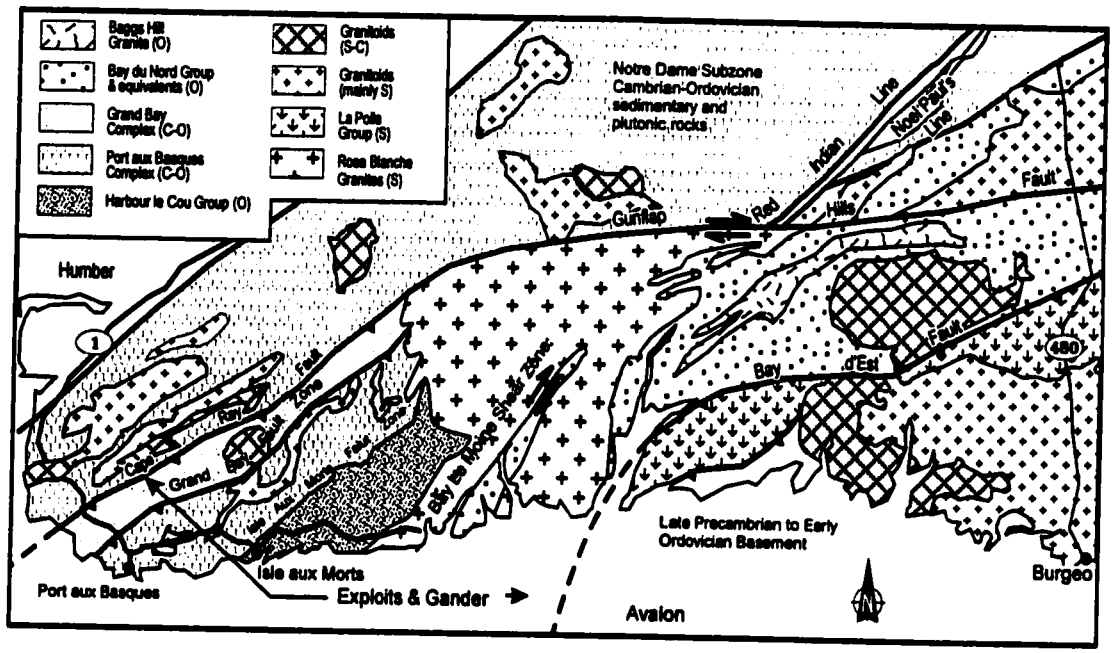

Fig. 2. Regional geology of the southwest coast of Newfoundland. Adapted form Lin et al., 1994.

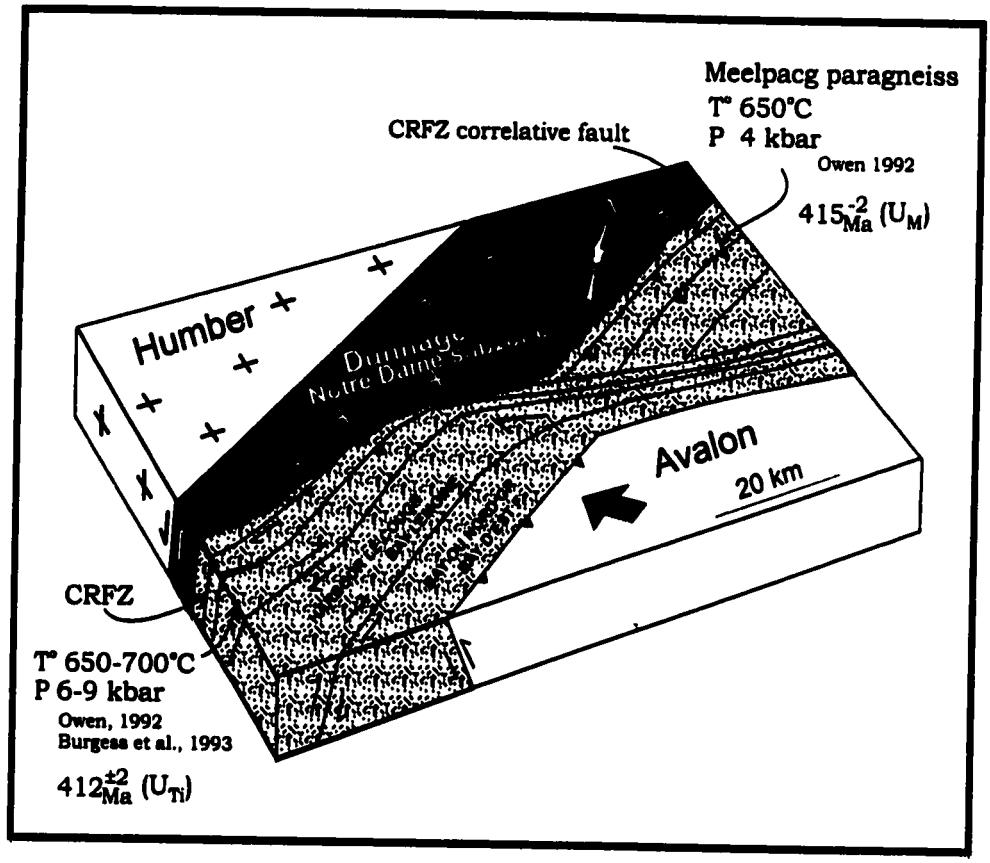

Fig. 3. Collisional geometry of the units of the southwest coast. From Dube et al., 1996.

CHAPTER 3 - METHODS.

3.1 Structural Mapping.

Mapping was concentrated on the coastal areas between the villages of Burnt Islands and Rose Blanche, as well as to the north of Harbour Le Cou, Lobster Cove and Gull Pond (see Maps 1 and 2). These coastal areas were selected for detailed mapping because they offer the best exposures of the RBG, often allowing for three-dimensional viewing of the structures and relatively easy access by vehicle or boat. The need to support AMS measurements with detailed structural and microstructural observations was an important factor in selecting the aerial extent and the scale of the mapping. Most structures were mapped on a 1:10,000 to 1:15,000 scale. Final map presentation (Maps 1 and 2) is on a 1:25,000 scale.

In order to facilitate description of the structures, lithologies and field relations, the mapped area has been subdivided into three sectors (see Maps 1, 2) - the Burnt Islands sector, the Barasway sector, and the Rose Blanche - Harbour Le Cou sector. The basis for this subdivision is the presence of map-scale geographically distinct RBG intrusions. No evidence was found to support subdivision of the area into structural domains. Subdivision of the field area into sectors is intended to facilitate descriptions of map-scale structures affecting the granite, geometry of separate intrusions, and locations of sampling sites.

Structural notation used to describe HLCG and RBG structures and fabrics is summarized in Table 2. Fabrics observed in the granite are described using a non-age-specific notation. Although this labeling approach does not conform with some of the generally accepted practices, determination of the structural age of the main granite fabrics was an important objective of the thesis. It was, therefore, decided to adopt an age-neutral labeling convention in order to avoid biasing data collection and interpretation.

Determination of the geometry of map-scale intrusions was given particular emphasis. Traverses were planned to follow and clearly define, where possible, the contacts between the RBG sheets and the surrounding HLCG metasediments. Because the exposure throughout the thesis area was observed to be good (between 60 and 100%), it was possible to walk out most of the contacts. Where this was not possible the contacts were interpolated and extrapolated by analyzing the orientation of nearby contacts, mesoscale structures observed in nearby RBG and HLCG exposures and geometry of the nearby large scale structures as established from previous mapping and/or air photo interpretation.

Most exposures of the RBG were observed to contain a weak to moderately strong foliation defined by preferential alignment of muscovite, biotite, and flattened quartz grains. These foliations were found to be relatively easy to measure in the field using a geological compass, however, measurements of the stretching lineations were more problematic. Most RBG outcrops were found to be weakly to moderately strained, and often partially covered with lichen. Most RBG exposures were also found to consist of an equigranular granite phase lacking sufficient quantities of elongate minerals (such as

amphibole) required to produce readily visible lineations at weak strains. Where possible, quartz stretching lineations were measured in the field (Benn et al., 1993, Rose Blanche sector). In other sectors quartz stretching lineations were measured from AMS cores (sampling procedure is described in section 3.3.2). A section containing the foliation plane was cut from the core, and the average rake of the elongate quartz grains within the foliation plane was measured. The true trend and plunge of this lineation were established using standard stereonet techniques. This procedure was carried out in the laboratory, after the end of the field season.

3.2 Microstructural Studies and Observations.

Oriented samples were collected for microstructural analysis from three separate map-scale RBG intrusions cropping out in each of the mapping sectors. Several shear zones were also sampled. RBG thin sections were cut from AMS cores and from several hand samples. One oriented thin section was cut for every AMS sampling site.

Recrystallization mechanisms active in a mineral at the time of deformation depend on pressure, temperature, and strain rate conditions to which the rock was subjected and, to a certain extent, on the amount of structural water locked within the crystal lattice of the mineral (Urai et al., 1987). Since the 1960's considerable amount of experimental and empirical work (e.g.Blachic, 1975; Carter et al., 1964; Evans, 1988; Prier, 1993; Tullis et al., 1973), has been done in documenting recrystallization mechanisms active in minerals (especially quartz in granites and quartzites) under various metamorphic conditions.

Microstructural observations can be used as supporting evidence in establishing the grade of metamorphism at the time of fabric formation. This, along with the need to petrographically document the mineralogical sources of susceptibility, was the primary aim of analysis carried out on RBG samples.

Microstructural study of the RBG samples included:

1.- visual estimation of modal mineralogy - identification of mineralogical sources of magnetic susceptibility;

2.- examination of biotite grains for signs of recrystallization and alteration in order to evaluate the significance of the AMS data;

3.- examination of deformation mechanisms which were active in the quartz and feldspars in order to constrain the nature of the fabric, primarily magmatic vs. primarily solid state, and estimate the metamorphic grade at the time of fabric formation, in the latter case.

Visual estimations of modal mineralogy of the RBG samples were considered sufficient for the purposes of this research, and consequently points were not counted.

In addition to the RBG samples, fifteen thin sections cut from samples of the HLCG pelites, semi-pelites, psammites and migmatites were examined. The focus of microstructural analysis of the wall rocks was different from analysis carried out on the RBG samples. The emphasis here was not on documenting mechanisms of recrystallization, but on establishing the relative timing of metamorphic mineral growth with respect to deformation. The primary aim of microstructural analysis of the HLCG wall rocks was to establish whether granite intrusion resulted in contact

metamorphism, or superimposed additional strain on the regional tectonic fabric - both processes which could not be observed macroscopically in the field. Results of this study were compared with data published by workers studying regional metamorphism in the area (Burgess et al., 1995; Dubé et al., 1996).

3.3 Anisotropy of Magnetic Susceptibility (AMS) Analysis.

3.3.1 AMS of rock-forming and accessory minerals.

Most rocks containing either structural, magmatic, or sedimentary fabrics exhibit magnetically anisotropic behaviour. Anisotropy of (weak field) Magnetic Susceptibility (AMS) is a non-destructive technique for measuring the magnetic susceptibility tensor in a small sample of rock (Borradaile, 1988). Sections below outline the theoretical basis behind this technique, its application to pluton emplacement studies, and the data collection, treatment, and interpretation methods used in the thesis.

Magnetic susceptibility is a measure of the response of a given substance to an applied magnetic field. It is defined by the following equation:

$$\mathbf{J} = k\mathbf{H} \qquad (1)$$

where $\mathbf{H}$ is the applied magnetic field vector, $\mathbf{J}$ is the induced polarization vector, and k is the volumetric magnetic susceptibility of the substance generally reported in units SI/unit volume. If the applied magnetic field $\mathbf{H}$ is weak, then

k is a constant - i.e. the material exhibits magnetically linear behaviour. If the material is perfectly isotropic then k is a scalar real number. If the material, like most rocks and minerals, is magnetically anisotropic then k becomes a second order tensor ($\mathbf{k}$) and equation (1) can be rewritten in its full vector form:

$$\begin{bmatrix} J_1 \\ J_2 \\ J_3 \end{bmatrix} = \begin{bmatrix} k_{11} & k_{12} & k_{13} \\ k_{21} & k_{22} & k_{23} \\ k_{31} & k_{32} & k_{33} \end{bmatrix} \times \begin{bmatrix} H_1 \\ H_2 \\ H_3 \end{bmatrix} \quad \textbf{(2)}$$

The eigenvalues of the magnetic susceptibility tensor are the principal susceptibilities:

K_1 - maximum susceptibility;

K_2 - intermediate susceptibility;

K_3 - minimum susceptibility.

Their corresponding eigenvectors are the principal susceptibility directions. The magnetic susceptibility tensor can be visualized as an ellipsoid with maximum (K_1), minimum (K_3), and intermediate axes (K_2). It is common practice to report the values of the principal susceptibilities normalized with respect to the average susceptibility K_m which is defined as: $K_m = (K_1 + K_2 + K_3)/3$.

In general, substances can be subdivided based on their behavior when placed in an external magnetic field. A substance whose orbital electrons are oriented to oppose the applied magnetic field exhibits negative susceptibility and is termed *diamagnetic*. In a *paramagnetic* substance the magnetic dipole moments of the orbital electrons are free to be oriented parallel to the magnetic field, resulting in a positive magnetic susceptibility value. In iron, cobalt and nickel strong paramagnetic interactions between atoms lead to the formation of fairly large (on the atomic scale) domains where the magnetic dipole moments of constituent atoms are oriented in the same direction. This behavior is called *ferromagnetism*, and it can produce susceptibilities $\sim 10^6$ times the magnitude of diamagnetic and paramagnetic substances. Ferromagnetic effects decrease with increasing temperature and disappear when the material reaches its Currie temperature. *Ferrimagnetic* materials contain two populations of magnetically opposing domains. One of the populations is usually dominant, resulting in a net ferromagnetic effect.

Rock forming minerals (e.g. feldspars, quartz, micas, etc. - see Table. 3) are either diamagnetic or paramagnetic. For diamagnetic minerals k is negative and typically on the order of -1×10^{-5} SI/unit vol. (Borradaile, 1988). Paramagnetic minerals have higher susceptibilities which are typically on the order of 10^{-4} SI/unit vol. The degree of magnetic anisotropy of paramagnetic minerals ($P = K_1/K_3$) is usually large. Values of susceptibilities and anisotropies of common rock-forming diamagnetic and paramagnetic minerals are given in Table 3.

AMS of diamagnetic and paramagnetic minerals is determined by the orientation of the crystal lattice and is not affected by the grain shape (Borradaile, 1988). Properties of the AMS ellipsoid of a single crystal (monocrystal AMS) depend on the symmetry of the crystal lattice. The AMS ellipsoid of many phyllosilicate grains, including biotite, can be effectively approximated by a uniaxial oblate ellipsoid of revolution with $K_1=K_2>K_3$ where K_3 is perpendicular to the (001) plane of the grain (Hrouda, 1987).

Some common accessory minerals found in metamorphic and igneous rocks are ferrimagnetic. Magnetite, hematite and pyrrhotite are the most important of these. Susceptibility of ferrimagnetic minerals is usually very large and positive (Table 4), frequently several orders of magnitude larger than for paramagnetic minerals. AMS of magnetite, the most important ferrimagnetic accessory mineral frequently found in granitoids, depends on the shape of the grain (when measured at low field strengths, multiple-domain magnetite) and not the orientation of the crystal lattice (Borradaile, 1988). Thus, in rocks where AMS is dominated by magnetite, it could be an indirect estimation of the magnetite shape preferred orientation (SPO). In those cases where magnetite replaces paramagnetic minerals, such as biotite, along crystallographic planes it could enhance, rather than overprint, the paramagnetic AMS fabric (Archanjo and Bouchez, 1994).

The relationship between the magnitude of K_m of the rock, the degree of anisotropy of the susceptibility ellipsoid ($P = K_1/K_3$), and the relative proportions of the constituent paramagnetic and ferrimagnetic minerals is an important consideration. Minerals and rocks with high bulk value of

susceptibility do not necessarily have a high degree of anisotropy. Although the magnitude of susceptibility - K_m for magnetite is relatively large (e.g. K_m = 6.2 SI/unit volume, Table 4), the typical value of magnetic anisotropy for this mineral can be very small (e.g. $K_1:K_2:K_3$ = 1.063 : 0.989 : 0.951, Table 4), due to the usually equant shape of individual grains. Anisotropies produced by strings of magnetite grains, formed by mimetic alteration growth for example, can be much larger than for paramagnetic silicates (Borradaile, 1988; Rochette, 1987). P of a paramagnetic mineral such as biotite (e.g. $K_1:K_2:K_3$ = 1.114 : 1.106 : 0.812, Table 3) is usually large, although K_m is much less than for magnetite (1230×10^{-6}, Ibid).

The mean bulk susceptibility for a sample of rock can be dominated by accessory minerals such as magnetite, whereas the anisotropy of the AMS ellipsoid can still be controlled by paramagnetic minerals, such as biotite, depending on the relative proportions of each of the minerals in a rock (Hrouda, 1987).

3.3.2 Whole rock AMS, mineralogy, microstructure and strain.

In all but the most weakly magnetic rocks the diamagnetic contribution to the bulk fabric can be ignored. In granites this accounts for the largest proportion of the matrix minerals - quartz and feldspars (Table 3). The paramagnetic component is an indirect estimation of the bulk petrofabric of the constituent paramagnetic minerals. In granites the main contributors to the paramagnetic subfabric are biotite and amphibole (see Table 3 for typical values susceptibility and AMS). However, accessory amounts of cordierite, tourmaline and garnet (an isotropic mineral which can contribute to K_m but not to P) can significantly affect the measurements (Jover et al., 1989). The ferrimagnetic component could represent either the petrofabric or the SPO fabric of the accessory minerals, depending on the accessory mineral species present and the timing of their growth with respect to the matrix minerals.

Separation of the paramagnetic and ferrimagnetic components of AMS, and identification of the mineralogical sources is

essential for the proper interpretation of the data. A number of techniques employing measurements of susceptibility at varying temperatures and field intensities (e.g. Rochette and Fillion, 1988) have been developed in order to identify and separate the contribution made by ferrimagnetic minerals. These are only briefly mentioned here as none of these techniques was applied in the course of this project.

In addition to the separation of subfabrics resulting from multiple sources of susceptibility, geological interpretation of AMS data involves making certain assumptions about formation and evolution of magnetic fabrics in response to strain. Strain response models, although they are necessarily imperfect simplifications of real deformation processes, provide a conceptual framework within which SPO and petrofabrics indirectly recorded by AMS can be related to deformation. Strain response models of March (1932) and Jeffrey(1922) have been widely discussed and treated in the scientific literature.

The March (1932), or the "line/plane", model treats the long axes of prolate particles as perfectly rigid lines, and the

short axes of oblate particles as poles to perfectly rigid planes, which rotate in a deforming matrix in response to strain (Fig. 4). Discussion of the mathematics involved in the model is beyond the scope of the thesis but a restatement of the underlying assumptions and implications for geological interpretation of AMS fabrics is useful and is given below. The model relies on the following assumptions:

1. The mineralogical sources of AMS can be approximated as perfectly rigid lines and planes which do not mechanically interact with one another.
2. The fabric is formed purely by passive mechanical rotation of purely rigid markers in response to strain - there is no mineral growth or recrystallization.
3. The deformation is linear in nature (March, 1932) - i.e. a straight line prior to deformation remains a straight line after.

During real deformation these assumptions are seldom satisfied. However, numerous numerical modeling studies have demonstrated that the March model produces fabrics which are very similar to those observed in real rocks (e.g. Benn,

1994; Hrouda, 1987). This is especially true for weakly to moderately deformed leucocratic granites whose main sources of susceptibility are dispersed biotite grains embedded in a matrix of quartz and feldspar.

The March model predicts that with increasing finite strain the long axes of prolate grains will be gradually aligned into parallelism with the maximum principal strain. The poles to oblate grains will be aligned along the direction of minimum principal strain. Thus prolate minerals such as amphibole will be aligned parallel to the stretching lineation and oblate minerals such as biotite will be aligned parallel to the foliation. Platy minerals, such as biotite, will also tend to be aligned in zones around the direction of maximum extension, as shown in Fig. 5, making it possible to produce a prolate fabric even if phyllosilicates with oblate monocrystal AMS ellipsoids are the only sources of susceptibility.

There have been many attempts to correlate the AMS ellipsoid with the finite strain ellipsoid (e.g. Hirt et al., 1995; Chen and Oertel, 1991; Hrouda, 1987). Most of these studies have applied the March model, largely due to its relative mathematical simplicity, with varying degrees of success. It has been demonstrated that in weakly deformed rocks, with simple magnetic mineralogy, correlations between AMS and strain ellipsoid orientations and shape parameters do exist (e.g. Chen and Oertel, 1991; summaries in Borradaile, 1988; Henry, 1989; Hrouda, 1987; Rochette, 1988). However, these studies have also demonstrated that the shape and orientation of the AMS ellipsoid depends to a much greater extent on the magnetic mineralogy than on the amount of finite strain experienced by a rock (Richter et al., 1991; Sun et al., 1995). For this reason AMS fabric studies must be accompanied by microstructural and, if necessary, demagnetization studies to separate the effect of changes in mineralogy from changes in the magnitude or type of strain.

3.3.3 AMS and pluton emplacement.

Magnetic fabric studies have been applied to a wide variety of geological problems. AMS analysis has been used to interpret paleocurrent directions in sedimentary rocks (e.g. Hrouda, 1971) and magma flow directions in dykes (e.g. Cadman et al., 1992). AMS fabrics have been used to study kinematics of shear zones, and strain in multi-deformed rocks (e.g. Henry, 1989, 1987; Richter et al., 1991; Chen and Oertel, 1991). Most studies have concentrated on deformed metamorphic and igneous rocks because these typically show the highest degree of anisotropy (Borradaile, 1988). AMS analysis offers a high degree of sensitivity to changes in petrofabrics, and a relatively rapid process of data acquisition, measurement and interpretation. Due to these advantages the technique has found especially wide applicability in structural studies of granitic plutons (e.g. Rochette et al., 1994; Bouchez and Gleizes, 1995).

Granites can generally be subdivided into paramagnetic and ferromagnetic types (Bouchez and Gleizes, 1995). From the

petrographic perspective the term "paramagnetic granite" encompasses those granitoid rocks whose parent magma lacked the iron oxide component - i.e. crustally-derived peraluminous granites typically found in collisional tectonic environments, such as two-mica S-type leucogranites (Barbarin, 1990). Paramagnetic granites have relatively uncomplicated magnetic mineralogy, with biotite being commonly, but not necessarily, the dominant source of susceptibility (Bouchez and Gleizes, 1995; Jover et al. 1989; Rochette et al. 1993; Benn et al., 1993). Significant contributions could also come from hornblende, cordierite, and ilmenite (Rochette et al., 1994; Jover et al., 1989). Because the monocrystal AMS of biotite is roughly coincident with the shape of the grains, the AMS fabric of a paramagnetic granite is an indirect estimation of the average biotite SPO fabric, provided that the grains have not been recrystallized, overprinted or altered by subsequent deformation and metamorphism. This highlights the importance of microstructural observations in interpretation of AMS data. Anatectic, or S-type, granites such as the RBG are almost invariably paramagnetic. Magnetic susceptibility of ferromagnetic granites is dominated by accessory iron-oxides and iron-sulfides such as magnetite and pyrrhotite.

A recently published study of the Mont-Louis-Andorra pluton in the Pyrenees (Bouchez and Gleizes, 1995) is an example of how a combined microstructural-AMS approach can be used to investigate the structural history of a granite body. Bouchez and Gleizes (1995) were able to map the petrographic zonation of the pluton by mapping the average magnitude of magnetic susceptibility (K_m) - an indirect reflection of pluton mineralogy. Directional AMS data (i.e. orientations of K_1 and K_3) were used by the above authors to map the stretching lineation and foliation patterns and identify two generations of fabrics preserved within the granite. The first generation of fabrics, characterized by NE-SW trends and magmatic microstructures, was interpreted to be related to pluton emplacement process, and the second, oblique to the first generation of fabrics and characterized by sub-magmatic microstructures, to later shear zones which formed in response to regional deformation. Microstructural observations were used to confirm that the fabrics preserved in the shear zones formed at a lower temperature, and therefore later, than the emplacement-related fabrics. Bouchez and Gleizes (1995) correlated the first generation of fabrics with an early Variscan thrust event which was, at the

time, becoming recognized elsewhere in the Pyrenees. The latter generation of fabrics was interpreted to record a dextral transcurrent-shearing event most commonly described as the main deformational episode in the Variscan Pyrenees which everywhere, except in the granites, overprinted the earlier thrust-related fabrics.

3.3.4 Sampling Methods.

Rock cores were collected at 34 sites covering three separate RBG intrusions located in the Burnt Islands, the Barasway, and the Rose Blanche-Harbour Le Cou sectors. These three areas were selected for sampling based on ease of access, availability of good exposure, and presence of clearly established structural relationships. Burnt Islands exposure is a granite sheet folded into an isoclinal synform. The Barasway exposure represents a hinge zone of a refolded fold, while the Rose Blanche sector was interpreted as a flank of a large-scale fold.

Sampling site locations were selected to provide an evenly spaced coverage of each of the three sectors. Three cores, each 1" in diameter and five to ten inches long, were collected at each site using a hand-held gasoline-powered drill with a diamond studded bit. Drilling points were selected so that the distance between any two cores for a given site would not exceed 5 m. This spacing was chosen to provide a good evaluation of the average fabric while

minimizing the effect of the AMS variation between cores caused by possible strain gradients.

AMS cores were collected by a team of two people. One person would operate the drill, and the other would be responsible for maintaining a steady flow of cooling water through the drill bit and determining core orientations. Core orientations were established using a custom built orientometer used in conjunction with a Brunton (or a modified Silva) compass.

3.3.5 AMS measurement and data treatment procedures.

The instrument used to make the AMS measurements was a KLY-2 Kappabridge manufactured by Geofyzika n.p. Brno, Czechoslovakia, and installed in the Structural Petrology Laboratory, Department of Geology, University of Ottawa. Software written and supplied by the manufacturer was used to calculate the magnitudes and orientations of K_1, K_2, K_3, the K_m (site averages) of the above parameters for each site, and the magnitudes of the associated errors.

Two 22 mm long samples were cut from each core. A 22 mm long cylindrical specimen with a 1" diameter contains approximately 10 cm^3 of rock - the optimum volume for the KLY-2 measuring apparatus. Orientation markings of the core were carefully transferred to each sample and subsequently used to determine orientation positions used in the measuring procedure. A total of six oriented AMS samples for each site were measured. Magnetic susceptibility was measured in 15 directions for each sample. Six of these measurements are independent and necessary to determine the

tensor, but 15 are taken in order to estimate residual errors, evaluate the reproducibility of the measurements and calculate the confidence ellipses for each of the principal susceptibility directions.

3.3.6 Analysis and interpretation methods.

Mineralogical sources of susceptibility were identified using transmitted-light petrographic observations. Rare ilmenite grains in the RBGrb phase were identified by the presence of titanite rims. In addition to ilmenite, very fine opaque grains were observed to have grown along the cleavage planes in some of the biotites and hornblendes in the RBGrb phase. The alteration mineral was too fine-grained for reflected-light microscopy to be effective. It was assumed to be late mimetic magnetite growth. Because only a small fraction of the samples were observed to contain this accessory mineral, uncertainty in its identity was not considered to seriously affect the overall interpretation (see discussions in Chapter 5).

Comparison of low-field AMS data with data for similar granites in published sources (Benn, 1994; Ben et al., 1993; Brun et al., 1990; Bouchez and Gleizes, 1995) and interpretation of K_m vs. P plots were used to support the identification of mineralogical sources of magnetic susceptibility in the RBG. An example of a K_m vs. P is shown in Fig. 6.

In a rock whose susceptibility is dominated by paramagnetic phyllosilicates P should not exceed 1.35 (Rochette, 1987). Anisotropy of biotite at room temperature is 1.37 (Rochette, 1987). If all of the biotite crystals in a sample of rock were perfectly aligned this value would represent the theoretical maximum of P for the sample, provided that its AMS was due solely to biotite. In reality this value is rarely attainable as in all weakly to moderately deformed rocks the phyllosilicates are never perfectly aligned. If the average susceptibly of biotite is taken as being approximately equal to 1300 x 10^{-6} SI (Table 4, Borradaile, 1988) and the contribution of the diamagnetic matrix is neglected, a 10% modal component of biotite will theoretically result in whole rock susceptibility of 130 x 10^{-6} SI. These assumptions can be used to roughly denote a

field on the K_m vs. P diagram (marked "10% biotite" in Fig. 6) which can be theoretically accounted for by this modal fraction of biotite, providing an indirect test for petrographic identification of mineralogical susceptibility sources.

Analysis of directional AMS data included interpretation of maps of K_1, maps of magnetic foliation (K_1-K_2 planes), and stereonet plots of K_1 and K_3, following approaches taken by other workers (e.g. Bouchez et al., 1995).

Plots of the degree of anisotropy ($P=K_1/K_3$) vs. the shape parameter $T = 2(\ln K_2-\ln K_3)/(\ln K_1-\ln K_3)-1$ are interpreted in a manner similar to the more conventional Flinn plots. Parameter T describes the shape of the AMS ellipsoid. It can vary between the values +1 and -1, with the former denoting perfectly oblate AMS ellipsoids and the latter perfectly prolate ones. The value P records the degree of anisotropy of the ellipsoid. An example of a P vs. T plot is shown in Fig. 7. Samples shown on this diagram are weakly anisotropic, clustering around the value of P = 1.1. The majority of samples have weakly to moderately oblate (above the horizontal axis) or prolate (below the horizontal axis)

AMS ellipsoid shapes, with roughly equal numbers falling into each field.

Maps showing distributions of T were used to support structural interpretations. Although the shape of the AMS ellipsoid is not equivalent to the shape of the strain ellipsoid, this parameter does provides a qualitative estimate of the nature and consistency of the fabric. Changes in it's value can reflect either changes in pluton mineralogy, or the nature of the mineral fabric.

Table 2. Structural conventions.

Primary sedimentary structures	S_0	-Bedding
D_1	S_1	-Foliation
D_2	F_2 L_2 S_2	-second generation folds -second generation stretching lineation -the main planar composite fabric in the area
D_3	F_3 S_3 L_3	-third generation fold -third generation foliation -third generation lineation
D_4	S_{4-s} S_{4-c} L_{4-str}	-s-foliation associated with a fourth generation shear zone -c-foliation associated with a fourth generation shear zone -stretching lineation observed in fourth generation shear zones
Granite Fabrics.	S_{bi} L_{qtz}	-biotite foliation observed in the RBG -quartz stretching lineation observed in the RBG.

Table 3. Examples of magnetic susceptibility and AMS data for common rock forming diamagnetic and paramagnetic minerals. From Borradaile, 1988.

A) Susceptibility data for common paramagnetic metamorphic minerals.

Mineral	Minimum Anisotropies			
	K_1	K_2	K_3	K_m (SI units/vol. $X10^{-6}$)
Actinolite	1.076	0.982	0.947	3560
Actinolite	1.083	1.027	0.899	6500
Hornblende	1.347	0.917	0.809	8920
Crocidolite	1.052	0.992	0.958	333
Glaucophane	1.094	1.006	0.908	787
Chlorite	1.093	1.060	0.864	358
Chlorite	1.287	1.058	0.734	70
Chlorite	1.128	1.023	0.866	1550
Chlorite	1.063	1.020	0.921	370
Biotite	1.114	1.106	0.812	1230
Biotite	1.098	1.095	0.832	1180
Biotite	1.107	1.096	0.824	998
Biotite	1.108	1.107	0.814	1290
Phlogopite	1.098	1.091	0.838	1180
Muscovite	1.159	1.052	0.820	165

B) Weakly susceptible, diamagnetic rock-forming minerals.

Mineral	**K_m (SI units/vol. $X10^{-6}$)**	**Standard Deviation**	**Anisotropy Ratio K_1/K_{23}**
Plagioclase	-2.78	0.34	
Quartz	-13.4	0.80	1.01
Calcite	-13.8	0.34	1.11
Talc	+5.4	0.82	

Table 4. Examples of magnetic susceptibility and AMS data for common ferrimagnetic accessory minerals. From Borradaile, 1988.

Mineral	K_1	K_2	K_3	K_m (SI/vol.)
Magnetite (crushed metamorphic)	1.063	0.989	0.951	5.8
Magnetite (detrital)	1.108	0.964	0.936	

Mineral	K_1 / K_3	K_1 (SI/vol.)
Hematite	> 100 : 1	0.001
Pyrrhotite	≅ 10000 : 1	1.0
Ilmenite-hematite	15 : 1	0.4

Mineral	K_m (SI/vol.)
Ilmenite	1.8
Titanomagnetite	0.01
Siderite	0.005
Limonite	0.003
Pyrite	0.001

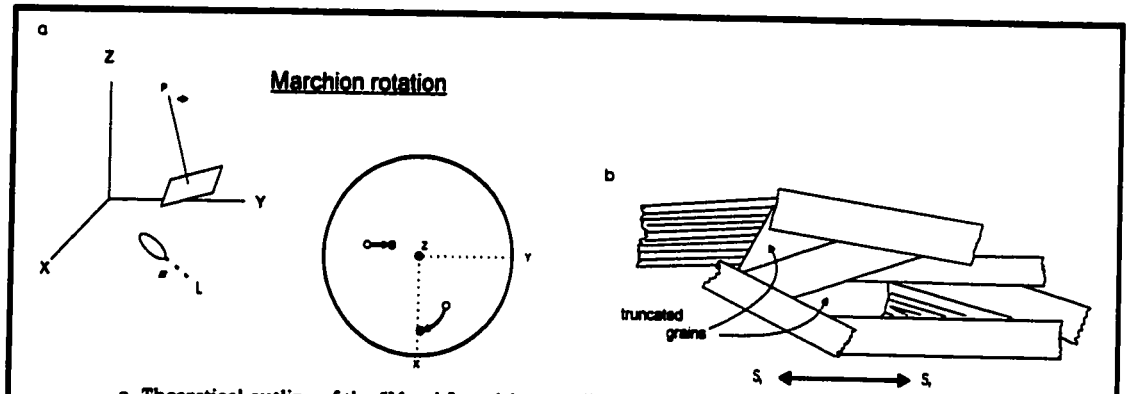

a. Theoretical outline of the "March" model as applied to the rotation and preferred orientation of the phyllosilicate grains. For strain axes $x \geq y \geq z$ the rotation of a pole *p* of a platelet is shown schematically as is the rotation of the long axis of a rod-like element. Such elements are considered to be dispersed and perfectly rigid.

b. Schematic cross-section of a typical natural preferred orientation of phyllosilicate grains defining a schistosity S_1. Grains with less favoured orientation are truncated and their volumetric contributions to the magnetic fabric may be reduced. Usually. the pattern of preferred orientation can only be explained by the March model to a limited degree.

Fig. 4. Diagram illustrating the rotation of the phillosilicate grains following the strain response model of March (1932). Figure and descriptive text from Borradaile (1988).

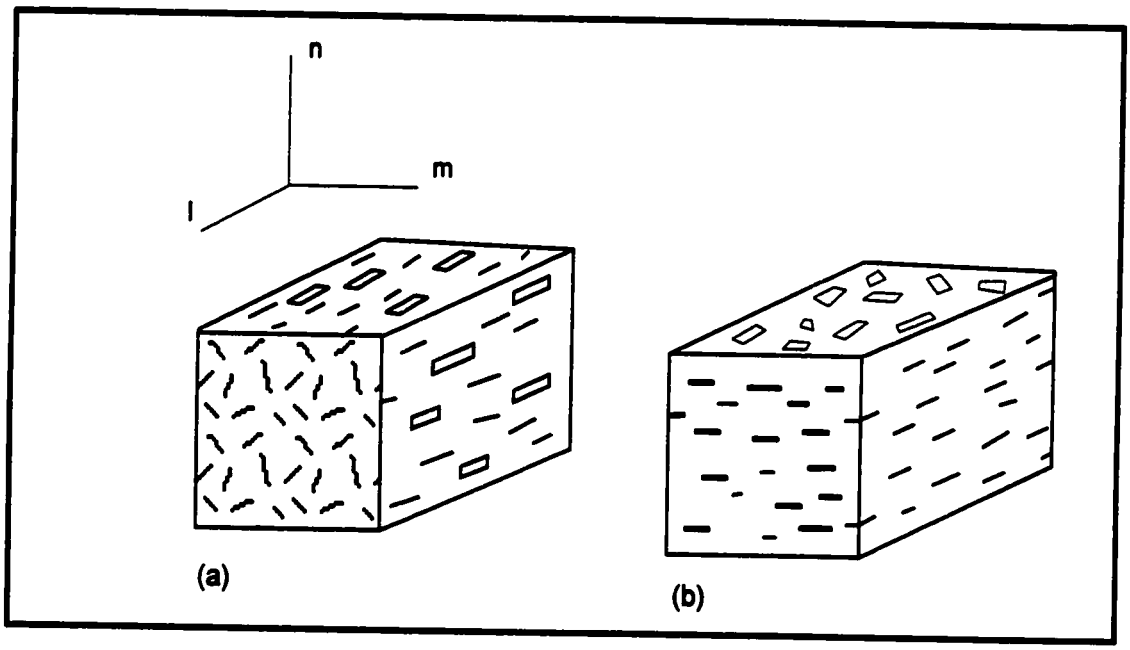

Fig. 5. Schematic block diagrams illustrating prolate (a) and oblate (b) fabrics produced by preferential orientation of phyllosilicate material grains. From Borradaile (1988).

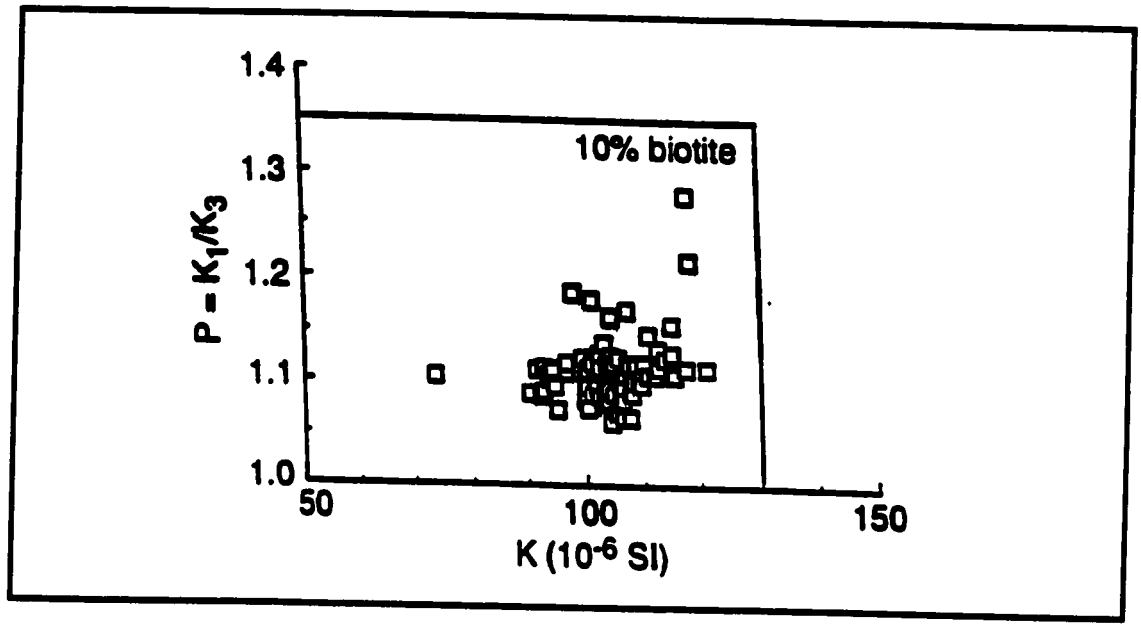

Fig. 6. Km vs. P plot from Benn et. al. (1993), which was used as supporting evidence that the AMS of samples collected from the pluton in the Rose Blanche-Harbour Le Cou sector was due entirely to biotite.

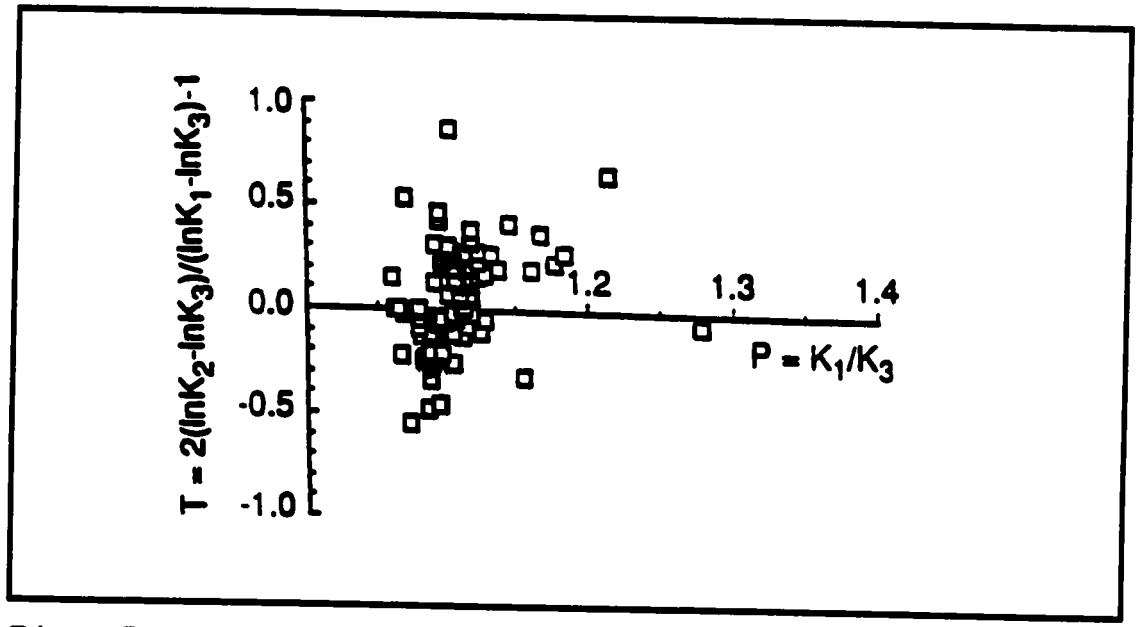

Fig. 7. T vs. P plot from Benn et. al. (1993) showing the variation of the ellipsoid shapes and the degree of anisotropy of samples collected from the pluton in the Rose Rlanche-Harbour Le Cou sector.

CHAPTER 4 - FIELD RELATIONS, STRUCTURE, AND MICROSTRUCTURE OF THE HARBOUR LE COU GROUP AND THE ROSE BLANCHE GRANITES.

4.1. Introduction.

This chapter presents the structural and microstructural data collected in the course of the field work and subsequent laboratory studies. It is organized into six sections. Lithologies and field relations of the HLCG wall rocks and the RBG suite are described in section 4.2. Structural history and style of the host HLCG metasediments are presented in section 4.3. Structures, fabrics and intrusive relationships of the RBG suite are described in section 4.4. Microstructures observed in the HLCG and the RBG are discussed in section 4.5. Section 4.6 is a synthesis of the findings.

4.2. Lithologies and Field Relations.

4.2.1. Lithologies and field relations of the HLCG wall rocks.

The HLCG wall rocks are a rather monotonous mixture of semi-pelitic to psammitic rocks generally lacking a clearly definable marker stratigraphy. True pelites or psammites were found to be very rare. The majority of the observed lithologies could be described as semi-pelites. Psammites occur in discontinuous patches or lenses embedded in the main body of semi-pelitic rocks.

Pelites and semi-pelites, typically medium-grained, rusty-coloured Gt-Mu-Bi-Amph-Gt-Sil-Ksp-Pl-Qtz schists with minor accessory amounts of iron-bearing sulfides and oxides, are the dominant lithologies in the area. The semi-pelites are very homogenous, ranging in composition from almost true pelites to relatively mica-poor semi-pelites. Sillimanite was observed in some pelitic outcrops and hand samples, although most HLCG semi-pelites in the study area were not observed to contain aluminosilicates. In most cases

sillimanite grains occur as clusters of fine grained needles visible on and between S_2 biotite-muscovite foliation planes (possibly the fibrolite variety). In several rare instances sillimanite pseudomorphs after kyanite were observed. In most cases the orientation of the sillimanite needles is parallel to L_2.

Amphibole and garnet were observed at many locations. Garnets frequently occur in lens-like concentrations. Where S_0 was clearly evident, occurrence of this mineral was restricted to the more pelitic beds. Garnets are typically relatively fine-grained (0.5 - 2.0 mm). Large garnet porphyroblasts are very rare. Amphibole was observed to occur as fairly small (2.0 - 5.0 mm long) black crystals growing in the S_2 foliation planes. As with sillimanite, the orientation of amphibole needles is nearly always parallel to L_2. In some rare instances amphiboles oriented parallel to minor F_3 hinges were observed. In pelitic beds many of the mica grains are sigmoidal or "fish like" in shape, suggesting that their grain shape has been modified by shearing after their growth.

Psammite, a quartz-feldspar rock with minor amounts of muscovite and biotite, was observed to be relatively free from rusty staining. Psammite layers usually occur as isolated pods, lenses or rootless small scale folds within the dominant semi-pelitic schist lithology, rather than well-defined strata. In a few locations, where sequences of beds were observed, psammites occur as thin quartzo-feldspathic beds alternating with pelitic layers (see Plates 1 and 2). True psammites are fairly rare. Most examples of this lithology contain an appreciable component of muscovite and biotite (10-20%) and are more accurately described as semi-pelites. Typical field appearance of these rocks can be seen in Plate 1.

When viewed under the microscope feldspar and quartz grains in psammite are equant and rounded in habit. The rocks are usually equigranular, with the average grain size being approximately equal to 0.5 mm. The grain boundaries between the quartz and feldspar grains are relatively straight to slightly curved. Quartz grains show undulose extinction and some tilt wall development. Samples collected near large RBG intrusions usually have coarser (1.0-2.0 mm) quartz grains with highly curved or lobate grain boundaries.

4.2.2. Lithologies and field relations of the RBG suite.

In the field the RBG suite was observed to consist of leucocratic, homogeneous, medium grained, weakly to moderately deformed granite and granodiorite sills and dykes. Detailed mapping revealed two mineralogically distinct but clearly genetically related phases of the RBG. The more common Rose Blanche (RBGrb) phase crops out near Burnt Islands, Rose Blanche, Harbour Le Cou, and further inland from Lobster Cove. This phase has a distinctly white appearance in the field and is characterized by the presence of accessory amounts of small pink garnet and muscovite and an almost total lack of mafic minerals such as hornblende and biotite. The Barasway phase (RBGba) crops out near the coast in the Barasway sector (see Maps 1 and 2). Larger content of mafic minerals gives this phase a light-gray appearance different from the RBGrb. The average modal mineralogy of each phase is given in Table 5.

Contacts between the two phases are exposed near the coast in the Barasway sector (see Maps 1 and 2), where the typically grayish, relatively fine-grained RBGba gradually

changes to the more leucocratic, and coarser grained RBGrb. The RBGba phase appears to be a compositionally distinct lens within the main RBGrb phase comprising most of the sheet. This is not entirely clear, however, due to the diffuse and patchy nature of the contacts. A trail of HLCG xenoliths crops out in a pattern which roughly coincides with the shape of the RBGba lens (see Maps 1 and 2). This could indicate that the differences in mineralogy between the two phases could be due to contamination of the RBGrb phase with absorbed HLCG wall-rock material.

Pegmatitic garnet and muscovite-bearing RBG dykes were frequently observed to cross-cut the fabrics and contacts in many RBGba and RBGrb exposures. Pegmatites also frequently occur at and near the contacts of several of the large-scale sheets. In the Burnt Islands sector, pegmatites occur all along the structurally lower contact of the synform (see Maps 1 and 2). The percentage and size of the pegmatitic grains increases on approach to the contact. The pegmatite layer is richer in potassium feldspar and plagioclase grains than the granite proper. These relations seem to indicate that the pegmatite was formed by accumulation of early-crystallized grains on the floor of the sheet.

Similar field relations are seen in the Barasway sector where large amounts of pegmatite occur in the roof zone of a medium scale sheet folded into an antiform (see Maps 1 and 2). In this instance the contact between the pegmatite and the granite proper is not gradational but rather sharp. The proportions of quartz and feldspars are roughly the same as in the granite proper. This pegmatitic layer likely formed in a fluid-saturated, near-roof zone of the sheet.

Migmatites were found to be ubiquitous near large RBG sheets located to the north and west of Lobster Cove. The percentage of leucosome in relation to semi-pelitic or psammitic protolith varies between 10 to 90 percent. In two instances, the relative percentage of leucosome was observed to increase on approach to large scale RBG sheets (Maps 1 and 2), although this was not always the case. In all cases as the percentage of the leucosome in the outcrop increases, the host schists become more mafic in composition. This can be seen in Plates 16A, 13B, where the pelitic layers are dark in appearance, depleted in quartz, feldspars and muscovite, and relatively rich in biotite, amphibole and

garnet. Structural history and origin of migmatites are treated in more detail in section 4.4.4.

4.3. Structural history of the HLCG wall rocks.

4.3.1. Deformational episodes, structures and fabrics of the wall rocks.

D_1

The evidence for D_1 deformation was indirectly inferred from the presence of a bedding sub-parallel mica foliation (S_1) in the hinges of F_2 folds (see Plate 1 B). It is not possible to describe the D_1 deformation other than to say that it probably represents a near bedding parallel fabric which developed as a result of burial or regional thickening of the sedimentary sequence, characteristic of the first fabrics to be developed during the orogenic cycle. This observation is consistent with the regional observations of Burgess et al. (1995).

D_2

F_2 folds were most frequently found at, or near to, clearly demonstrable F_3 hinges, where they were observed to be recumbent, and verging to the northwest. Plate 2 shows the structural style associated with this deformational episode.

F_2 folds, when viewed down plunge at F_3 hinges have an S-symmetry. The limbs are attenuated, and the hinge zones are thickened. F_2 folds contain a strong axial planar foliation S_2 (Plate 1 B), which overprints S_0 and the much weaker S_1, defined by preferential alignment of biotite and muscovite. It was possible to observe these relationships only at F_3 hinges. On the limbs of large-scale F_3 folds evidence of S_0 or D_1 fabrics has been obliterated by tightening of S_2 foliation in response to strain imparted during D_3.

The dominant fabric (S_2) in the area is a very well developed, composite foliation defined by the preferential alignment of the micas, cm-scale psammite lenses, and small quartz veins with sheared off limbs. This fabric is folded by F_3, and is invariably axial planar to F_2 folds. Typical field appearance of this fabric can be seen in Plate 1 B (in psammite), Plate 5 B (in pelite), and Plates 9 and 7 B (in migmatite).

A well developed stretching lineation L_2 was observed to be associated with S_2 (Plate 5 B). Defined primarily by the elongate aggregates of quartz and feldspar, this lineation is the strongest linear fabric in the field area. Rarely, a

weak mineral lineation defined by amphibole and/or sillimanite was observed to be parallel to L_2.

Lower-hemisphere, equal-area stereonet projections of D_2 fabrics are shown in Fig. 8 A, B, and C. Poles to S_2 are concentrated in the SE quadrant, with a peak at a trend/plunge of 157/55. The stretching lineations L_2 appear to be distributed along a great circle (Fig. 8 B), with a characteristic concentration at 231/10 and 45/15. The distribution of L_2 hinges also shows scattering along a great circle, which is very similar to the scattering of the stretching lineation. L_2 and F_2 were frequently observed to be parallel. This is clearly evident at many locations in the Barasway sector (see Map 2).

D_3

D_3 was observed to be characterized by upright to steeply inclined periclinal folds. A weak axial planar foliation defined by preferential alignment of biotite was observed to be associated with some F_3 folds, but this fabric was relatively rare and much weaker than the main S_2 fabric. The style of F_3 folds is very well exemplified by the many RBG dykes and sills folded during this episode (Fig. 10). The

overturned limbs of the steeply inclined D_3 folds are usually, but not always, thinned.

On an equal area stereonet F_3 axes define three concentrations at 358/40, 31/36, 278/36 (Fig. 8 D). This supports field observations and exemplifies the non-cylindrical, doubly-plunging nature of D_3. Poles to S_2 foliation, which have been rotated by nearly isoclinal F_3 folds into close parallelism with the S_3 axial-planar foliation, are concentrated at 130/6 - testifying to the fact that F_3 are generally nearly upright and verge to the southeast.

L_2 are almost always nearly horizontal, with plunges rarely exceeding 10-15 degrees, and are concentrated around a NE-SW axis. F_3 hinges commonly plunge at 30-40 degrees, and trends are most commonly due North and West. This is an important observation to note, as it will be discussed further in the context of interpreting AMS fabrics presented in Chapter 5.

D_4

This phase of deformation manifests itself in late strike-slip shear zones, which cross-cut D_3 structures. These

usually show well developed, proto-mylonitic S-C fabrics, and subhorizontal stretching lineations (Fig. 8 E). Reliable field observations of the shear sense could be made only on shear zones cutting through the RBG, all of which were dextral. Strike-slip displacement along most of the shear zones appears to have been relatively minor as the trends of large-scale D_3 structures do not appear to be disrupted or offset (see Maps 1 and 2), although the lack of clearly definable marker stratigraphy in the wall rocks precludes accurate estimations. Infrequently, a weakly developed spaced cleavage was observed in the HLCG rocks in the vicinity of D_4 shear zones.

4.3.2. Synthesis of the deformation history of the wall rocks.

Field observations, maps and stereonet analysis can be used to construct a general model of deformation, fabrics and structural style observed in the HLCG wall rocks. The relative importance and structural style associated with each episode are summarized below.

D_1 - this episode of deformation is very poorly constrained because nearly all of the associated structures have either been obliterated by the intense D_2 and D_3 deformation, or never formed. Presence of a weakly-developed bedding sub-parallel foliation suggests that this episode represents early regional metamorphism in response to bureal, or tectonic thickening of the sedimentary sequence.

D_2 - is characterized by development of asymmetric, non-cylindrical, recumbent folds with a strong associated axial-planar foliation and a well-developed hinge-subparallel stretching lineation. The structural style and symmetry of folds associated with D_2 indicates that the structures were produced by non-coaxial westerly directed reverse shearing, consistent with observation made by workers studying regional geology (Burgess et al, 1995).

D_3 - is characterized by non-cylindrical, steeply-inclined, southeast-verging folds and weekly-developed penetrative fabrics which may have formed during an overall transpressional event.

D_4 - is characterized by the development of late dextral strike-slip shear zones and an associated spaced cleavage. Structures produced by this episode are localized and displacements across them are relatively minor. Many of the shear zones are parallel to the limbs and axial planes of F_3 folds - an indication that D_4 was either controlled by D_3 fabrics or is an evolutionary continuation of the latter.

A schematic block diagram showing the geometry and relative orientations of F_2 and F_3 is shown in Figure 11.

4.4 Structural History of the RBG.

4.4.1 Geometry and Fabrics of the Intrusions.

Maps 1 and 2 show the outcrop pattern of the suite in the field area, as well as detailed views of the of the contacts and foliation and lineation patterns observed in the Burnt Islands and the Barasway sectors. The majority of the RBG intrusions were observed to be sheet-like in geometry, and folded by the nearly upright, southeast-verging F_3 folds. Viewed on a map scale (see Map 1) granite bodies are elongate parallel to the trend of large-scale F_3 hinges. Some of the sheets have a fairly simple folded geometry with a thickened and an attenuated limb, with the latter, in some cases, being used by a late shear zone (Map 1, 2, the Burnt Islands intrusion). Other bodies, such as the ones mapped in the Barasway sector show a more complex folding pattern.

Map 2 (the Barasway sector) shows an F_3 dome with several parasitic folds clearly defined by an RBG sheet (northeast corner of the sector, inland). The largest RBG exposure immediately near the coast has a rather complex pattern of

contacts (southwest corner of the sector immediately along the coast). The overall shape of the body is roughly elliptical, with the major axis of the ellipse trending parallel to a large scale F_3 antiform. Within the body two elongate exposures of HLCG semi-pelite were carefully mapped out. These exposures were found to contain fabrics clearly consistent with those observed in the surrounding country rocks. In particular, numerous small-scale symmetrical F_3 folds were observed. The foliations and lineations in the granite wrap around these exposures (see Map 1). The exposures are interpreted as outcropings of hinge zones of an F_3 synform-antiform pare which folded this pluton, as opposed to country rock xenoliths. Along strike, and to the southwest, of the exposures, the hinges can be clearly observed in the HLCG pelites (Plate 5 A). A structural crossection of this intrusion is shown in Fig. 12 A (see also Maps 1 and 2, section A-B). The section reveals that this body is a Christmas-tree laccolith which has been folded by tight, southeast-verging F_3 folds. A structural cross section through another granite body cropping out north of Harbour Le Cou (section A'-B' on Maps 1 and 2, Fig. 12 B) shows very similar geometry.

Particular attention was paid to the determination of internal foliation and lineation patterns in the RBG intrusions (see Maps 1 and 2). This was not a particularly easy task (especially in the dominant RBGrb phase), as these granites are leucocratic and lack the necessary proportions of elongate or platy minerals necessary for the development of strong fabrics at moderate strains. Sections below deal entirely with "conventional" structural data acquired in the field, or in the laboratory, from cores and hand specimens. AMS data are treated separately in Chapter 5.

Maps 1 and 2 show the patterns of foliations and lineations. The structure mapped out in the Burnt Islands sector is a relatively simple southeast-verging synform. Geometry of the granite contacts defines a folded body with a thickened and an attenuated limb. The attenuated northwestern limb contains a strong fabric with an ambiguous sense of shear and appears to be involved in a late shear. The rest of the granite body contains a fairly weak foliation defined by preferential alignment of biotite (S_{bi}) and flattened quartz grains. The granite body belongs to the RBGrb phase and is very leucocratic and garnet-bearing. Lineation data could not be obtained in the field and were measured from the AMS

cores as described in Chapter 3. The trace of the main foliation S_2 closes around the hinge zone. The trace of the biotite foliation in the granite (S_{bi}) parallels both the contacts and the trace of S_2. Neither S_{bi}, nor S_2 define a trend axial planar to the synform.

The lineations - L_2 and L_{qtz} generally show a trend very close to the strike of the foliation (Map 2). Near the hinge of the synform both L_2 and S_{bi} are oriented at a fairly high angle to the regional trend. Near the limbs L_2 and L_{qtz} are parallel to the regional structural NE-SW trend. These observations suggest that both the HLCG and RBG fabrics have been folded by F_3. The similarity of the trends of the RBG fabrics to those in the HLCG suggests that the fabric in the granite is D_2 in origin (also supported by microstructural evidence see section on microstructure below).

Several folded granite sheets are exposed in the Barasway sector. The pattern of folding is more complex than in the Burnt Islands sector, as evidenced by a dome structure in the northeast corner of the sector. As in the previous example, the strike of S_2 and the trend of L_2 are oriented

at high angles to the regional structural trends and close in the immediate proximity to the granite contact closures.

Stereonet analysis of S_{bi} and L_{qtz} reveals their similarity to S_2 and L_2. Distributions of S_2 and S_{bi} are remarkably similar (Fig. 8). So are the distributions of L_2 and L_{qtz}. Stereonet distributions of RBG fabric data support field observations, and indicate that fabrics in the granite are D_2 in origin, and have been folded by F_3 folds just as the fabrics of the HLCG wall rocks have been.

4.4.2. Contacts, Folded Dykes, and Xenoliths.

Granite contacts were observed to be straight and largely concordant with S_2 (see Plate 6 A). However, numerous examples of dykes and sills cutting across the S_2 trends and then swinging back into concordance were observed. This is clearly shown in Plate 6 B, and Plate 7 B. RBG contacts show no evidence of chilling, in fact the granite was very frequently observed to gradually become coarser and, in places, even pegmatitic approaching the contact (Plates 6 A, 8 B).

The entire field area is intruded by a multitude of small-scale RBG dykes and sills. Many of these have folded geometries, which exemplify map-scale bodies. Virtually all of the dykes show effects of two deformational episodes and both concordant and discordant intrusive relationships with respect to the D_2 fabrics. Figure 9 shows an interpretation of one such example. The contacts of the dyke clearly cut across the main foliation (S_2) in the HLCG semi-pelite. Offshoots from the dyke intrude concordantly into the main foliation, and along with S_2 are folded by small and relatively open (in this case) F_3 folds. The pen outlined in Fig. 9 is parallel to a weak but evident biotite foliation in the dyke, which is parallel to S_2. Many smaller dykes show a "hook" interference pattern produced by the folding of a small RBG dyke by D_2, and subsequent refolding By D_3. Examples of refolded RBG dykes are shown in Fig. 10, and in Plate 8 B.

Xenoliths of HLCG semi-pelites were observed to frequently occur near the contacts of the larger RBG intrusions. The xenoliths were commonly elongate in shape and oriented parallel to both the fabric in the granite and the fabric in the nearby country rocks. Most did not show any evidence of

mechanical rotation related to forceful magma injection and flow. Although some were clearly rotated after their separation from the wall rock, the vast majority were observed to be oriented concordantly with the fabric in the nearby wall rocks, as shown in Plate 6 A. Here sheets of HLCG semi-pelite are embedded in the pegmatitic, near-contact zone of the Burnt Islands intrusion. The shape of these xenoliths is clearly controlled by S_2 in HLCG, and their orientation is parallel to both the granite contact and S_2. The xenoliths contain a well-developed S_2 foliation.

Two more characteristic examples of xenoliths in the RBG are shown in Plate 8. In Plate 8 A, a tabular pelitic xenolith (Rose Blanche - Harbour Le Cou sector) contains the characteristic S_2 foliation. Both the foliation in the xenolith, and the xenolith-RBG contact are folded by small open F_3 folds. Plate 8 B shows an even more characteristic relationship. This photo was taken at the contact between the large-scale RBGba granodiorite and the HLCG pelite (the Barasway sector, near the coast, see Map 1). The main contact of the sheet is pegmatitic and parallel to S_2 in the wall rocks. Small dykes coming off the larger body are folded by two events. A small F_2 closure is visible to the

right of the tip of the hammer handle. The same dyke shows characteristic D_3 folds. To the left of the hammer handle, an angular xenolith is included in another offshoot from the main sheet. The xenolith contains S_2 but the F_3 folds evident in the wall rocks are very poorly developed. This is viewed as evidence that the granite surrounding the xenolith mechanically shielded the xenolith from D_3.

4.4.3. Migmatites.

Migmatitic rocks were observed throughout the field area. They were found to be particularly common further inland, to the north of Lobster Cove and Gull Lake Pond. In some cases migmatites were observed to grade into RBG sheets. This was definitely the case with the sheet to the west of Harbour Le Cou (Maps 1 and 2, Rose Blanche-Harbour Le Cou sector), and with several smaller-scale sheets north of Gull Lake Pond. Near the Harbour Le Cou intrusion the lithology was observed to gradually change from semi-pelite to a mixture of semi-pelite and leucosome, and finally into granite proper. RBG sheets cropping out elsewhere along the coast did not show such gradational contacts.

Typical exposures of migmatite are shown in Plate 9. Both of these photographs were taken north of Gull Lake Pond, where migmatitic rocks were ubiquitous. Migmatite contains remnants of the S_2 foliation and recumbent F_2 folds, which are in turn folded by relatively open, upright F_3 folds. Plate 9 A shows a partially melted, boudinaged psammite bed. The boundaries between the granitic leucosome and the psammite boudin are gradational (except for the boundary closest to the bottom of the photo where it is fairly sharp. Well developed asymmetrical pressure shadows filled with RBG leucosome, c′ shears, and highly asymmetrical F_2 indicate a tops to the northwest sense of shear in this vertical outcrop face. Pelitic rocks visible in the photo are very mafic in appearance and contain a multitude of leucosome bands. In areas of migmatization the restite is always much more mafic in composition than un-migmatized HLCG rocks. Observations such as these suggest in-situ generation of the RBG magma by partial melting of both pelitic and psammitic lithologies of the HLCG. This view is supported by regional metamorphic and geochemical ivestigations (Burgess et al., 1995; Whalen et al., 1995).

4.5 Microstructures of the RBG and the wall rocks.

4.5.1. Microstructures of the HLCG wall rocks.

Microstructures observed in the HLCG wall rocks record a history of deformation and metamorphism consistent with field observations. Evidence for the existence of two biotite foliations is shown in Plate 10 A. Concentrations of small garnets and relatively coarse biotite grains define the remnants of pelitic beds (S_0). The first generation of coarse biotite and muscovite (S_1) is folded and kinked around an F_2 hinge. The limbs of the fold (S_1) are oblique to the second generation of smaller biotite and muscovite grains which define an axial planar foliation (S_2).

A typical porphyroblast-matrix relationship is shown in Plate 10 B. The main S_2 foliation defined by muscovite, biotite and flattened quartz grains wraps around a euhedral garnet porphyroblast. Inclusion trails of quartz, biotite and muscovite grains, oriented at a high angle to the matrix foliation, have been preserved in the center of the porphyroblast. Quartz and biotite are evident in the pressure shadows. Notably, quartz inclusions appear to be

relatively strain free (no undulose extinction) compared to the nearby matrix grains. The included grains are smaller in size than the ones in the matrix. The rim of the garnet is inclusion free. These microstructures are indicative of continued garnet, quartz, biotite and muscovite growth during D_1 and D_2.

Kyanite and sillimanite are the aluminosilicates observed in the more pelitic units of the HLCG. Kyanite grains were observed to contain quartz inclusion trails. Sillimanite occurs as either pseudomorphs after kyanite or anastomosing aggregates of fine grained needle-like crystals oriented parallel to S_2 (fibrolite, Plate 11). Some sillimanite grains are sometimes kinked around small scale F_3 folds.

4.5.2 Microstructures of the RBG.

Both phases of the RBG show remarkably similar fabrics, grain sizes, microstructures and histories of crystallization. In fact, as mentioned above, the only observed difference between the two is that RBGba is slightly more mafic and contains accessory amounts of hornblende and opaques instead of garnet. The average modal mineralogy of the two phases is given in Table 5. In the discussions below the most characteristic microstructures of the RBG suite as a whole are described.

The RBG is equigranular with grain size ranging from 1 to 3 mm. The grain boundaries between the major constituent phases (quartz, microcline, plagioclase, muscovite, and biotite) are generally straight or slightly curved. Grain boundaries between plagioclase and microcline show extensive myrmekite development. Plagioclase grains are subhedral to euhedral whereas quartz and microcline grains are anhedral.

In the field, and in thin section, muscovite and biotite define a weak to moderately well developed foliation.

Microscopic observations reveal that the micas within the larger granite sheets are generally undeformed. Muscovite and biotite grains are euhedral and lack any optically visible signs of deformation such as undulose extinction, kinking, or recrystallization. A small percentage of the mica grains impinging on plagioclase crystals were observed to be slightly bent or kinked. Chlorite alteration along cleavages was observed on some biotite grains.

Euhedral crystals of plagioclase (An_{68}-An_{70}) appear to have been the first phase to crystallize as they are frequently observed as inclusions in quartz and microcline. They display strong optical zoning and a high degree of sericitization. Many highly altered euhedral plagioclase cores were observed to be rimmed by zoned plagioclase of different composition (which was not estimated optically due to lack of twinning and fine grain size). The rims are unaltered (Plate 13 A), indicating that alteration of early plagioclase crystals to sericite likely occurred in the magmatic state. Most plagioclase crystals show extensive replacement by muscovite along cleavages. Matrix muscovite appears to be a euhedral magmatic phase which grew in equilibrium with the other minerals (i.e. not a replacement

mineral). It is likely that this alteration also occurred in the magmatic state and not as a solid state metamorphic overprint, although post-crystallization growth of a second generation of metamorphic muscovite cannot be ruled out.

Most plagioclase crystals show little evidence of crystal plastic deformation. Many of the grains are slightly fractured, and some show pull-apart microstructures (Plate 13 A). Quartz grains can be seen in the pull-aparts. In a few rare instances microstructures indicative of grain boundary migration were observed. Plate 13 B, shows evidence for possible grain boundary migration between two plagioclase grains. The grain boundary depicted in this figure shows a series of bulges. Subgrain boundaries appear to be developing at the neck of some of the bulges and the enclosed material is optically slightly misoriented with respect to the host grain. This type of microstructure may be indicative of a dynamic recrystallization process known as 'bulge nucleation' (Urai et al., 1986). Dynamic recrystallization through grain boundary migration in plagioclase is a high temperature process, generally thought to occur at temperatures greater than 550° C (Pryer, 1993). Growth of quartz grains in pull-apart microstructures is

indicative of low temerature strain. This does not necessarily contradict the occurrence of high-temperature microstructures because field relations indicate that the RBG have been subjected to at least two episodes of deformation, and consequently to sets of P-T-strain conditions. The fact that both high-temperature and low temperature microstructures can be observed supports the macroscopic structural field evidence.

Potassium feldspar observed in the RBG shows crosshatched twinning characteristic of microcline. Evidence for mechanical twinning was observed in many perthitic grains. Although some grains show slight undulose extinction, no evidence of dynamic or static recrystallization, or grain size reduction was observed. Fracturing was observed in some grains.

Another common petrological and microstructural feature observed in the RBG is the widespread occurrence of myrmekite. Two types of myrmekite were observed. Type 1 is represented by euhedral, myrmekitic plagioclase crystals included within larger anhedral microcline grains. The grain boundaries between plagioclase and microcline are straight

and show no optically discernible signs of reaction. This texture is probably igneous in origin, and may reflect either eutectic crystallization of plagioclase and quartz, or crystallization at large undercooling, which could be indicative of microquenching of a magma due to exolution of water (Hibbard, 1979).

Type 2 myrmekite appears to conform to the model of Simpson and Wintsch (1989). It is commonly located at high strain sites between adjacent plagioclase and microcline grains. Quartz blebs in the myrmekite are often in optical continuity with adjacent independent grains of quartz, when observed at a triple junction between quartz, microcline, and plagioclase. The grain boundaries between Type 2 myrmekitic plagioclase and microcline are embayed and irregular, commonly with the same optically continuous quartz blebs being included by both plagioclase and microcline. These observations support the potassium feldspar to plagioclase plus quartz alteration reaction proposed by Simpson and Wintsch (1989) and also described by Stel and Breedveld (1993).

Quartz represents the most abundant mineral phase of the RBG, and it appears to have accommodated almost all of the ductile deformation. Most quartz grains are slightly to moderately elongated and the volumetric proportion of dynamically recrystallized fine grains is small (about 5-10% of total matrix quartz, mostly found in areas of locally high strain between feldspar grains). This is consistent with field observations showing that the RBG is moderately to weakly deformed. Most quartz grains show fairly well developed tilt walls and subgrains. This suggests that recovery processes were dominant, which indicates relatively high temperatures. Formation of tilt walls requires dislocation climb, which is a high temperature process (Nicolas and Poirier, 1976, p. 137).

Quartz microstructures indicate that dynamic recrystallization was operating during deformation. Typical grain boundaries are serrated, lobate or bulged (Plates 15 A, 14 B), and dissection microstructures are common (see Plate 14 A). These features are usually associated with grain boundary migration (Urai et al., 1986). Plate 15 A is a close up view of the grain boundaries in a typical dissection microstructure. A weakly strained quartz grain

appears to be consuming a more highly strained grain. The grain boundaries appear to be migrating outward from their centers of curvature into the grain showing more evidence of deformation (greater degree of undulose extinction, more extensive subgrain development). This is indicative of dynamic recrystallization driven by volume forces (Urai et al., 1986) rather than post deformational annealing, which is characterized by grain boundaries migrating towards their centers of curvature under the influence of surface energy driving forces. Fine, recrystallized grains of quartz observed in local areas of high strain appear to have been formed by the bulge nucleation mechanism described above for feldspars.

4.5.3. Interpretation and Synthesis of the Microstructural data.

Microstructures recorded in the HLCG wall rocks record a history of metamorphic mineral growth which is very similar to the one described by workers studying regional metamorphism (Burgess et al., 1995, see Table 2):

1. D_1 - is characterized by growth of garnet, muscovite, biotite;

2. D_2 - continued growth of garnet, muscovite, biotite, quartz, potassium feldspar, kyanite and sillimanite;
3. D_3 - partial replacement of garnet and biotite by chlorite, sericitization of plagioclase grains, partial replacement of sillimanite by muscovite.

Estimation of temperature and pressure conditions from available experimental data using microstructural criteria is not straight forward. This is because P-T domains occupied by recrystallization mechanisms depend strongly on strain rate and presence or absence of structural water during deformation. Experiments of Neville et al. (1964) on quartzite showed that abundant plastic deformation of quartz could be achieved at 500° C and 5 Kb. The same authors concluded that in natural environments recrystallization of quartz could occur at temperatures as low as 500° C. Tullis et al. (1973) report observing grain boundary recrystallization in quartzite at temperatures higher than 650° C. at a geologically very high strain rate of 10^{-7}/sec. Pryer (1993) empirically correlated the transition from crystal plasticity to cataclasis in feldspars with the

change from lower amphibolite to upper greenshist in metamorphic grade (temperature between 450 and 500° C.).

Microstructural observations agree with the field evidence. They show that the fabric in the granite is dominated by solid-state microstructures. The solid state overprint must have formed at a temperature above the temperature necessary for the onset of grain boundary migration in quartz, but just below that necessary for the onset of pervasive crystal plasticity in plagioclase and microcline (some feldspar grains do show some evidence of grain boundary migration). These observations loosely bracket the temperature of solid-state fabric formation in the RBG at around 650° C and agree with thermo-barometric estimations of local peak metamorphic conditions made by Burgess et al. (1995) of 650-700° C.

4.6 Summary.

Evidence presented in this chapter shows that regional deformation imparted four distinct generations of structures into HLCG wall rocks. D_1 was responsible for the development of a bedding sub-parallel foliation in the HLCG psammites

and semi-pelites, and probably represents either regional burial, or thickening of the sedimentary sequence prior to full-scale continental collision. The bedding and the early S_1 foliation were overprinted and transposed by the development of recumbent F_2 folds and a strong axial planar fabric. A well-developed L_2 stretching lineation, trending NE-SW, suggests that D_2 structures formed in response to a highly non-coaxial phase of deformation likely associated with west-directed overthrusting. D_2 transposition of previous fabrics largely obliterated the previously existing stratigraphy, with psammite layers being folded into recumbent isoclines and locally sheared-off into lens-shaped bodies. D_3 deformation tightly folded the HLCG rocks into steeply-inclined, southeast-verging, periclinal folds. D_3 fabrics were found to be poorly developed in comparison to the D_2 fabrics. D_4 is a phase of local deformation characterized by the development of steep, mostly dextral shear zones with S-C fabrics and a sub-horizontal stretching lineation.

The RBG suite occurs as a multitude of sheets and dykes folded by F_3, and in some cases by both F_2 and F_3. The sheets contain a foliation defined by the preferential alignment of

the micas, and a lineation defined by slightly elongated quartz grains. These fabrics are dominated by solid-state microstructures and are commonly folded by F_3. Migmatites associated with some granite sheets appear to have been generated by partial melting of the HLCG lithologies in-situ, and are folded by both F_2 and F_3. Xenoliths observed in the granite contain D_2 fabrics and structures but lack those associated with D_3. Structural cross sections of intrusions in the Barasway and Rose Blanche-Harbour Le Cou sectors show that granite bodies which crop out there are, in fact, Christmas-tree laccoliths which have been folded by F_3. It is likely that many of the granite sheets were emplaced as sills formed during laccolith growth.

Structural and microstructural histories preserved in the HLCG wall rocks are identical to those described by workers studying regional geology of southwestern Newfoundland (Burgess et al., 1995, Dube et al., 1996, Lin et al., 1993, 1994). Intrusion of the RBG did not result in significant deflection of, or generation of additional fabrics in the wall rocks.

Table 5. Average modal mineralogy of the two RBG phases (visual estimations of 34 thin sections).

Phase	RBGzb	RBGba
Mineral	Mode	Mode
Qtz	45	35
Microcline	23	25
Plagioclase	20	30
Biotite	5	7
Muscovite	5	3
Garnet	Tr	-
Chlorites	Tr after biotite	Tr after biotite
Hornblende	-	Tr
Zircon	Tr	Tr
Apatite	Tr	Tr
Tourmaline	Tr	-
Opq	-	Tr

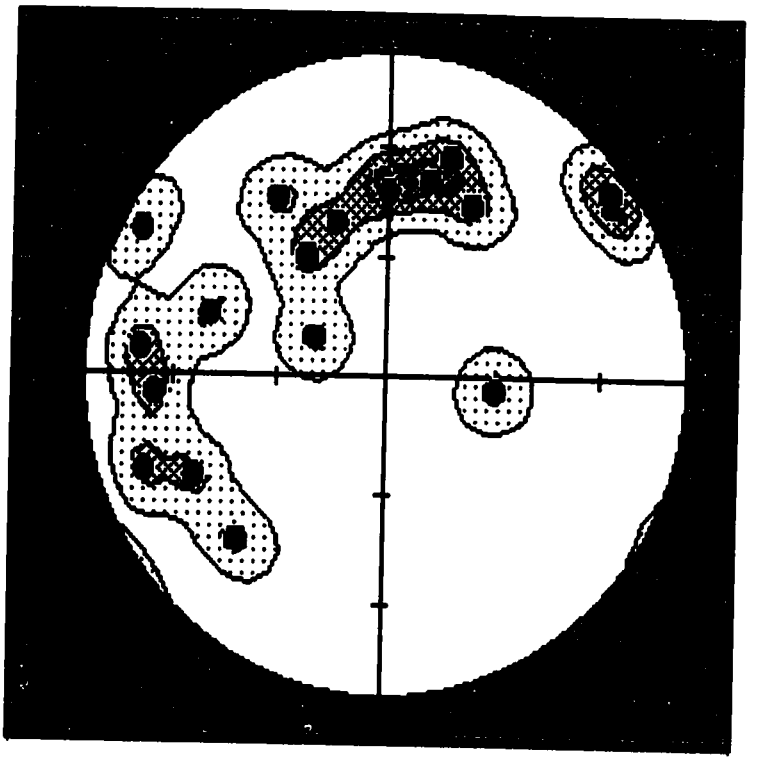

Fig. 8. Stereonets of the fabrics and structures ofserved in the HLCG wall rocks and the RBG.

A) Stereonet distribution of the F_2 hinges.

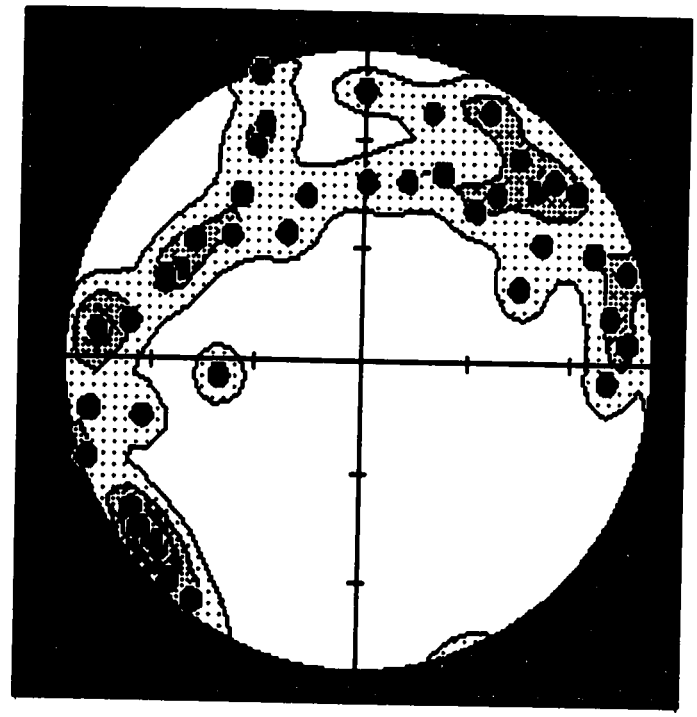

B) Stereonet distribution of L_2 lineations in the HLCG.

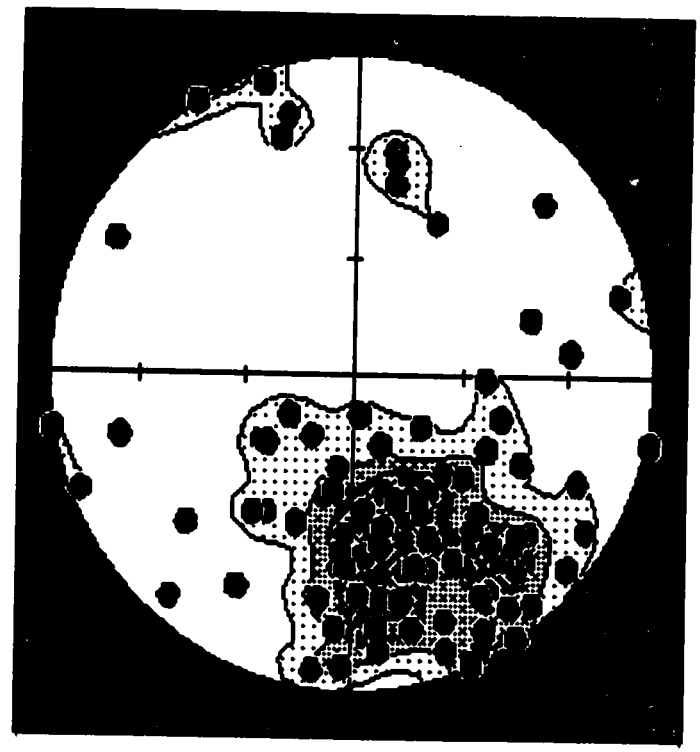

C) Stereonet distribution of poles to the S_2 foliation in the HLCG.

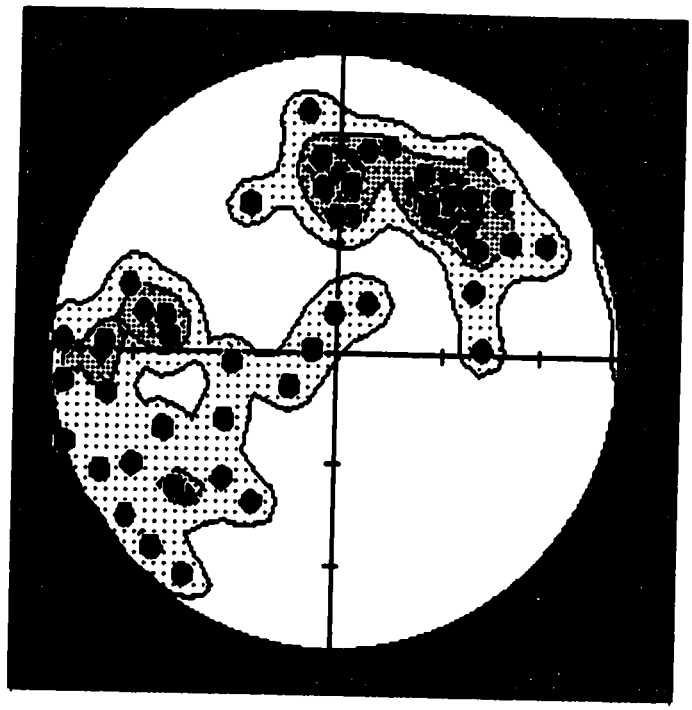

D) Stereonet distribution of the F_3 hinges in the HLCG.

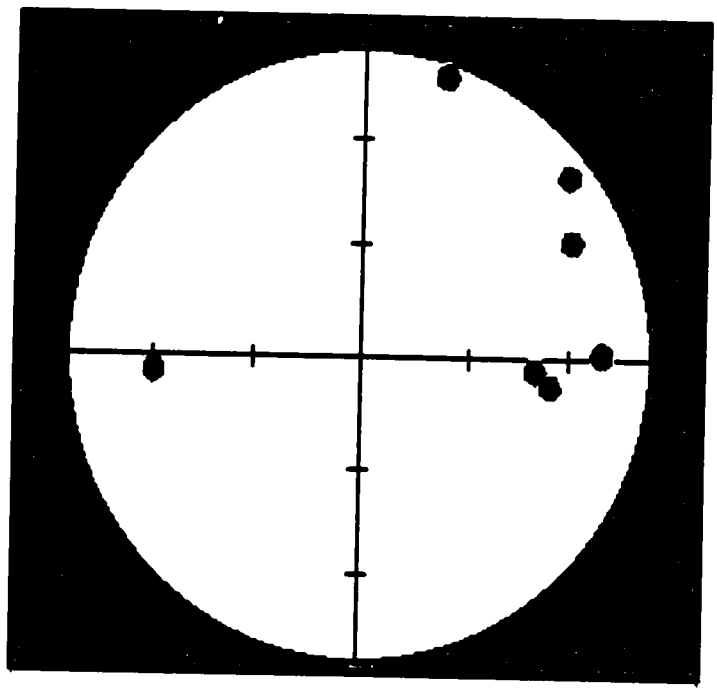

E) Stereonet distribution of $L_{4\text{-}str}$ lineations.

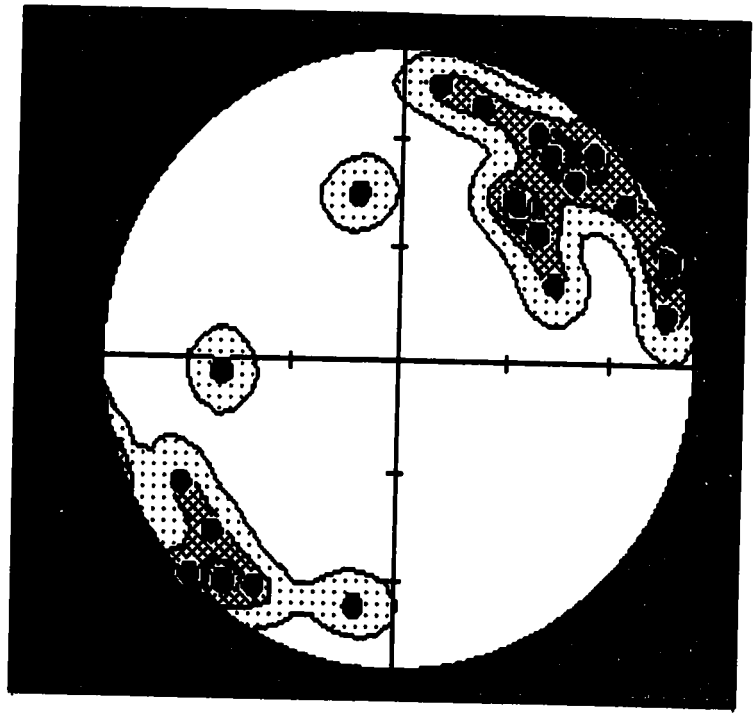

F) Stereonet distribution of quartz stretching lineations (L_{qtz}) in the RBG.

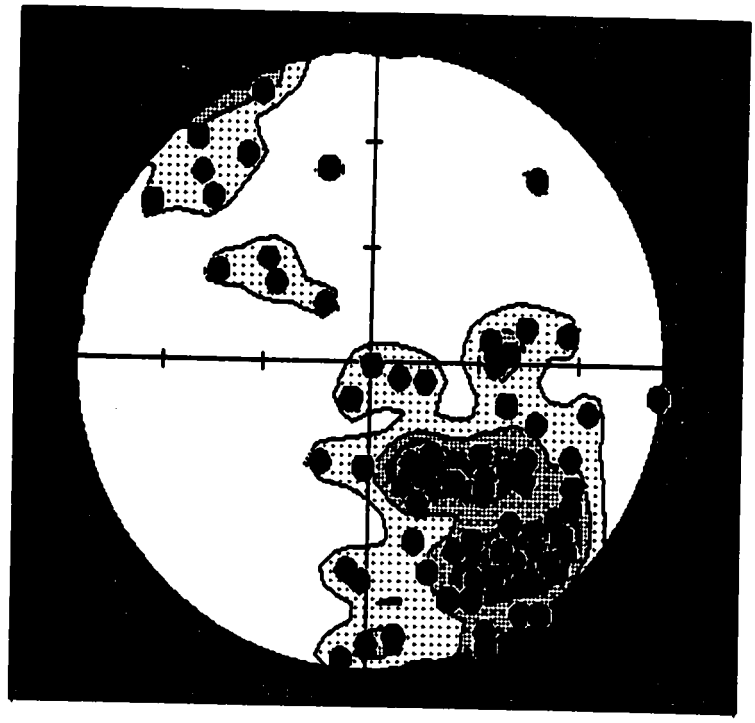

G) Stereonet distribution of poles to biotite foliation S_{bi} in the RBG.

Fig. 9. An example of a syn-D_2 RBG dyke - interpretation of the structures evident in Plate 6 B.

Fig. 10. Structural style of F_2 and F_3 as demonstrated by folded RBG dykes.

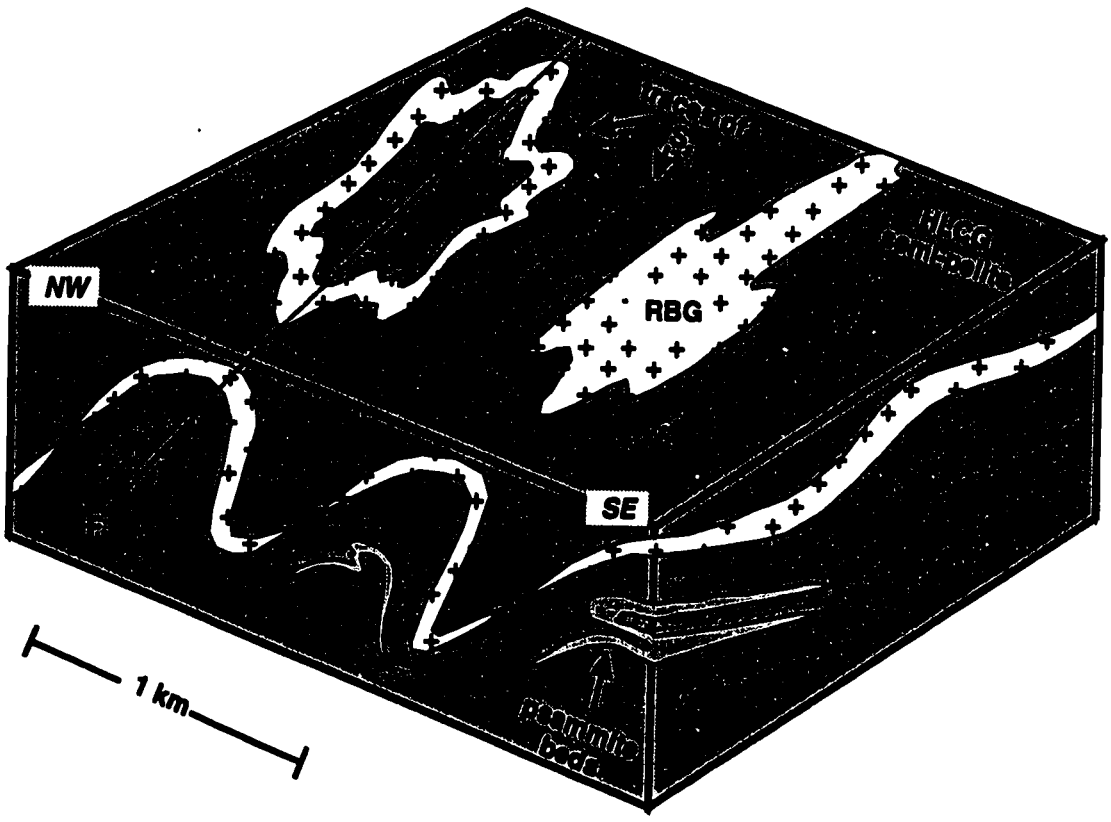

Fig. 11. Schematic block diagram showing typical geometry, vergence and relative orientation of F_2 and F_3 in the HLCG. An RBG sill is shown as a marker outlining F_3. Periclinal F_3 folds produce distinctive outcrop shapes evident in map view (see Maps 1 and 2). F_2 can be observed at F_3 hinges, where discontinuous psammite beds often serve as markers. Observed at F_3 hinges, F_2 folds are recumbent, and have a symmetry which indicates non-coaxial shearing directed to the northwest.

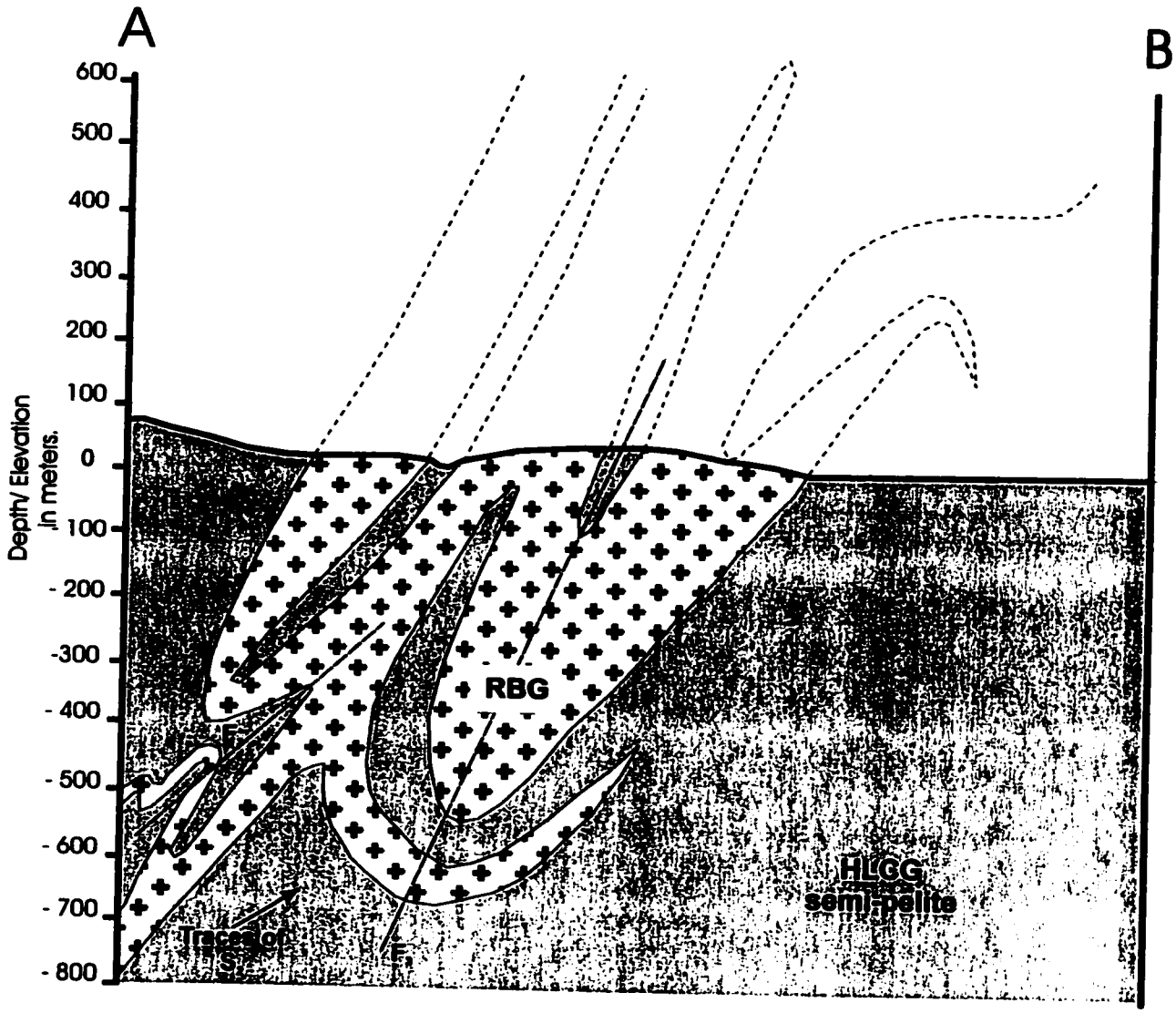

Fig. 12. A) Structural crossection of the intrusion in the Barasway sector (see Maps 1 and 2). The pluton has the shape of Christmas-tree laccolith, which has been folded by tight F_3 folds.

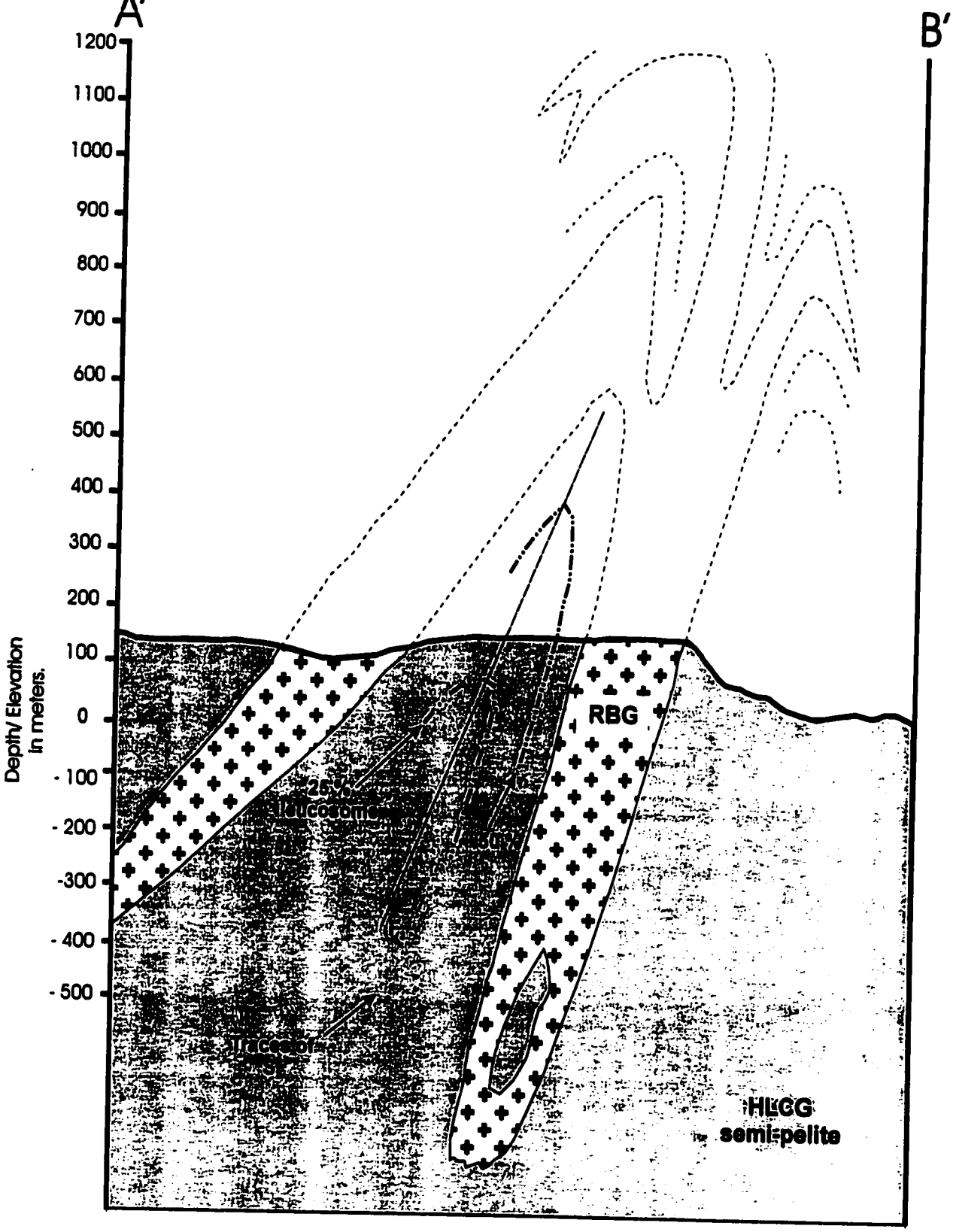

Fig. 12. B) Structural crossection of the intrusion north of Harbour Le Cou (see Maps 1 and 2). The pluton has the shape of a laccolith, which has been folded by tight F_3 folds.

Plate 1. Evidence of S_0, S_1, and S_2.

A) S_0 in the HLCG wall rocks, Barasway sector.

B) Close-up of a hinge of one of the psammite beds in A showing a weakly developed bedding sub-parallel foliation S_1, which is overprinted by a stronger axial-planar foliation S_2.

Plate 2. F_2 fold, Barasway sector.

Plate 3. An RBG dyke which cuts across S_0, S_2, and is folded by F_3. Photo was taken north of Gull Lake pond.

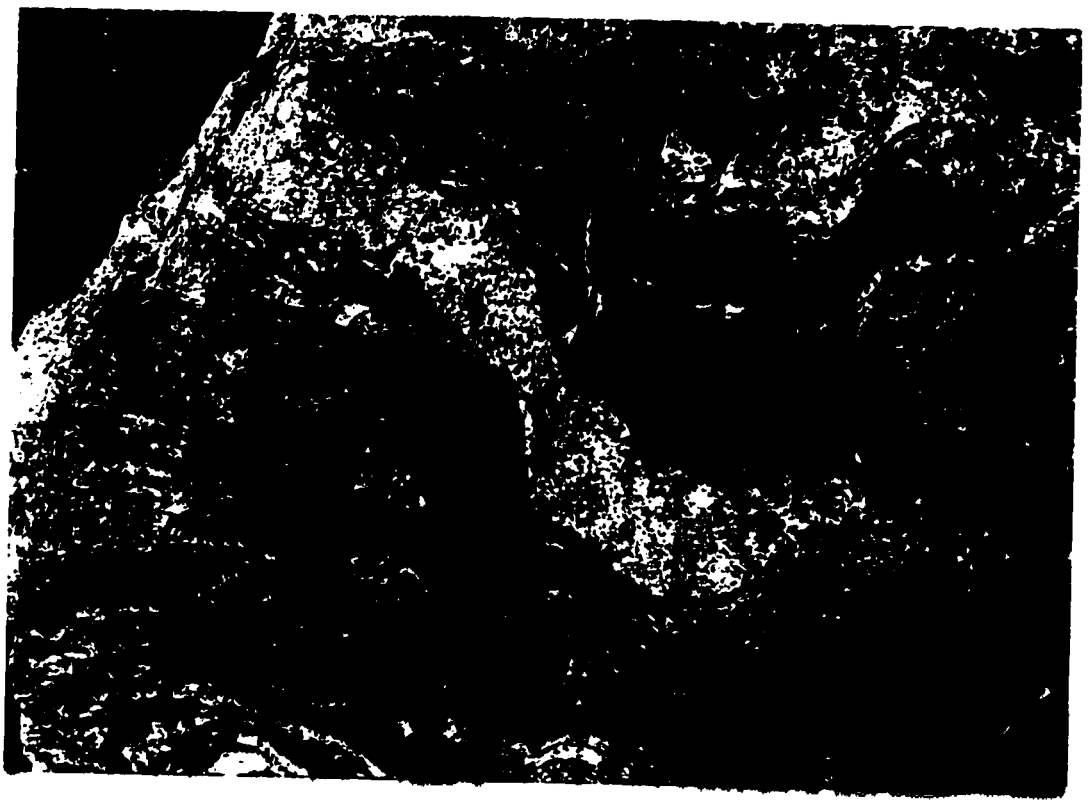

Plate 4. Geometrical relations between F_2 and F_3 folds.

A) An F_3 hinge cropping out in the Barasway sector.

B) An F_2 hinge visible on an orthogonal face of the same outcrop (indicated in A).


F
F_2

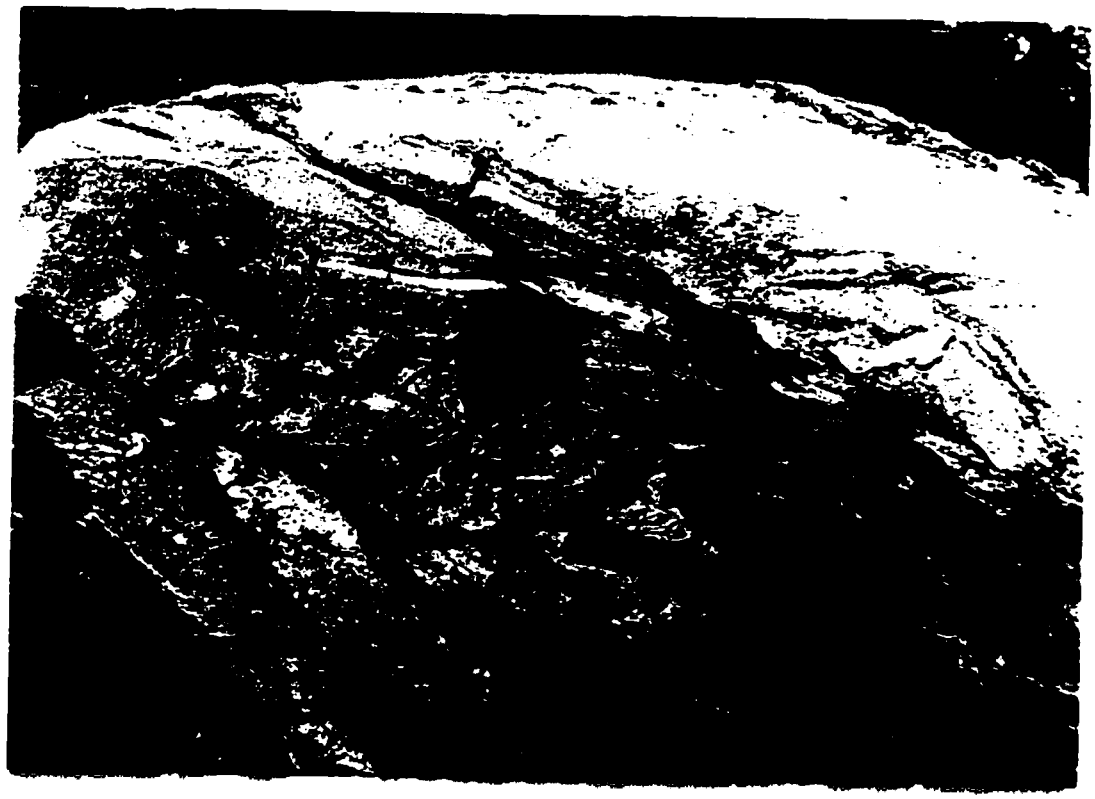

Plate. 5. Geometrical relations between F_3 and second-generation fabrics.

A) An F_3 hinge cropping out in the Barasway sector.

B) Close-up of the folded pelitic bed in A. The pen is oriented parallel to the L_2 stretching lineation, the hammer handle is parallel to the hinge and points down plunge.

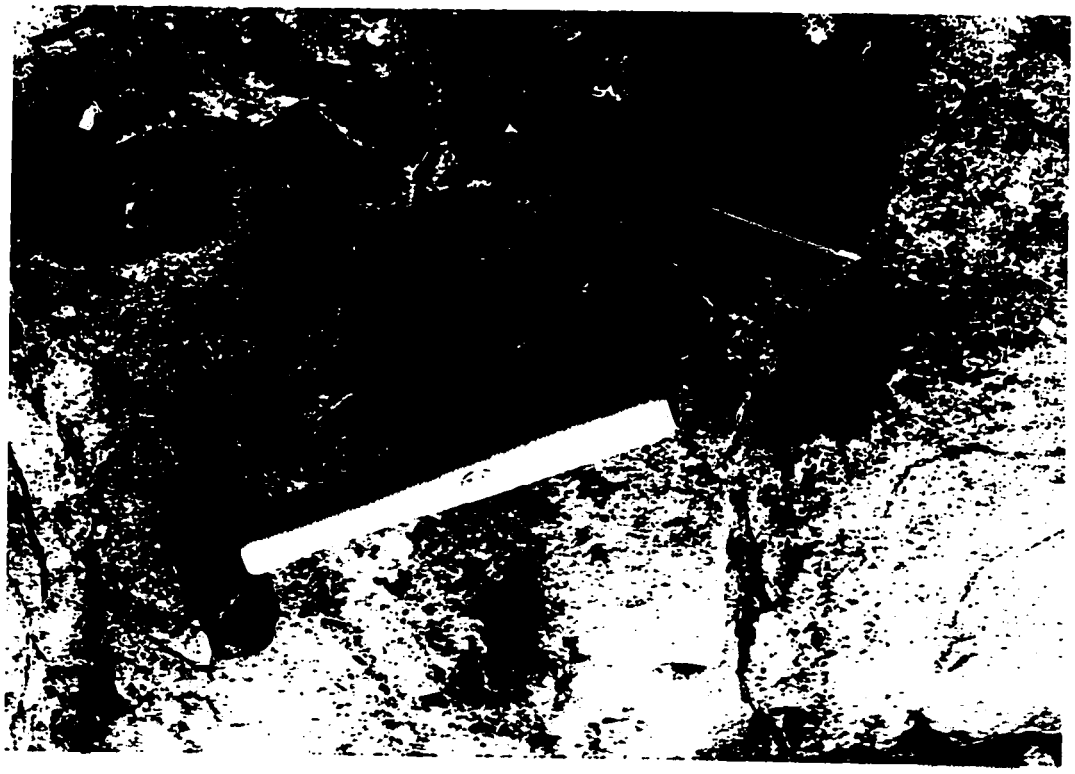

Plate 6. Typical RBG-HLCG contact relations.

A) Close-up of a typical RBG-HLCG contact. The granite is pegmatitic in the immediate proximity to the contact. Sheets of the HLCG country rock are included in the pegmatite. The sheets are concordant with, and contain, the S_2 foliation.

B) An example of a typical RBG dyke. The main contact of the dyke cuts across the composite S_2 foliation in the HLCG rocks. Offshoots from the dyke intrude concordantly into the foliation. Both the offshoots and the foliation are folded by small, open F_3. The pen shown in the photo is parallel to the trace of the foliation in the dyke, which is concordant with S_2 in the country rocks. Interpretation of the structures and fabrics shown in this plate is given in Fig. 9.

Plate 7. Typical geometries of S_{bi}, S_2 and the RBG-HLCG contacts.

A) Obliquities between S_{bi}, S_2 and the contact. The black pen in the photograph is parallel to S_{bi}, and the red one is parallel to S_2.

B) S_{bi} in the granite is parallel to S_2, but oblique to the granite contact.


S2


F3
S2

Plate 8. Examples of HLCG xenoliths observed in the RBG.

A) A tabular pelitic xenolith containing the characteristic S_2 foliation observed in the Rose Blanche-Harbour Le Cou sector. Both the xenolith and the contact are folded by F_3.

B) Blocky xenoliths and folded RBG dykes in the Barasway sector.

Plate 9. Boudinaged, partially melted psammite bed.

A) Close-up of one of the boudins in B (center of the photo, near the label c').

B) View of the nearly vertical outcrop face. Several well developed shear sense indicators are clearly visible. The sense of shear is tops to the northwest.

SE NW

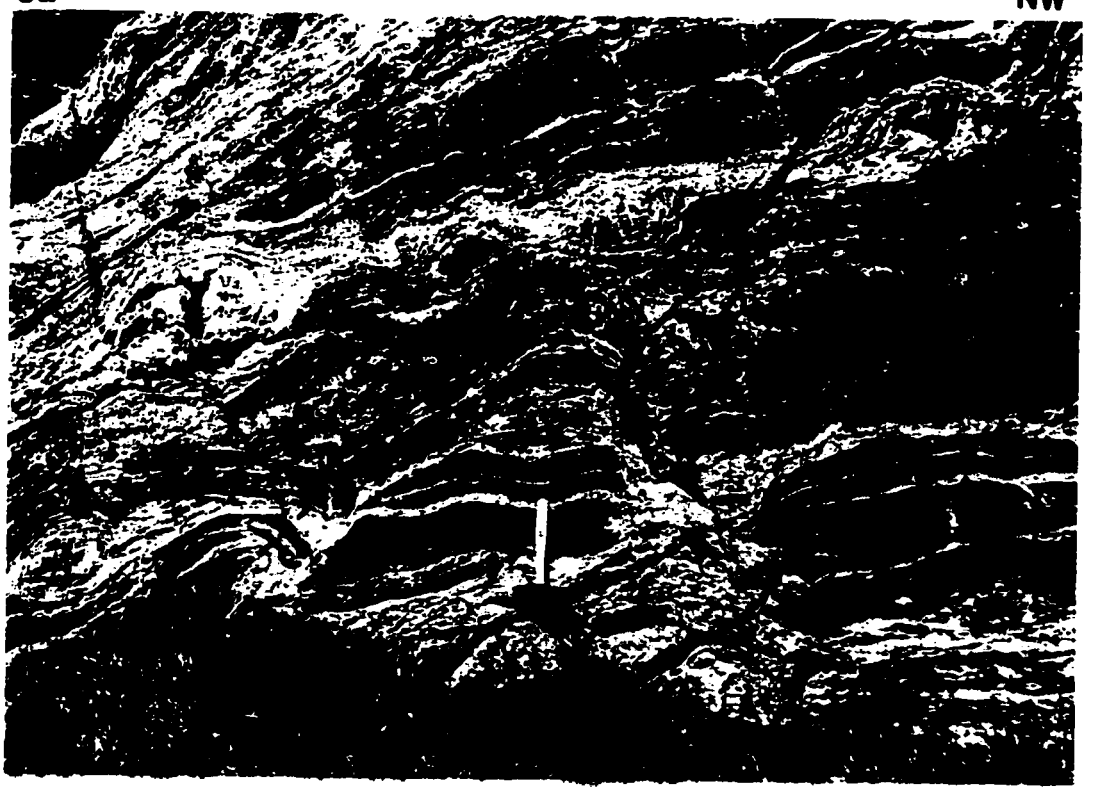

Plate 10. Porphyroblast-matrix relations in the HLCG pelites.

A) Two generations of biotite grains in the matrix. S_1 is defined by coarser biotite grains, which are folded and kinked at the hinge of an F_2 fold. Smaller biotite grains define an axial planar foliation S_2 to the fold. Plane polarized light.

B) Garnet porphyroblast in a pelitic bed. Rims of the garnets are inclusion free. Trails of fine quartz and biotite inclusions in the cores of the garnets are oriented at a high angle to the matrix foliation defined by much coarser grains of biotite, muscovite and quartz. Crossed polars.

S2
S1

Plate 11. Sillimanite needles in an HLCG pelite. Some of the needles are either being replaced by muscovite, or growing as fibrolite on muscovite. Crossed polars.

Plate 12. Mineralogical sources of susceptibility in the RBGba phase. Hornblende (Hb) is partially replaced along cleavages by very fine-grained opaques. Faint traces of alteration by opaque minerals can also be seen in the biotite grain below and to the right. A larger opaque grain to the right of Hb is rimmed by sphene - an indication that the opaque is ilmenite. Plane polarized light.

Plate 13. Microstructures in Plagioclase feldspar.

A) A pull-apart microstructure indicative of brittle deformation. Crossed polars.

B) Bulged grain boundaries between two plagioclase grains. This microstructure is indicative of grain boundary migration - an amphibolite grade process in plagioclase feldspar. Crossed polars.

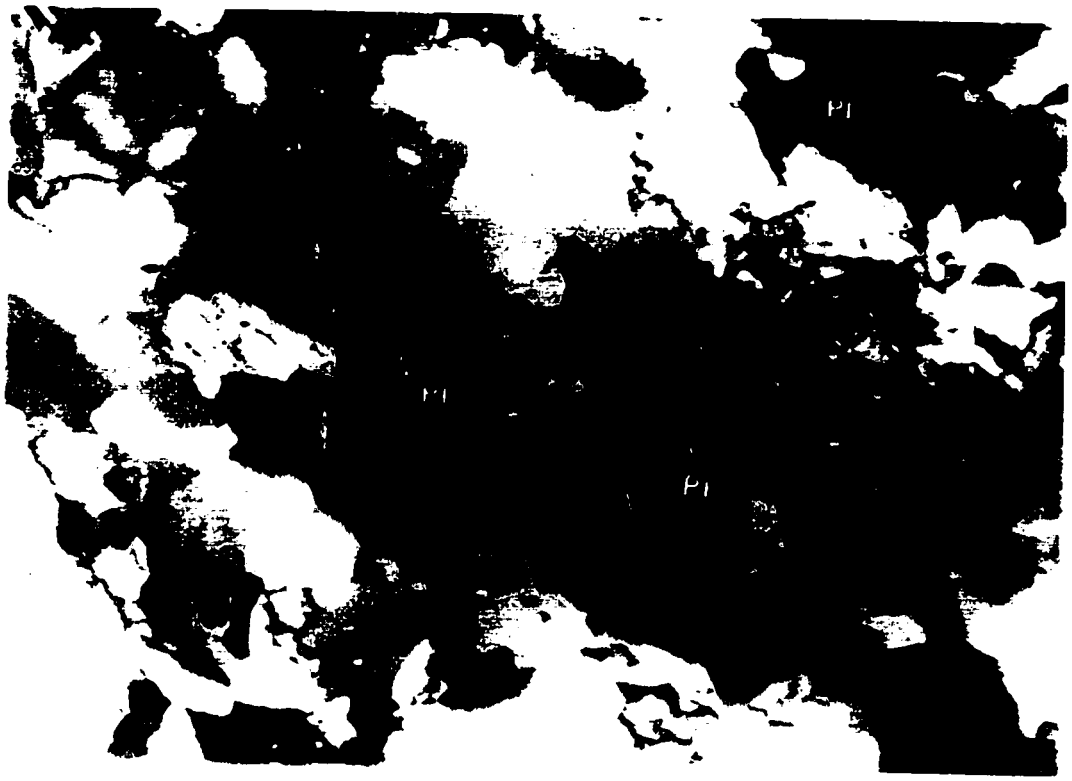
PI
PI
PI


PI

Plate 14. Microstructures and recrystallization mechanisms in quartz.

A) Dissection microstructure.

B) Highly lobate grain boundaries between two quartz grains.


Qtz


Qtz

Plate 15. Microstructures in quartz.

A) Close-up of the grain boundaries of a dissection microstructure. Crossed polars. The grain boundaries migrated into the more highly strained grain (the one near extinction).

B) Well developed tilt walls in quartz. Crossed polars.

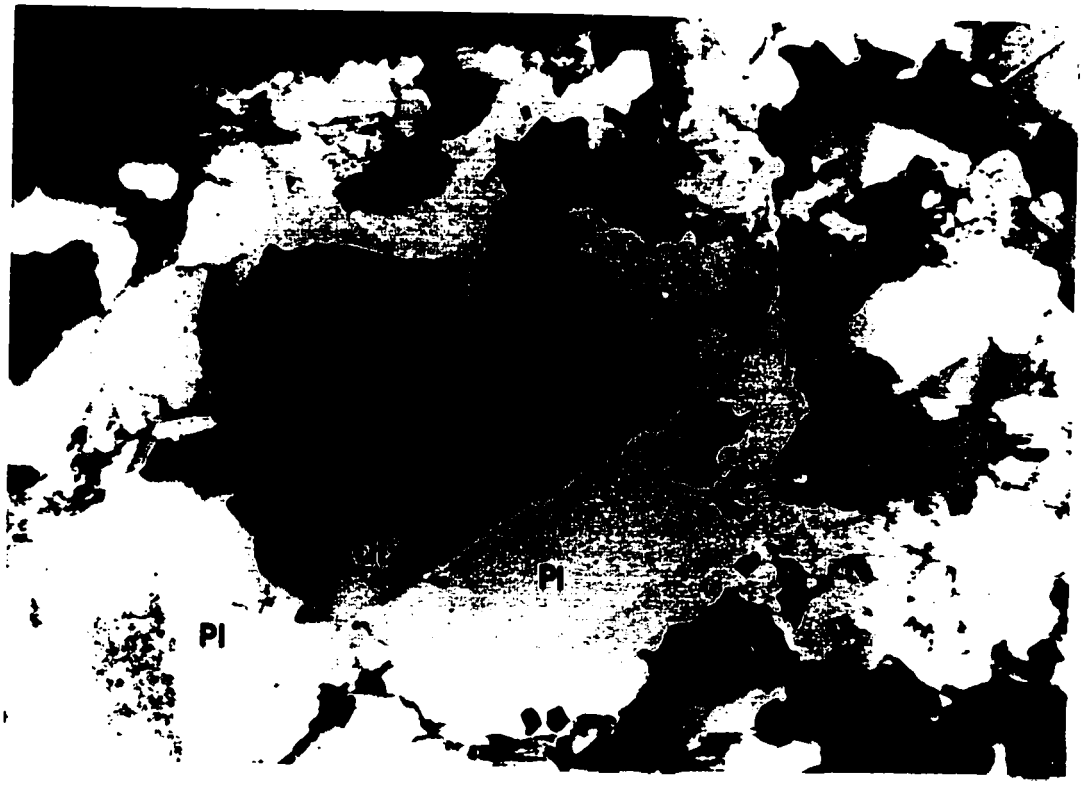
Pl
Pl

CHAPTER 5 - AMS FABRICS OF THE ROSE BLANCHE GRANITES.

5.1 Introduction.

AMS analysis has often been used to infer patterns of magmatic and solid-state lineations and foliations in plutons. In many cases AMS fabrics characterized by weakly anisotropic ellipsoids, and supported by microstructural observations suggesting low amounts of superimposed solid-state strain, have been interpreted as evidence of magmatic flow directions (e.g. Bouchez et al., 1990; Bouchez and Gleizes, 1995). Recent computer modeling indicates that weak AMS fabrics can be rapidly overprinted by small strains (Benn, 1994).

In Chapter 4 it was shown that intrusions comprising the RBG suite are typical examples of weakly to moderately deformed, paramagnetic, leucocratic granites. It was demonstrated, via

conventional structural techniques, that many granite sheets and dykes were folded by two episodes of regional deformation - D_2 and D_3. The microstructural study has demonstrated that the fabric in the RBG is characterized by microstructures indicative of amphibolite-grade solid-state deformation.

This chapter presents analysis of the AMS data. In the following sections mineralogical sources of susceptibility in the RBG will be identified and discussed. It will be shown that in all of the mapping sectors analysis of directional and non-directional AMS data supports the conclusion that magnetic fabrics of the RBG accurately record solid-state strain imparted during regional D_2.

5.2 Mineralogical sources of susceptibility of the RBG.

In Chapter 4 it was shown that the RBG suite consists of two phases - RGBba and RBGrb. Petrographic observations indicate that biotite is the only paramagnetic mineral (see Chapter 3, Table 4 for susceptibility characteristics of biotite) present in the RBGrb phase. No opaque accessory minerals

were observed in any of the samples collected from the RBGrb phase. Petrographic observations carried out on samples collected from the RBGba phase revealed that accessory amounts of opaque minerals were present (Plate 12). Rare grains of ilmenite were observed to be rounded and equant in habit and frequently rimmed by titanite (Plate 12). Another opaque mineral, most likely magnetite, was observed to occur as aggregates of very fine grains replacing biotite along cleavages (Plate 12).

Table 6 is a summary of all site-average AMS data presented in the thesis. AMS data from the Rose Blanche sector were discussed by Benn et al. (1993), and are not summarized in this table. Locations of the AMS sites are shown in Fig. 14. A histogram of site-average K_m values for all of the sites sampled in the Burnt Islands and The Barasway sectors is presented in Fig. 13 A. The majority of the sites have K_m values below 200 x 10^{-6} SI. The four sites collected from the more mafic RBGba phase do not show systematically higher values of K_m than sites from the RBGrb phase (Table 6, Fig. 13 A). Three of the sites, two from the RBGrb phase (g93rb9, g93rb8) and one from the RBGba phase (g93rb17) record anomalously high values of susceptibility. Significant

amounts of accessory opaques were observed in one of these sites (g93rb17) collected from the RBGba phase. No accessory opaques were observed in thin sections from sites g93rb9 and g93rb8. This does not necessarily preclude their occurrence. Site average AMS records the average fabric and susceptibility in about 60 cm^3 of rock - a much greater amount than covered by a single thin section. It is possible that ferromagnetic accessories were present even though none were observed in thin section.

The P vs. K_m plot of all samples collected from the Burnt Islands and the Barasway sectors is shown in Figure 13 B. Samples cluster around the low values of P=1.1, K_m=105 x 10^{-6} SI. The majority of the samples are grouped between the values K_m=60 to K_m=200 x 10^{-6} SI and cluster around the value of P=1.1. A small number of samples show anomalously high values of both K_m and P. In these samples either magnetite or ilmenite almost certainly make a contribution. The most probable explanation for this anomalous behaviour is the presence of mimetic magnetite growth along cleavage planes of the biotite grains (Plate 12). Mimetic magnetite grains and grain aggregates can produce very high values of both K_m, and P, resulting in drastic variations of the shape

parameter (T), but directional AMS data are not likely to be seriously affected (Archanjo et al., 1994).

Data presented in Figures 13 A and B support the petrographic observations indicating that biotite is the dominant contributor to the AMS in the RBGrb phase. The AMS from three of the RBGba sites also appears to be controlled by biotite. Benn et al. (1993, see Chapter 3 for discussion) showed that all of the samples collected from the Rose Blanche sector plotted well within the P-K_m field (maximum boundaries - P=1.35, K_m=130 x 10^{-6} SI). This can be theoretically produced by a 10% modal biotite component (see Chapter 3 for discussion). The majority of samples collected in the Burnt Islands and The Barasway sectors also fall within this field (Fig. 13 B). Only a few of the samples fall outside of the 20% biotite field (Fig. 13 B). Most of the samples, with the exception of ten, plot well below the theoretical maximum value of P for rocks whose susceptibility is dominated by paramagnetic minerals (Rochette, 1987).

Petrographic observations presented in Chapter 4 indicate that the modal proportion of biotite is under 10% in both

the RBGba and the RBGrb phase. Many of the samples from the Barasway and Burnt Islands sectors have values of K_m slightly greater than can be accounted by 10% modal biotite. This can be explained either by a minor contribution to K_m from accessory ferromagnetic minerals such as ilmenite and mimetic magnetite (Archanjo et al., 1994), real fluctuations of modal fraction of biotite which were not detected by thin section observations, or presence of significant amounts of other paramagnetic minerals such as garnet (garnet can contribute to K_m but not to P), cordierite and tourmaline in addition to biotite (Rochette et al., 1994). It is, therefore, reasonable to conclude that in both phases paramagnetic minerals, primarily biotite, dominate the AMS of the RBG. AMS measurements in all but three sites represent indirect estimations of biotite SPO (see discussions in Chapter 3).

5.3 Directional data analysis.

Equal area, lower hemisphere projections of K_1 and K_3 are shown in Figure 15. K_1 data define a sub-horizontal, northeast-southwest trending cluster. The orientations of the two main concentrations of K_1 on an equal-area stereonet are nearly identical to the orientations of the main concentrations of L_2 in the HLCG (Fig. 15 A). The stereonet distribution of K_3 shows an orientation distribution very similar to that of S_2 - the main foliation observed in the HLCG wall rocks (Fig. 15 B). The AMS data show considerably less scatter. There are two possible explanations for this: 1 - conventional field data inherently include a larger component or random error, while AMS measurements are relatively precise; 2 - there are fewer AMS sites than conventional sites and their spatial distribution is not as broad. Overall the stereonet distribution of K_1 and K_3 is remarkably similar to L_2 and S_2 in the HLCG, although the clusters of the AMS data are tighter.

Maps of K_1 in the Burnt Islands, the Barasway, and Rose Blanche sectors are shown in Figures 16 and 17. In the Rose

Blanche sector (Fig. 16 C) magnetic lineations trend parallel to the north-western contact of the granite sheet, which, in turn, is oriented parallel to the regional trend of both S_2 and F_3 axes. A similar pattern is seen in the Barasway sector (Fig. 16 B) where the folds affecting RBG intrusion are relatively complex (Map 1). Magnetic lineations maintain the characteristic northeast-southwest trending, shallowly-plunging pattern. In the Burnt Islands sector, at the hinge zone of the fold structure, the trend of the shallowly-plunging K_1 lineations clearly turns around at a high angle to the regional northeast-southwest trend (Fig. 16 A). This pattern of orientation was observed to be typical of L_2 and S_2 in the nearby HLCG (Maps 1 and 2).

Patterns of magnetic foliations (planes orthogonal to K_3), shown in Figure 17, paint a very similar structural picture. In the Rose Blanche-Harbour Le Cou and the Barasway sectors magnetic foliations consistently strike parallel to the main regional northeast-southwest trend, and dip steeply to the northwest. This orientation is consistent with both the regional S_2 foliation, as observed on the limbs of the nearly isoclinal F_3, and with map traces of F_3 axial planes (Fig. 17 B, C, Maps 1 and 2). The pattern of magnetic

foliations in the Barasway sector is similar, with the foliations striking consistently northeast-southwest, even in the immediate vicinity of the interpreted locations of F_3 hinges (Fig. 17 B). This is not the case in the Burnt Islands sector where the strike of the magnetic foliation in the immediate vicinity of the hinge zone is at a high angle to the regional trend (Fig. 17 A).

The sites in question in The Barasway sector (g93rb16 and g93rb17, Fig. 14) are located in the RBGba phase. Accessory opaque minerals were observed in thin sections cut from cores collected at these sites (Plate 12). Both sites have anomalously high values of susceptibility (Fig. 13 A). It is reasonable to conclude that in these two sites the AMS is controlled by late accessory ferromagnetic minerals which grew syn-D_3. In the Burnt Islands sector sites with AMS fabrics which trend at high angles to regional fabrics do not show any petrographic evidence for presence of late accessory minerals (Fig. 17 A, Fig. 13 A).

5.4 Fabric shape analysis.

The P vs. T plot for the entire population of site averages is shown in Fig. 18 A. Most of the samples cluster around the value of P = 1.1 ± 0.5, with the majority of samples with small to moderate magnitudes of T falling in the oblate field. A small proportion of the samples have large values of T in either prolate or oblate fields. Clustering of the data around this small value of P supports qualitative field observations attesting to the fact that the RBG contain a moderately well developed fabric, and that in general the intensity of this fabric does not vary greatly. Sites from the Barasway and Burnt Islands sectors, where the RBG exposures have preserved evidence of folding, have predominantly oblate AMS ellipsoid shapes (see Figure 19).

Several of the sites with prolate AMS ellipsoid shapes were collected at the Burnt Islands and the Barasway sectors close to the granite contact with the wall rocks (Fig. 14). Anomalous prolate ellipsoid shapes could be produced by a significant contribution to the susceptibility by an

accessory mineral with prolate single-mineral AMS, such as tourmaline or hornblende (Borradaile, 1988), or aggregates of fine grained magnetite crystals within hornblende (Borradaile, 1988). The latter explanation appears to be likely for sites g93rb17 (The Barasway) and g93rb9 (Burnt Islands) which show anomalously high values of K_m (see Figures 13 A, 14, and 19).

Sites from the Rose Blanche sector (discussed by Benn et al., 1993) are evenly distributed between weakly to moderately prolate to oblate AMS ellipsoid shapes (Fig. 18 D). Spatial distribution of the T parameter reveals no systematic variation (Fig. 19 C). The AMS data, coupled with microstructural observations, support qualitative field observations attesting to the fact the fabric in this pluton is the result of homogeneously distributed solid-state strain.

5.5 Synthesis and discussion.

Analysis of the AMS fabrics presented in this chapter shows that:

1. AMS of the RBG is dominated by biotite, and, consequently, that the magnetic fabrics are indirect estimations of biotite SPO;
2. Directional AMS fabrics are coaxial with D_2 fabrics in the HLCG - where this is not the case, the AMS is probably influenced by presence of late accessory minerals;
3. AMS shape fabrics are dominantly oblate and show no systematic spatial variation.

In some of the recently published AMS-microstructural pluton emplacement studies (e.g. Bouchez and Gleizes, 1995) the authors have used changes in directional and scalar AMS data coupled with changes in grain-scale microstructures to identify domains of emplacement-related and later tectonic deformation. It was not possible to identify domains characterized by magmatic, sub-magmatic and solid state microstructures in this study. Microstructures observed in

all of the AMS sampling sites are consistently indicative of amphibolite-grade, solid-state deformation (Chapter 4) and show little variation in type or intensity.

A systematic transition from prolate to oblate AMS fabrics from the interior of a pluton to the contacts with the wall rocks, coupled with a transition from magmatic to solid-state microstructures, could be indicative of emplacement related flow and subsequent expansion (e.g. Brun et al., 1990). Systematic transitions such as this have been used as supporting evidence for proposed emplacement mechanisms. In the Burnt Islands and The Barasway sectors, where the RBG contain a visually relatively well developed fabric and preserve fold closures, AMS ellipsoid shapes are dominantly oblate. No systematic spatial variations in AMS fabric shape are evident. In the Rose Blanche pluton, where the visible fabric in the granite is relatively weak and no clear evidence of folding has been preserved, the values of T are scattered equally between oblate and prolate fields - again without systematic spatial variation.

Undoubtedly, early in their emplacement history the RBG contained a magmatic flow, or syn-crystallization, fabric.

In fact, possible magmatic foliations defined by alignement of feldspar laths (Patterson et al., 1989) appear to have been locally preserved in some pegmatites, and occasionally near the RBG-HLCG contacts (Chapter 4, Plate 7). However, neither scalar nor directional AMS analysis, nor microstructural data show any evidence suggesting that magmatic flow fabrics have been preserved in the RBG suite as a whole. A number of recent studies have noted that AMS lineations preserved in syn-tectonic leucogranites record regional stretching lineations (e.g. Rochette et al., 1994). Brun et al. (1990) have noted that AMS fabrics of syn-tectonic plutons do not necessarily reflect magmatic flow but may be strain-controlled, even in domains with magmatic microstructures.

Petrographic and microstructural observations can be used to support the choice of strain response model which will serve as a conceptual framework for the geological interpretation of the AMS data. Biotite grains, the primary sources of AMS, are dispersed and undeformed, while the quartz matrix in which they are embedded consistently records small to moderate amounts of solid-state ductile strain. Although feldspar grains show no evidence of ductile deformation, and

therefore can also be viewed as embedded rigid particles, they were generally observed to be dispersed and rarely in contact with other feldspar or biotite grains. The March (1932) strain response model, which treats biotite grains as perfectly rigid plates passively rotating in a ductile, homogeneously deforming medium in response to strain (see discussion in Chapter 3), can be considered as a realistic conceptual framework for interpretation of the AMS fabrics. Jeffrey's (1922) model, which treats target minerals as rigid particles rotating in a viscously flowing medium, offers an alternate way of relating fabric formation to strain. Like the March model, Jeffrey's model relies on a number of assumptions which are rarely satisfied during real deformation. It is more complex, and in this case offers no substantial advantage over the simpler March model.

According to the March (1932) model, rigid plates (biotite grains) will tend to become arranged in a zone around the X axis of the finite strain ellipse. The orientation of this zone defines the orientation of K_1 in a sample of rock. Poles to biotite plates will also be rotated into parallelism with the Z axis of the finite strain ellipse. Consequently, in a rock whose AMS fabric was produced under

March-type conditions, K_1 will be parallel to the stretching lineation and K_3 to the foliation poles. Analysis of directional AMS data from the RBG is consistent with this interpretation. K_1 in the RBG are coaxial with L_2 - the stretching lineation in the HLCG wall rocks, while K_3 are coaxial with poles to S_2.

While it is not possible to establish a quantitative correlation between finite strain and the shape of the AMS ellipsoid due to lack of information about the initial fabric, the AMS fabric in the RBG accurately records the orientation of the stretching lineation and the associated foliation produced by D_2. Dominantly oblate AMS shape fabrics indicate that the fabric preserved in the RBG was produced by tectonic, solid-state strain (Brun et al., 1990).

Table 6. Site average values of K_m, the principal susceptibilities, P and T.

12	g93rb1	Burnt Islands	RBGrb	29.82	1.0697	1.0498	0.8804	1.215	0.79
14	g93rb2	Burnt Islands	RBGrb	174.45	1.0313	1.0099	0.9589	1.076	0.409
100	g93rb3	Burnt Islands	RBGrb	22.9	1.0252	1.008	0.9667	1.061	0.412
101	g93rb4	Burnt Islands	RBGrb	88.42	1.0383	1.0068	0.9549	1.087	0.244
102	g93rb5	Burnt Islands	RBGrb	187.92	1.0585	0.9905	0.951	1.113	-0.264
103	g93rb6	Burnt Islands	RBGrb	75.41	1.0302	0.9929	0.977	1.054	-0.402
106	g93rb7	Burnt Islands	RBGrb	227.73	1.0238	1.0055	0.9706	1.055	0.312
107	g93rb8	Burnt Islands	RBGrb	344.63	1.0566	1.0177	0.9257	1.141	0.406
108	g93rb9	Burnt Islands	RBGrb	867	1.1565	0.9957	0.8478	1.364	-0.042
109	g93rb10	Burnt Islands	RBGrb	245.47	1.0285	1.0158	0.9557	1.076	0.651
111	g93rb12	The Barasway	RBGrb	112.23	1.0578	1.0069	0.9352	1.131	0.17
112	g93rb13	The Barasway	RBGrb	103.8	1.0658	1.009	0.9252	1.152	0.191
113	g93rb14	The Barasway	RBGba	119.95	1.0424	1.0162	0.9414	1.107	0.48
114	g93rb15	The Barasway	RBGrb	73.36	1.0341	1.0209	0.945	1.094	0.703
115	g93rb16	The Barasway	RBGba	235.17	1.0383	1.0088	0.953	1.09	0.309
116	g93rb17	The Barasway	RBGba	742.12	1.107	0.9847	0.9083	1.219	-0.231
117	g93rb18	The Barasway	RBGrb	135.67	1.0559	1.0323	0.9119	1.158	0.672
118	g93rb19	The Barasway	RBGrb	121.28	1.0419	1.0193	0.9388	1.11	0.562
209	92r1	Rose Blanche	RBGrb	105.50	1.0316	1.0012	0.9673	1.067	0.054
210	92r2	Rose Blanche	RBGrb	106.45	1.0482	0.9958	0.956	1.096	-0.136
211	92r3	Rose Blanche	RBGrb	105.13	1.0437	1.0046	0.9517	1.097	0.151
212	92r4	Rose Blanche	RBGrb	120.69	1.0526	1.0008	0.9466	1.112	0.021

213	92r5	Rose Blanche	RBGrb	97.23	1.0362	0.998	0.9658	1.073	-0.085
214	92r6	Rose Blanche	RBGrb	103.70	1.0403	0.9984	0.9614	1.082	-0.063
215	92r7	Rose Blanche	RBGrb	106.47	1.0547	1.0002	0.9451	1.116	0.006
216	92r8	Rose Blanche	RBGrb	97.00	1.0473	0.9921	0.9606	1.09	-0.273
217	92r9	Rose Blanche	RBGrb	104.25	1.0499	1.0034	0.9467	1.109	0.1
218	92r10	Rose Blanche	RBGrb	98.32	1.045	1.0047	0.9503	1.1	0.149
219	92r11	Rose Blanche	RBGrb	105.38	1.0691	0.9956	0.9353	1.143	-0.1
220	92r12	Rose Blanche	RBGrb	109.07	1.052	0.9863	0.9617	1.094	-0.455
221	92r13	Rose Blanche	RBGrb	105.39	1.0449	1.0107	0.9444	1.106	0.319
222	92r14	Rose Blanche	RBGrb	104.59	1.0552	1.0031	0.9418	1.12	0.081
223	92r15	Rose Blanche	RBGrb	105.02	1.048	1.0105	0.9416	1.113	0.295

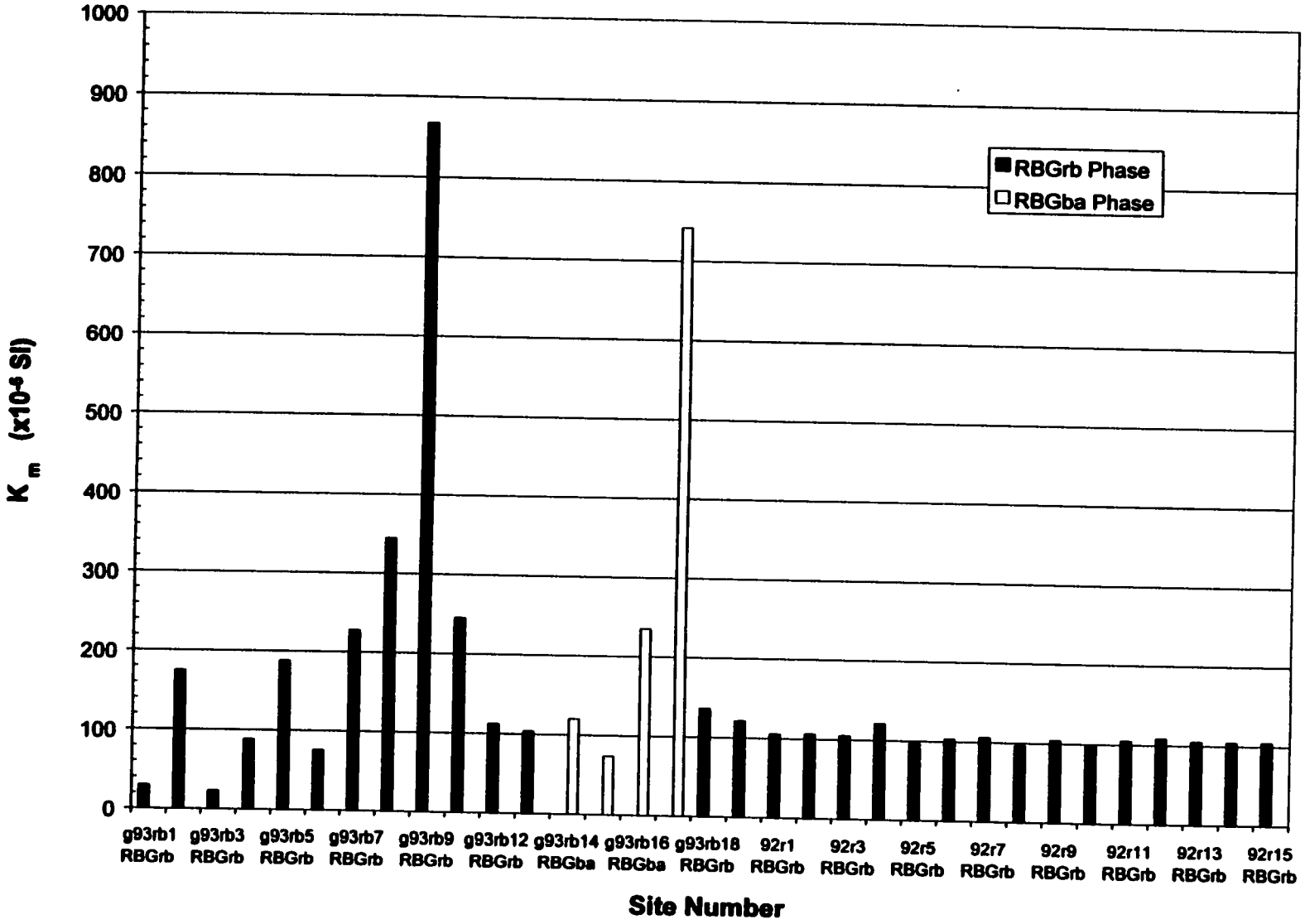

Fig. 13. A) Bar graph of site-average susceptibility values (K_m) given in Table 6.

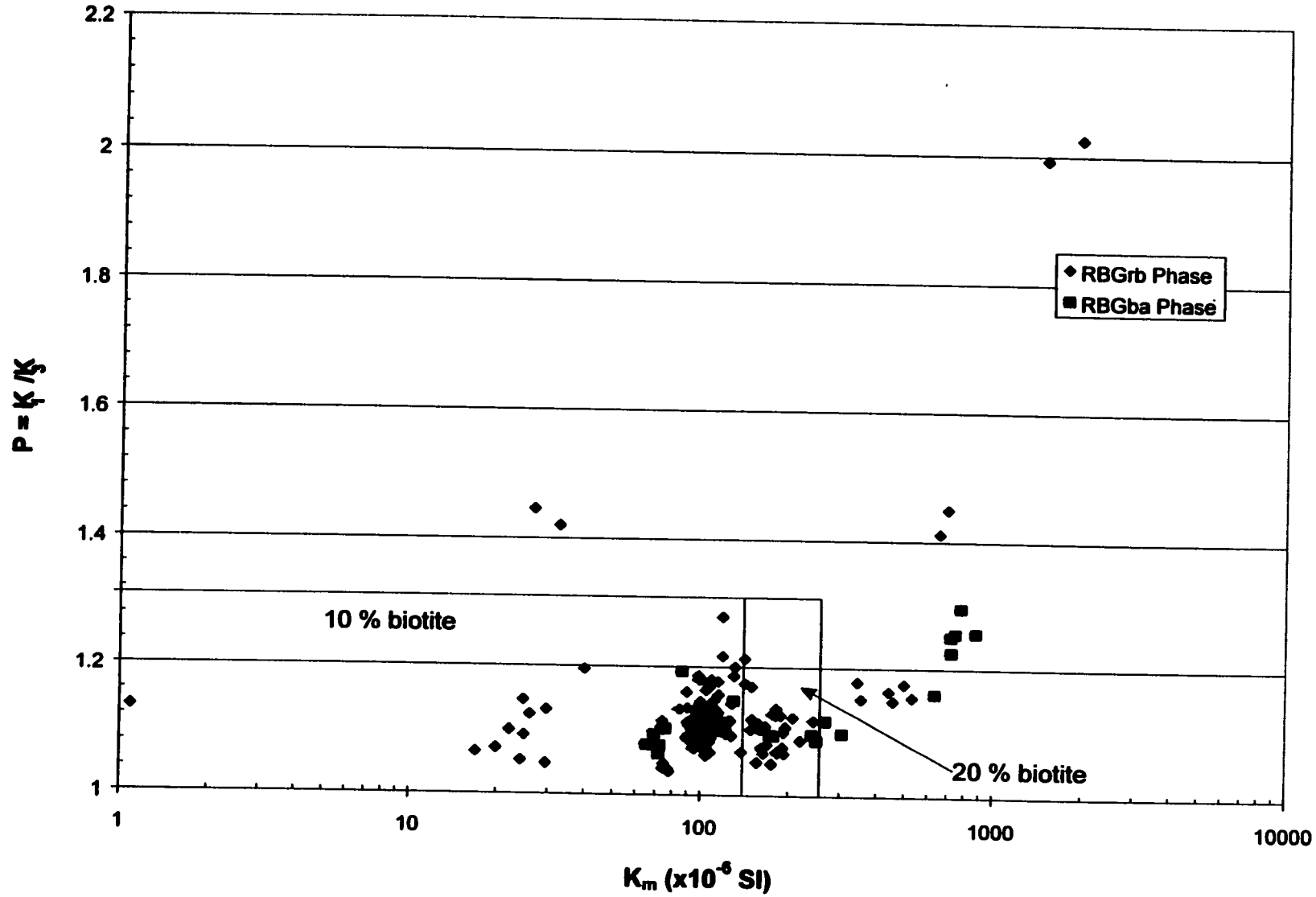

Fig. 13. B) P vs. K_m plot for all samples.

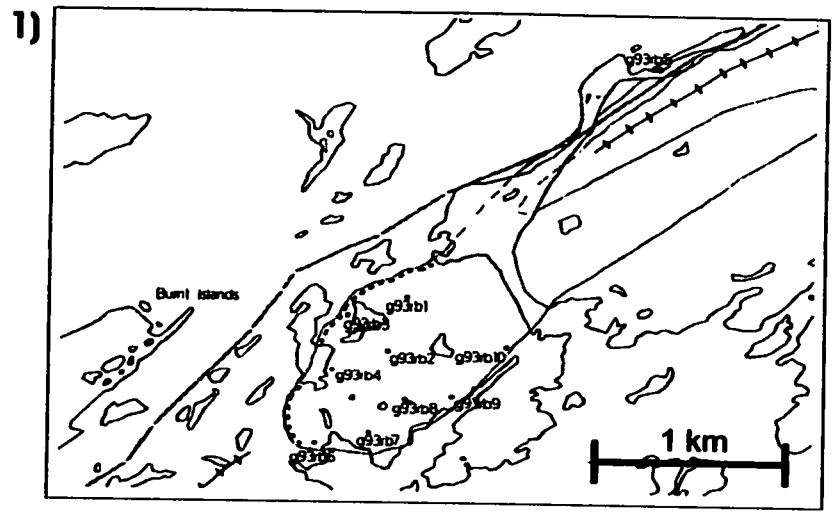

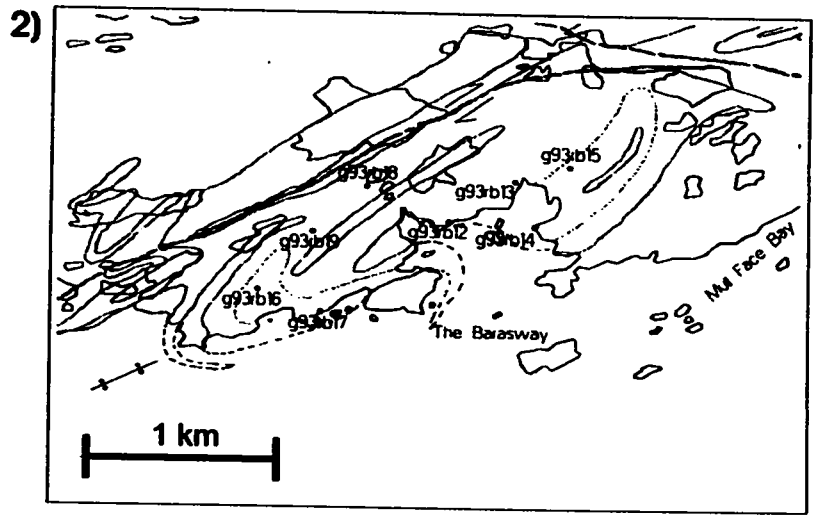

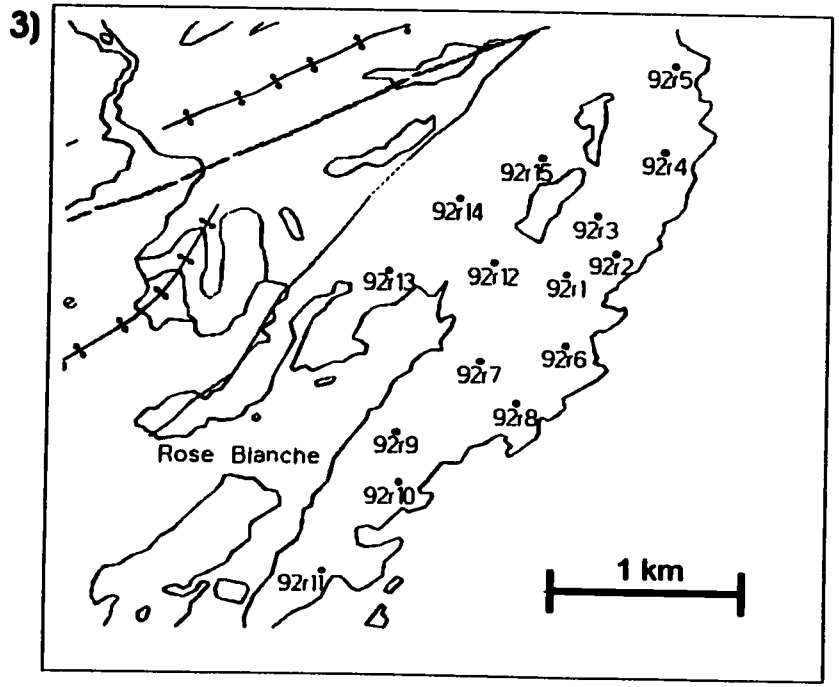

Fig. 14. AMS drill site locations in 1) Burnt Islands, 2) The Barasway, and 3) Rose Blanche-Harbour Le Cou sectors.

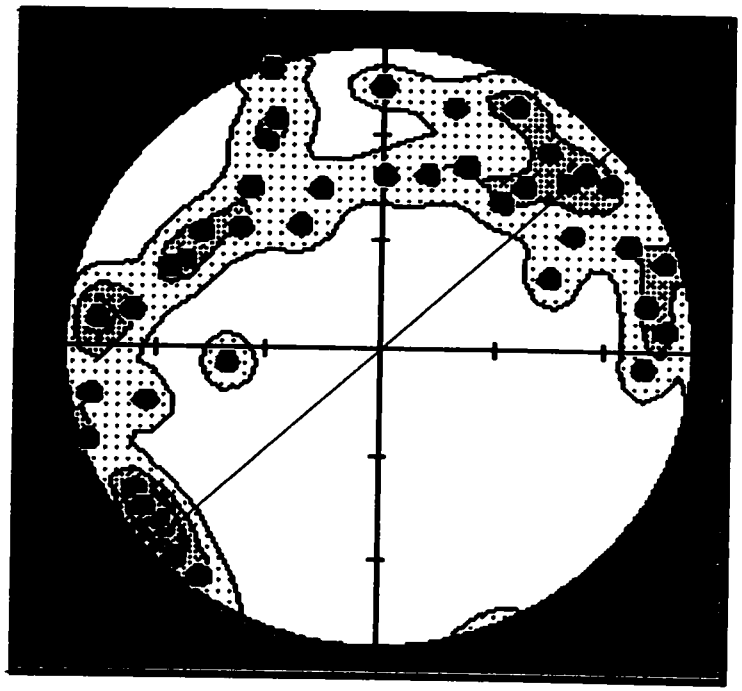

A) Stereonet distribution of L_2 stretching lineations in the HLCG wall rocks.

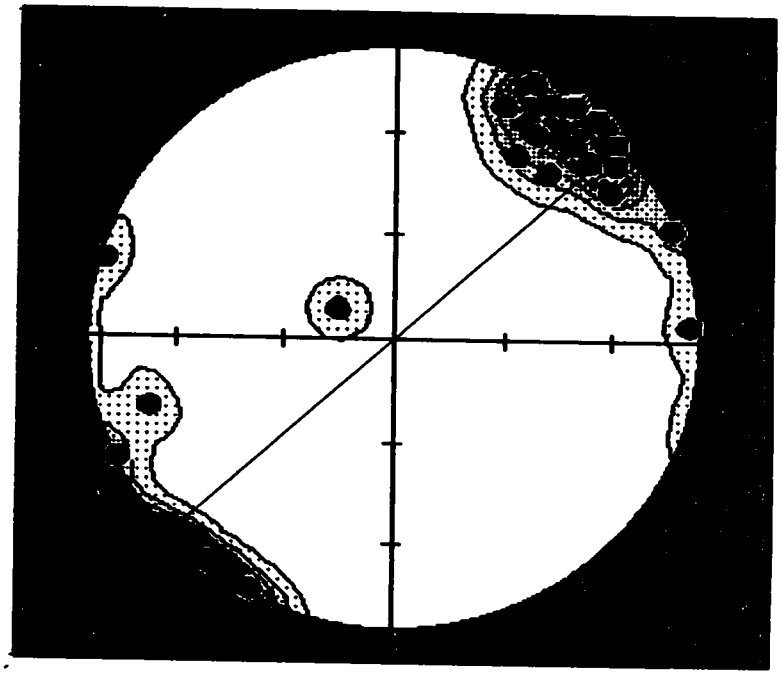

B) Site average maximum susceptibility orientations for all sites.

Fig. 15. A comparison of second generation fabrics in the HLCG with AMS fabrics of the RBG.

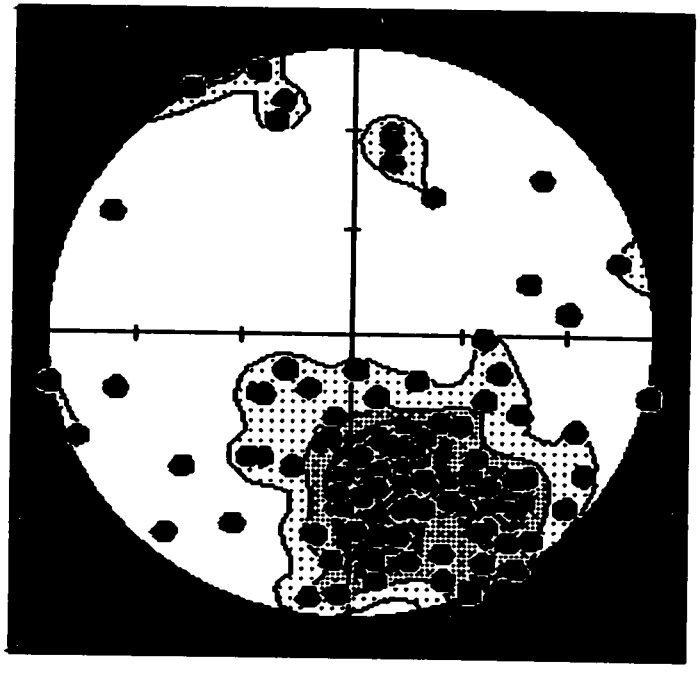

C) Stereonet distribution of poles to the S_2 foliation.

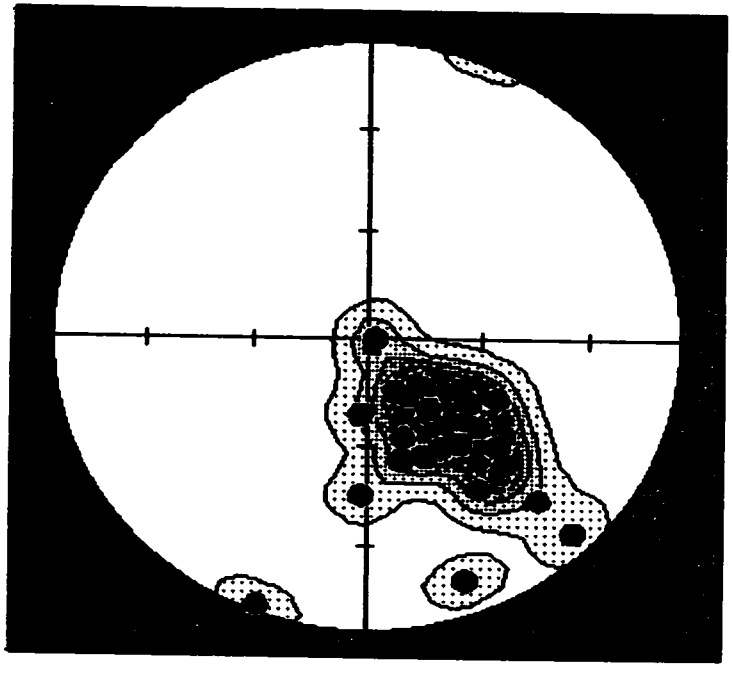

D) Stereonet distribution of K_3, or poles to the magnetic foliation.

Fig. 18. P vs. T diagrams of site average values.

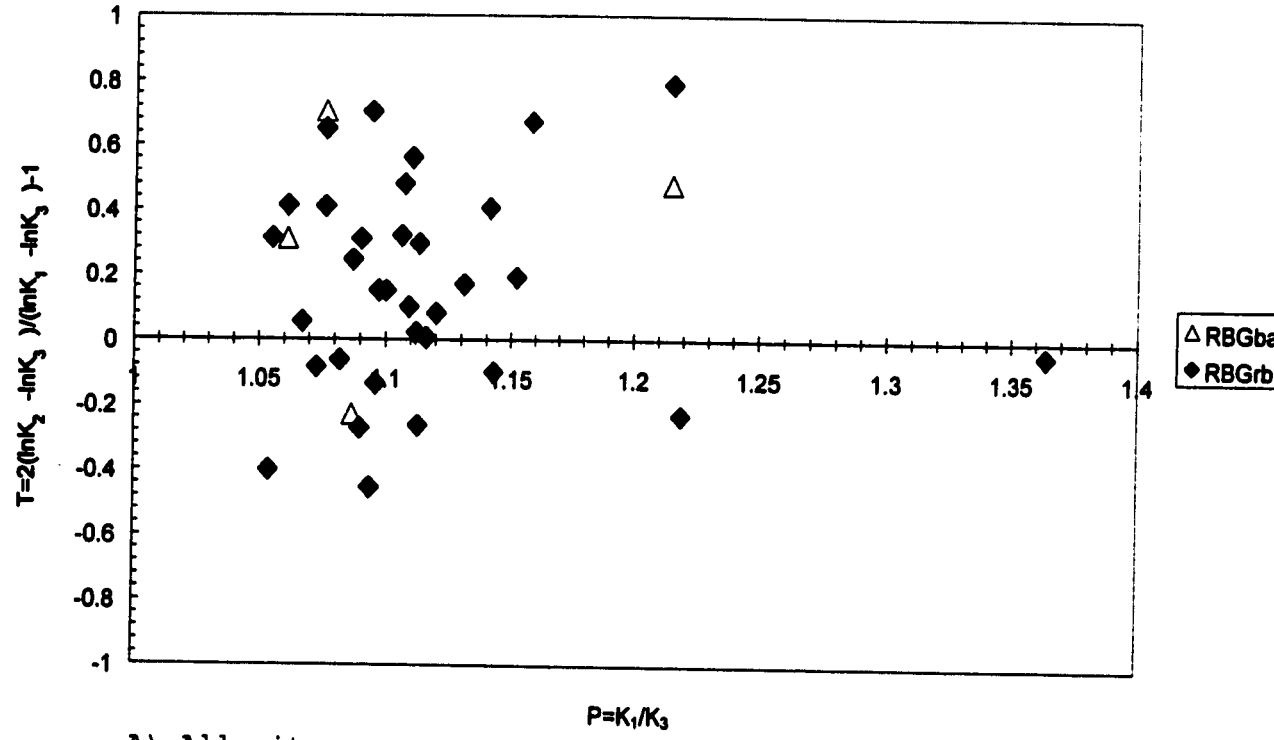

A) All sites.

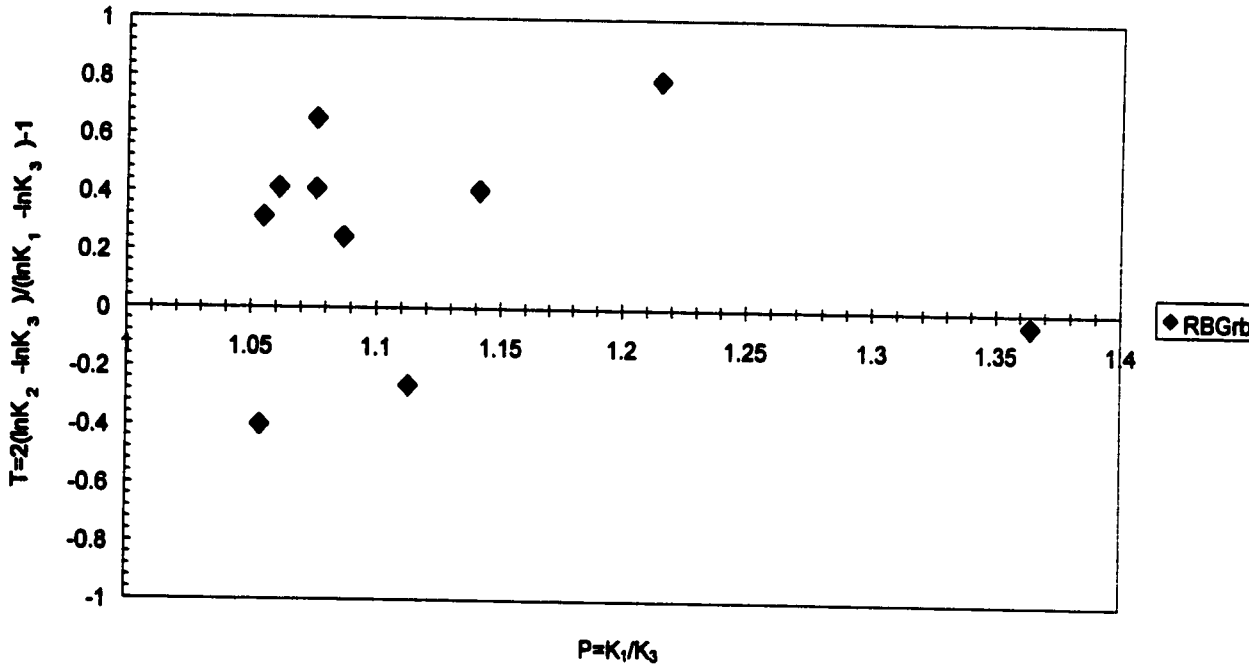

B) Burnt Islands sector.

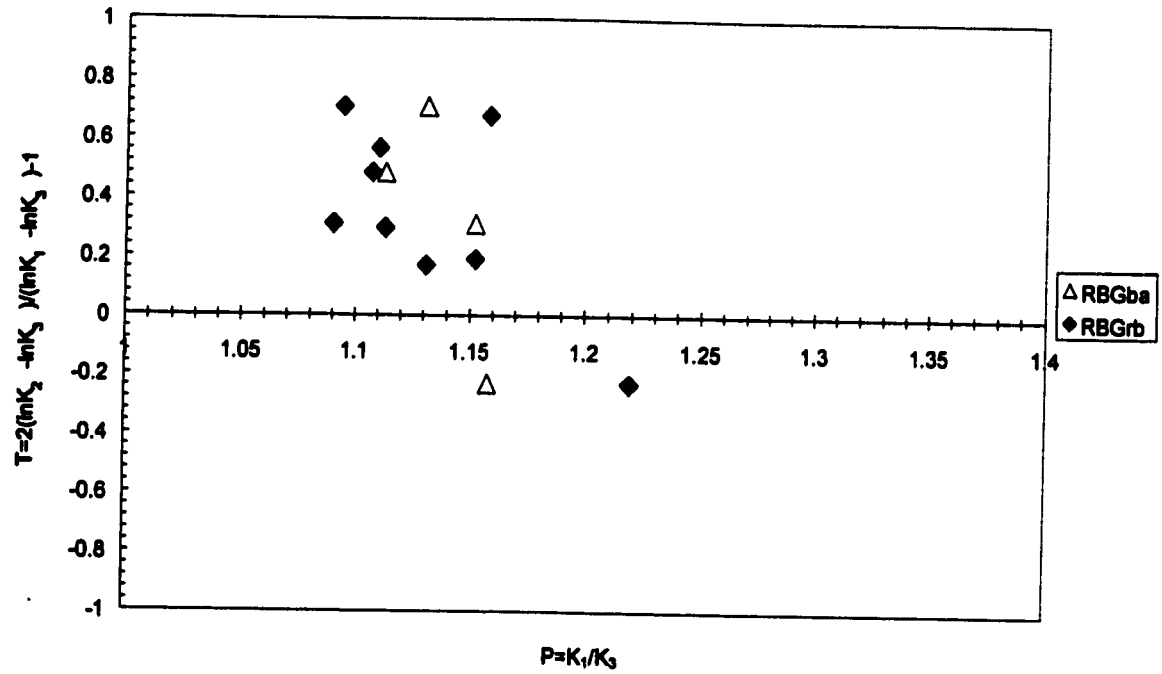

C) The Barasway sector.

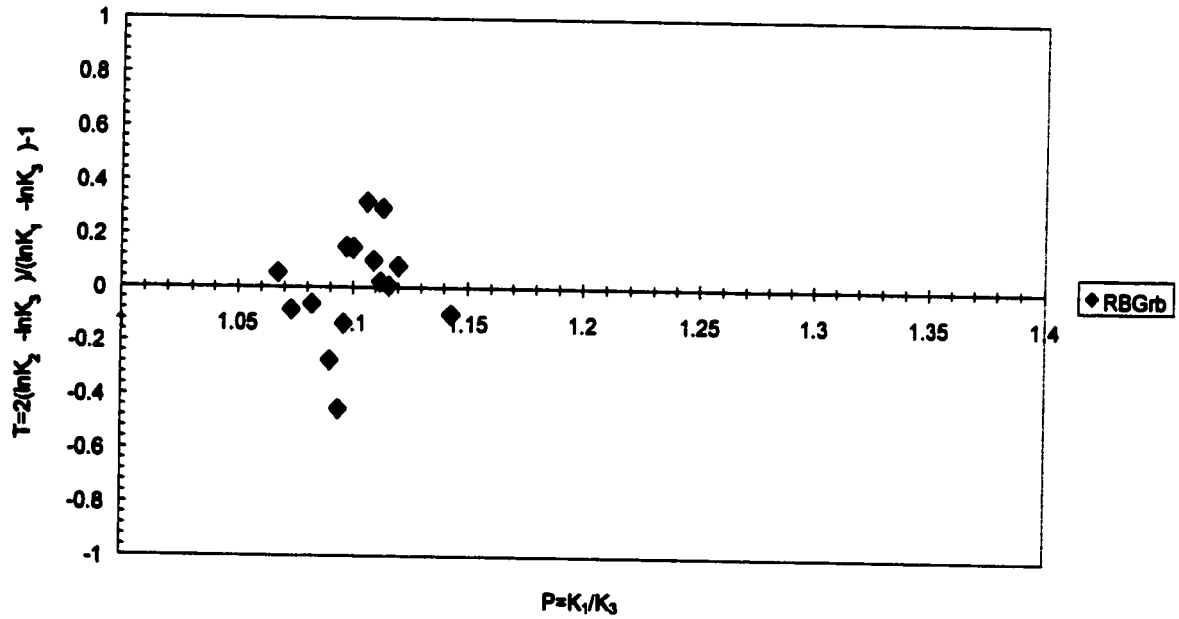

D) The Rose Blanche sector.

A)

B)

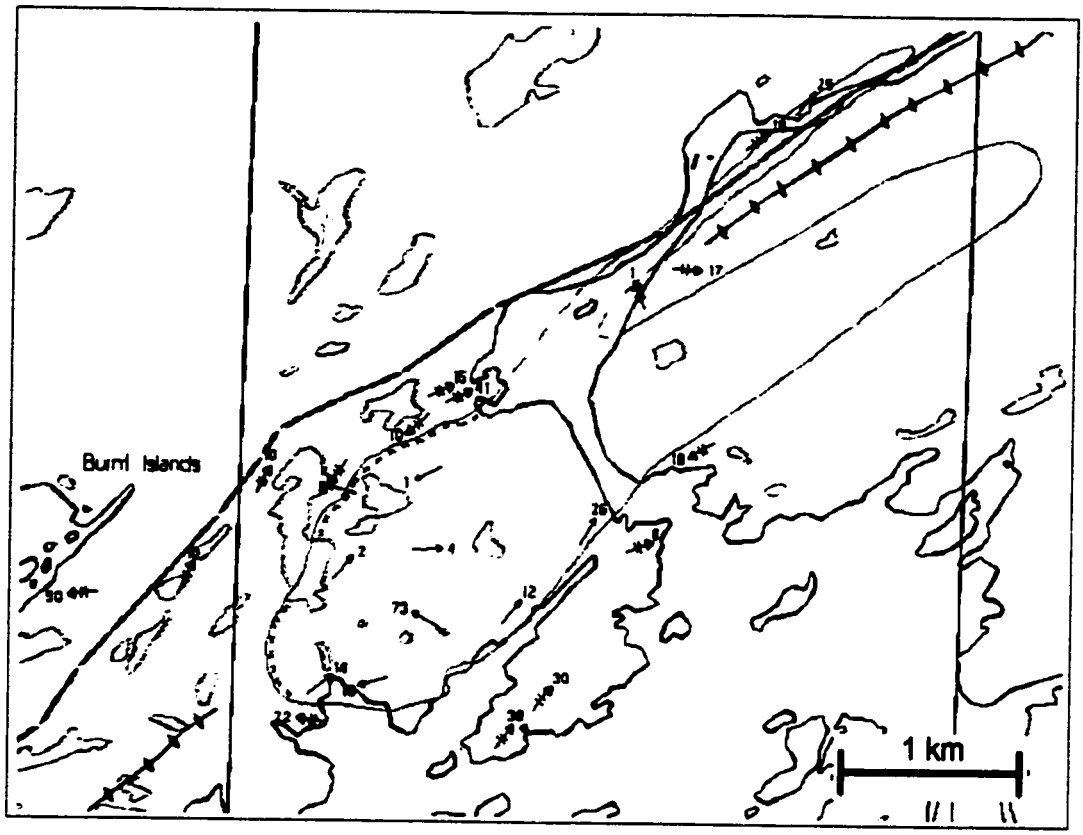
Burnt Islands
1 km

C)

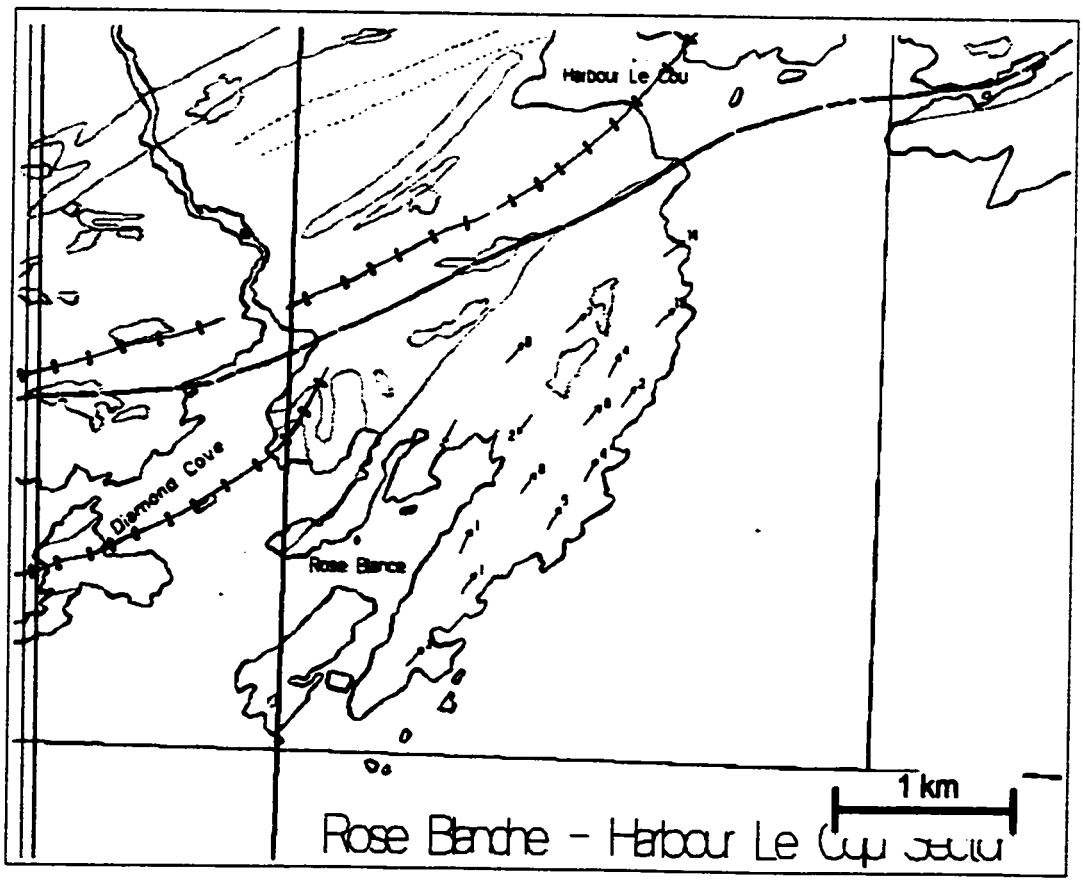
Harbour Le Cou
Diamond Cove
Rose Blanche
1 km
Rose Blanche - Harbour Le Cou

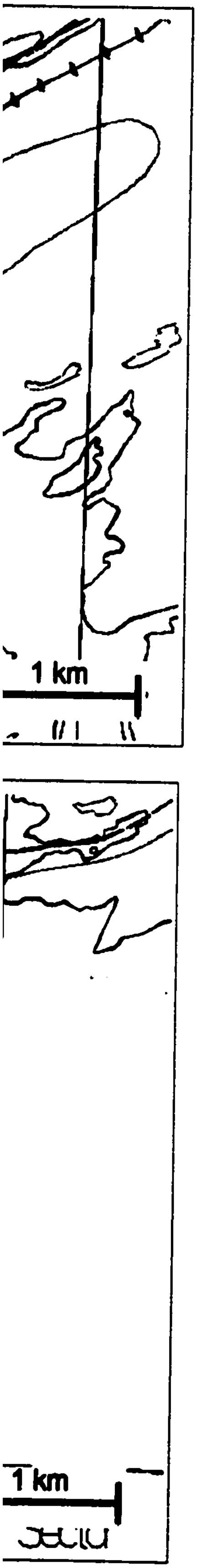

B)

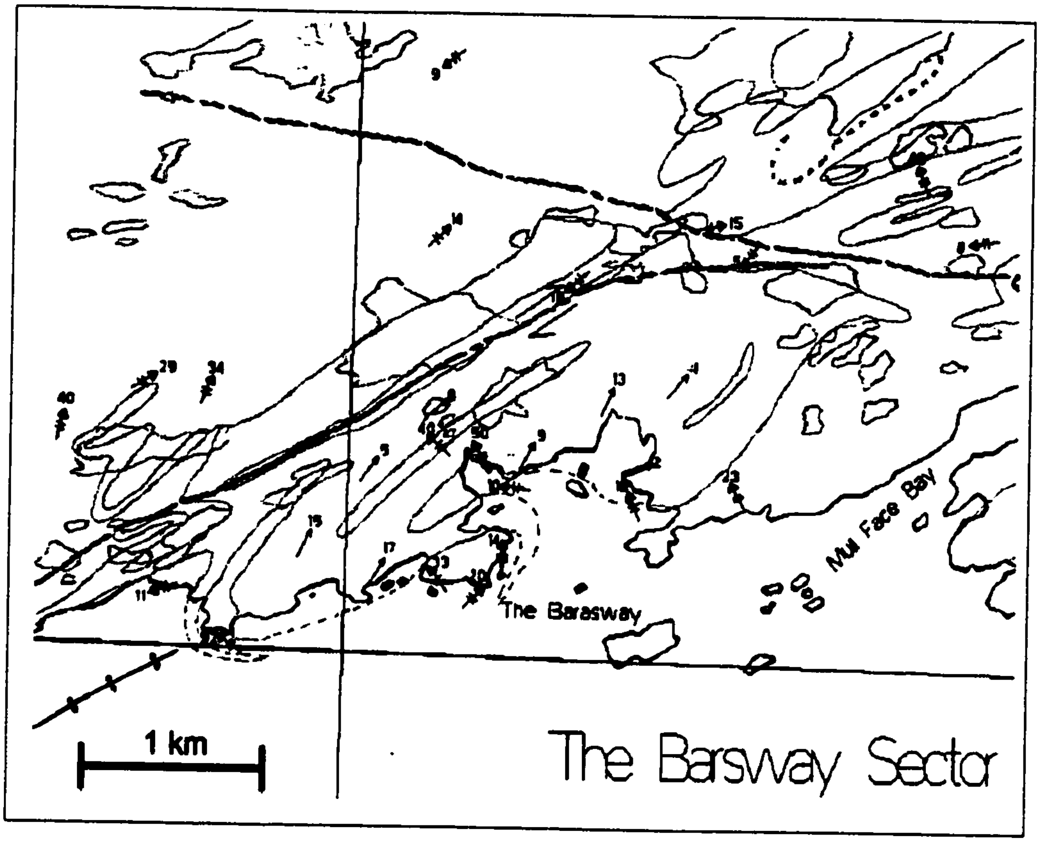

→ K_1

→ L_2

The rest of symbology is as defined in Maps 1 and 2.

Fig. 16. Patterns of K_1 and L_2 in A) Burnt Islands, B) The Barasway, and C) Rose Blanche-Harbour Le Cou sectors.

A)

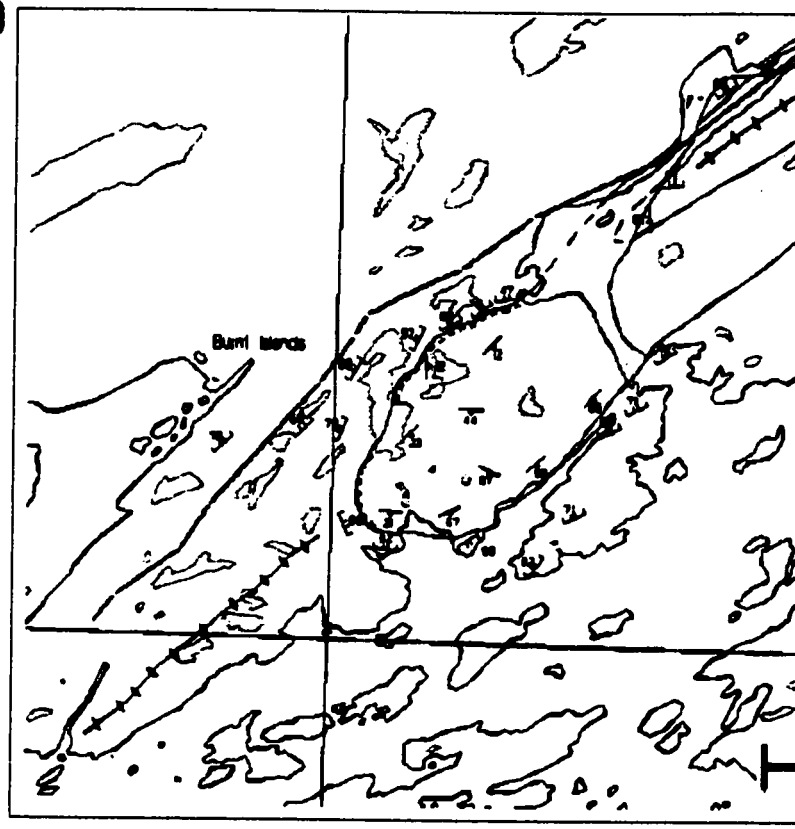

C)

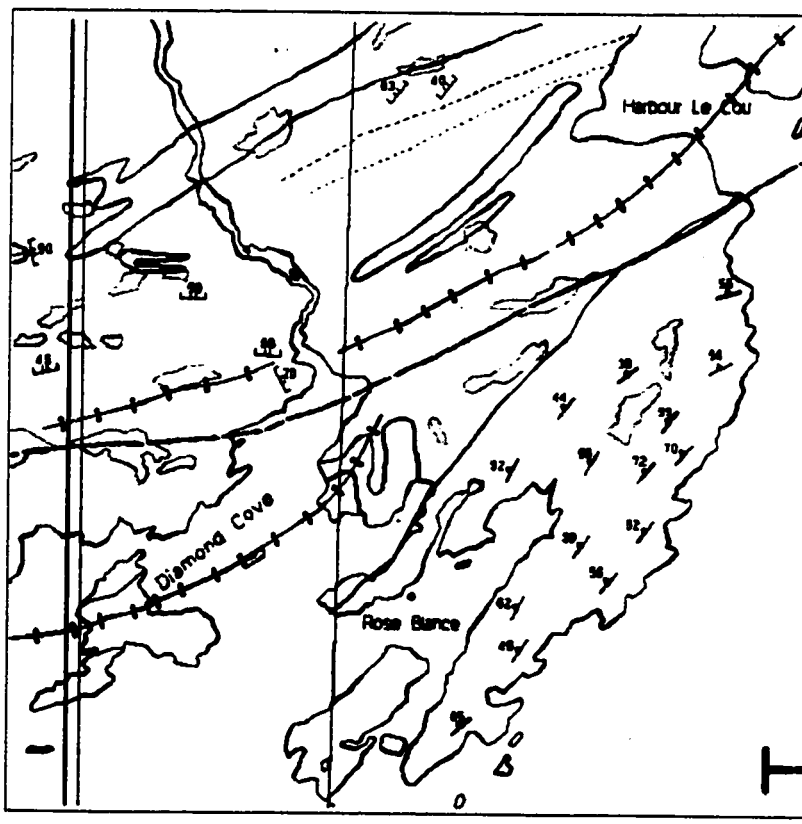

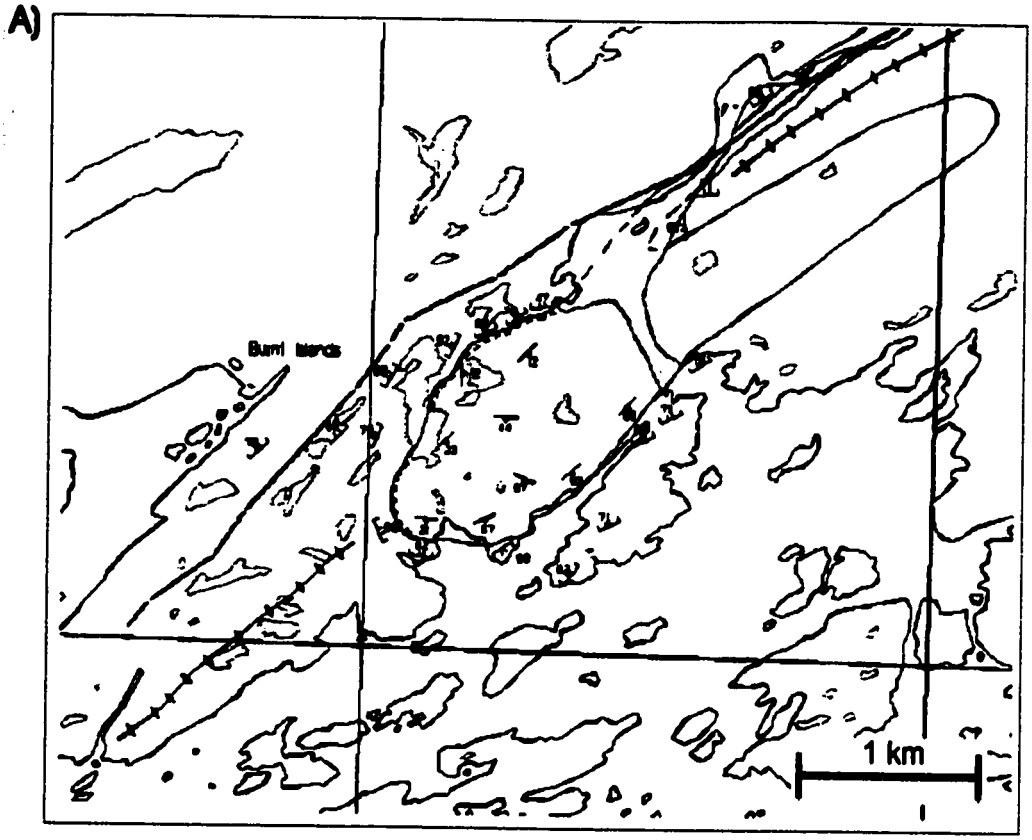

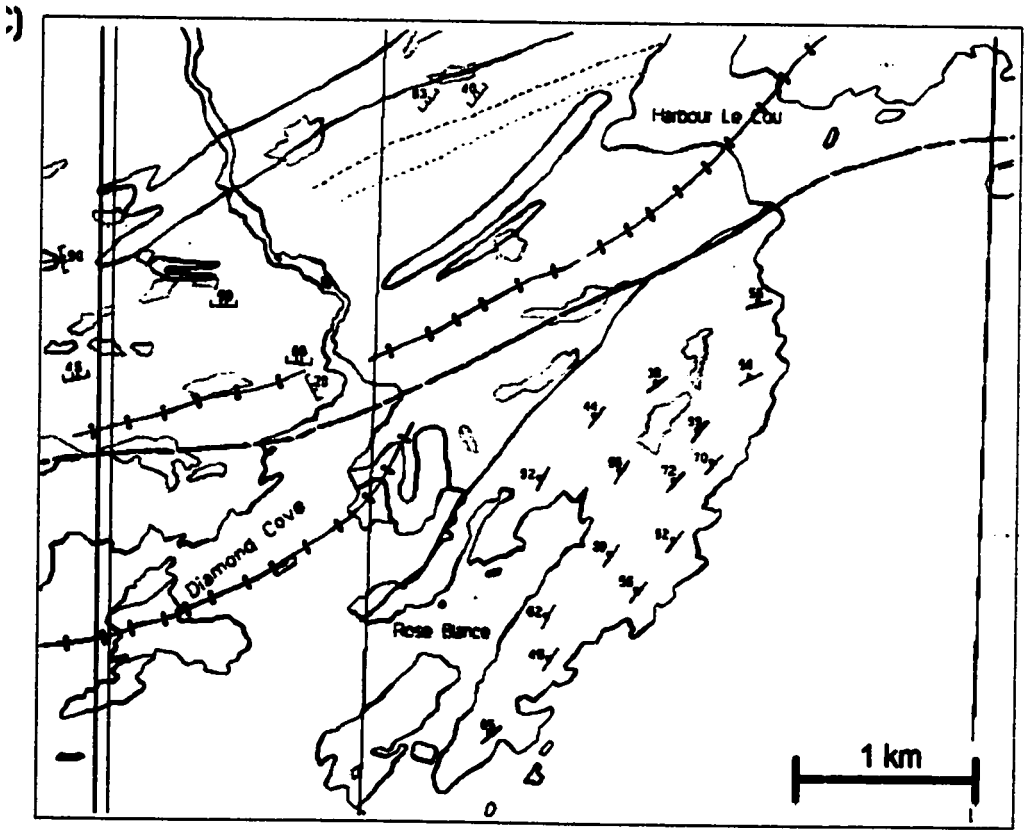

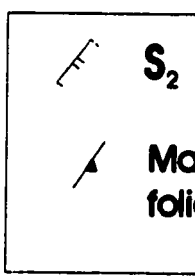

Fig. 17. K
foliations,
B) The Bara
sectors. Sy
1 and 2.

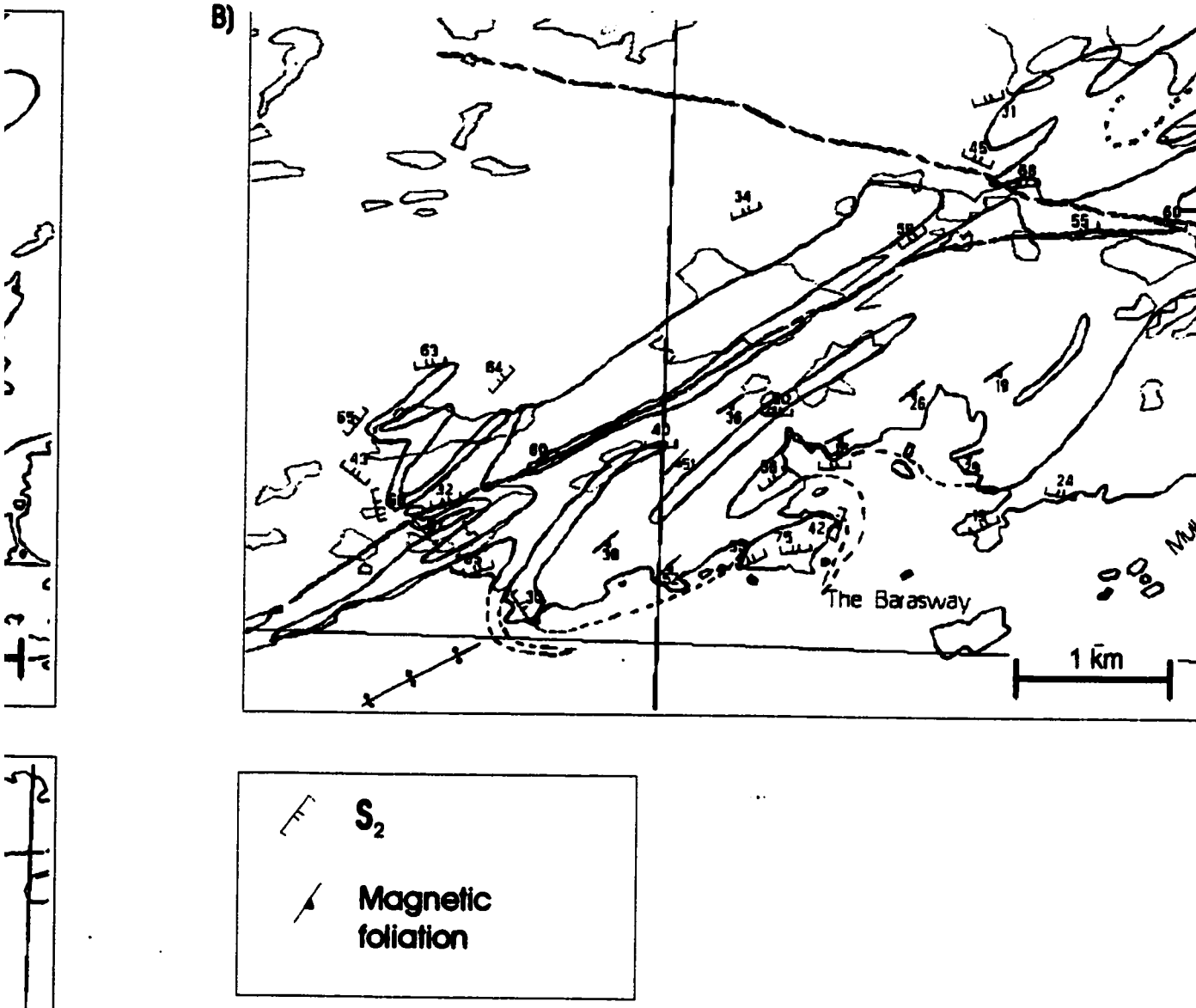

Fig. 17. K_1 - K_2 planes, or magnetic foliations, in A) Burnt Islands, B) The Barasway, and C) Rose Blanche sectors. Symbology is as shown in Maps 1 and 2.

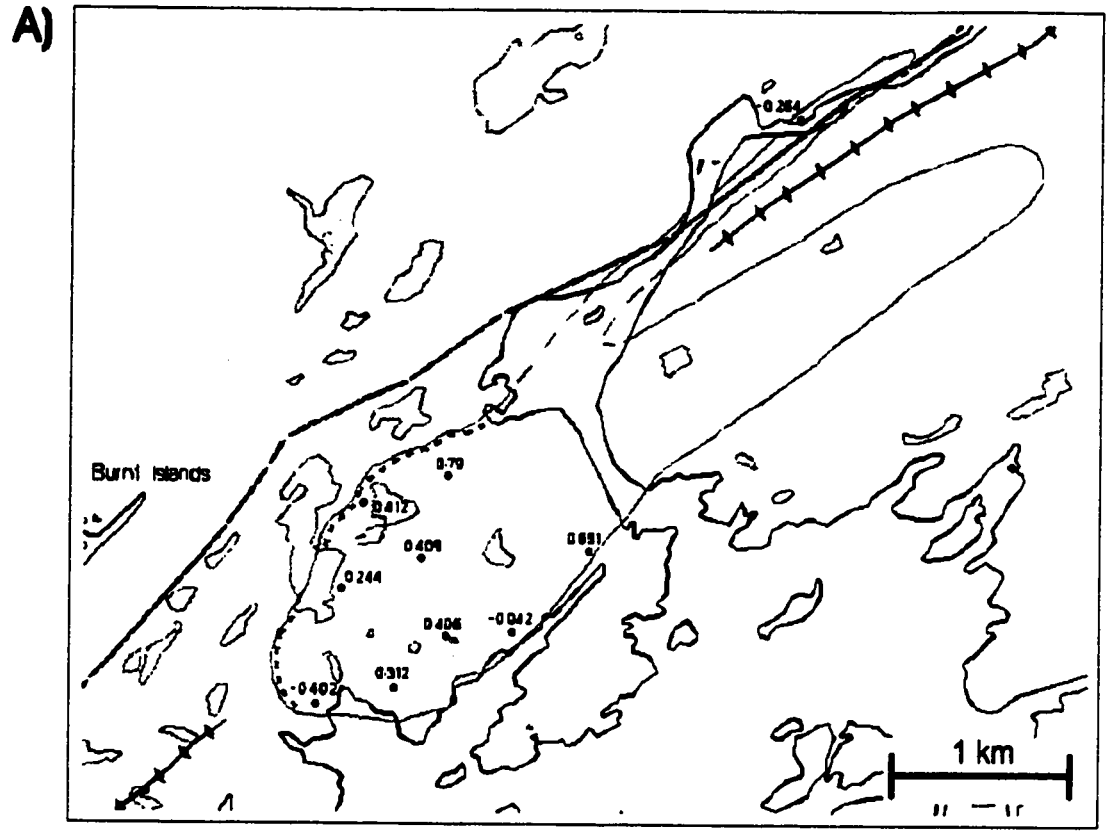

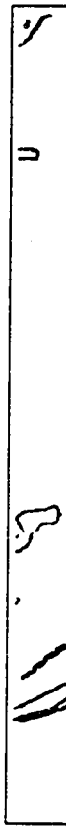

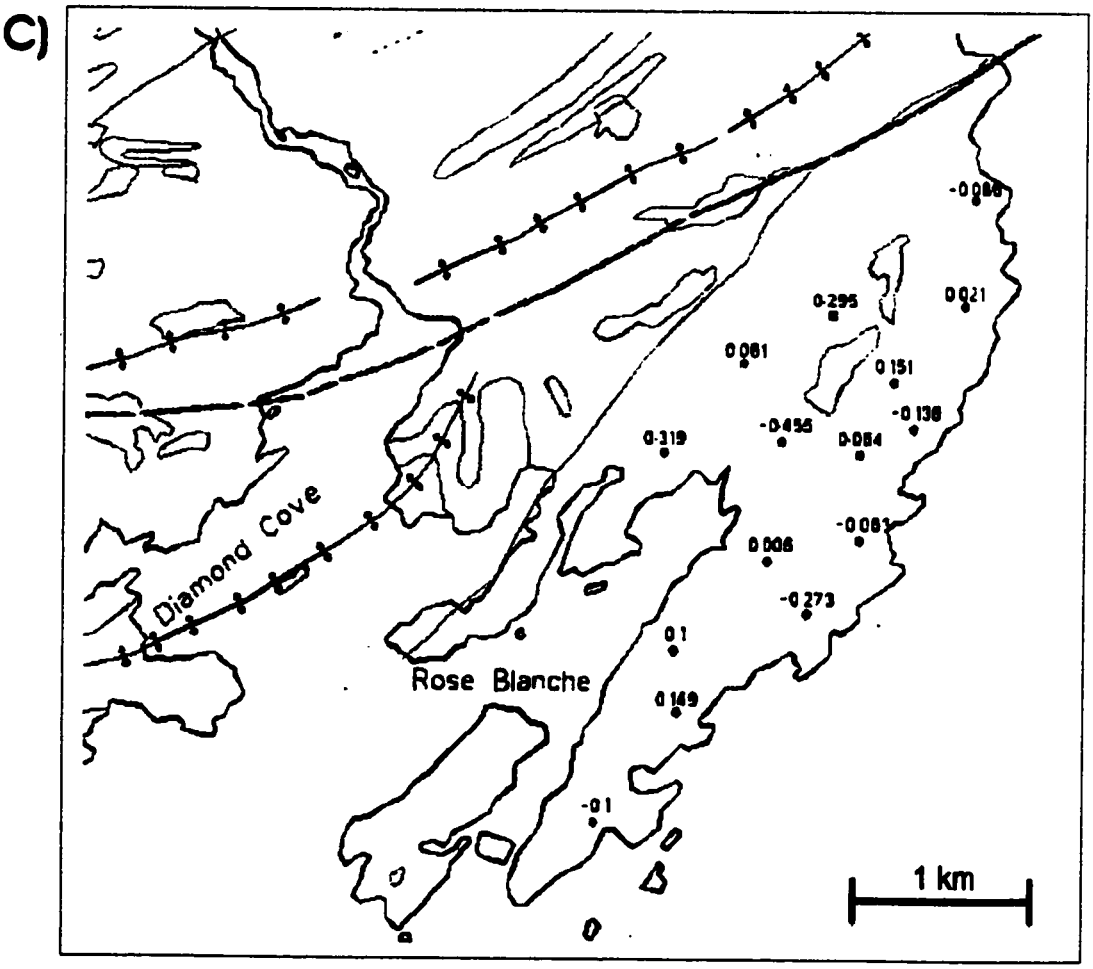

Fig.
Isla
Symb

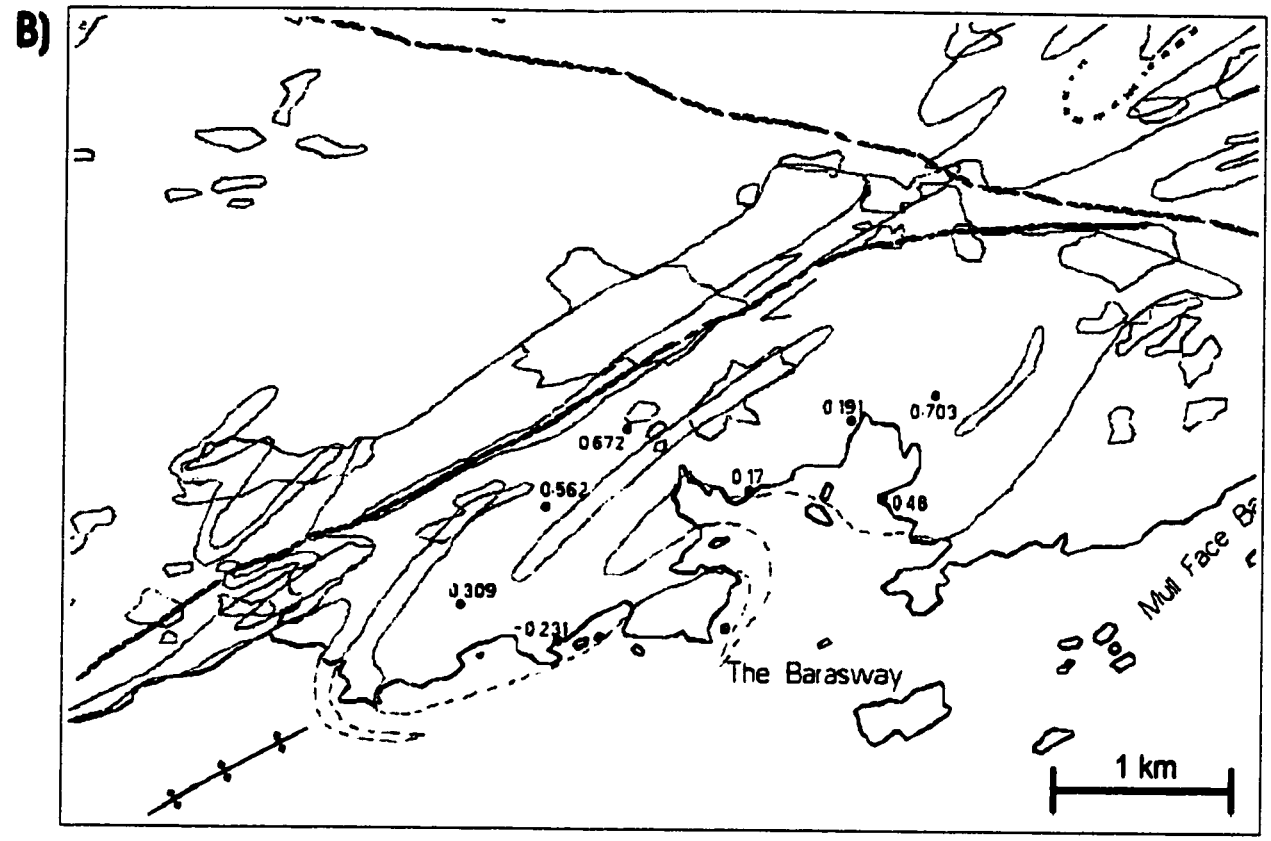

Fig. 19. Spatial distribution of the AMS shape parameter T in A) Burnt Islands, B) The Barasway, and C) Rose Blanche-Harbour Le Cou sectors. Symbology is as in Maps 1 and 2.

CHAPTER 6 - TIMING AND MODEL OF EMPLACEMENT - A DISCUSSION.

6.1 Introduction.

Granite emplacement mechanisms are hotly debated topics in the current scientific literature (e.g. Patterson and Fowler, 1993). Emplacement of plutons may involve a combination of several processes such as diapirism, magma transport by fracture propagation (Clements and Mawer, 1992), stoping, and buoyancy-driven ascent along shear zones. Different processes may dominate at different structural levels within the crust in response to changes in rheology and metamorphic conditions. When a particular process is clearly dominant it is expected to produce a characteristic structural signature. For example, diapirism and post-emplacement ballooning will result in a significant deflection of the regional fabrics and possible formation of foliation triple points (Guglielmo, 1993). An emplacement model can be proposed only if the relative timing of

emplacement can be established, as pre-tectonic, post-tectonic and syn-tectonic scenarios can often produce similar end-result structures (Guglielmo, 1993).

6.2 Emplacement of the RBG.

In Chapters 4 and 5 it was demonstrated that all of the RBG exposures in the thesis field area contain a solid-state fabric which is coaxial with the main D_2 fabric in the wall rocks. Many of the HLCG-RBG contacts have concordant-discordant geometry with respect to S_2. Larger plutons are largely concordant bodies with laccolithic shapes, as demonstrated in Chapter 4 (Fig. 12, A and B).

Mechanics of laccolith emplacement and growth have been described in detail by Corry (1988). Following his classification, granite bodies mapped out in the Barasway and Rose Blanche-Harbour Le Cou sectors (Maps 1 and 2) have geometries characteristic of Christmas-tree laccoliths. Christmas-tree laccoliths most frequently form at mid-crustal levels, where the ductile rheology of the wall rocks

more readily accommodates the mechanics of emplacement (Corry, 1988).

Corry (1988) describes the emplacement and growth of laccoliths in four stages: 1 - transport of magma vertically through the lithosphere; 2 - cessation of vertical transport transport of the magma and onset of horizontal spreading; 3 - cessation of horizontal spreading and commencement of vertical thickening; 4 - large scale deformation of the overburden. Clements and Mawer (1992) present a model which describes the mechanics of magma transport through the crust in propagating fractures. According to their model, when a propagating fracture encounters a ductile zone in the crust, it's progress is arrested and the transported magma spreads laterally forming laccolithic shapes (Clements and Mawer, 1992). The fact that larger RBG intrusions are frequently associated with migmatites is consistent with this hypothesis. The RBG magma could have been generated by partial melting at lower crustal levels, transported upwards in dykes, and emplaced as laccoliths when the dykes encountered a zone of migmatization. Structures shown in Fig. 12 B, where the first sill of a laccolith intrudes

immediately above a mapped-out zone of migmatite, are particulary indicative of this scenario.

Migmatites observed in the field area also preserve evidence for melt formation and segregation. Frequently observed networks of melt-filled veins cross-cutting folded psammite beds, and occurrence of stromatic migmatites with leucosome offshoots which cross-cut the foliation and intrude small scale shear zones (leucosome entering c' shears in Plate 9 B) suggest that melting was accompanied by fluid overpressure-driven fracturing and subsequent magma transport in dykes. This is also consistent with the model of Clements and Mawer (1992). What is the genetic relationship between the larger RBG plutons and the migmatites?

Metamorphic work of Burgess et al. (1995) shows that the promontory-promontory collision of Laurentia and Gondwana was accompnied by clock-wise P-T-t path. Peak metamorphic conditions reached the levels necessary for anatectic melting (Whitney, 1988) during D_2. Anatexis likely began in the pelitic units of the HLCG at temperatures close to 750°C via muscovite breakdown reactions such as:

Muscovite + Quartz + Na-Plag. = Sillimanite + K-spar + Liquid (Whitney, 1988).

This conclusion is supported by field observations indicating that migmatite melanosome is depleted in muscovite, and that the feldspar-rich psammite layers are involved in the melting (Plate 9 A). Burgess et al. (1995) also noted that the textural relationships evident in the leucosomes are indicative of crystallization of the constituent phases (K-feldspar, Plagioclase, and Quartz) from a melt and in-situ.

Structures showing leucosome concentrations in dilatant sites, such as the one shown in Plate 9 A, are indicative of leucosome movement parallel to the planes of the foliation via the dilatancy-pumping melt segregation mechanism (Brown, 1994). Regional deformation, therefore, must have played an important role in assisting the segregation of the magma from its HLCG source, although gravitational compaction of the restite must also have contributed to the process (Clements and Mawer, 1992).

Geochemical evidence summarized in Chapter 3 indicates that the most likely source for the RBG magma are the host

Harbour Le Cou Group rocks (Whalen et al., 1995). It is likely that many portions of the RBG suite were generated essentially in-situ, although clearly many of the larger intrusions were generated at lower structural levels, and emplaced as laccoliths after substantial vertical travel through the crust.

6.3 Timing of emplacement.

Structural, microstructural, and AMS data presented in Chapters 4 and 5 support the syn-D_2 emplacement scenario for the RBG suite. Arguments in support of this theory are summarized below.

None of the RBG exposures observed in the field area were found to contain dominantly D_3 fabrics. Structural, microstractural and AMS data presented in Chapters 4 and 5 show that the RBG plutons contain fabrics produced by solid-state, amphibolite-grade deformation which are coaxial with D_2 fabrics in the wall rocks. The plutons are folded by F_3. It was not possible to identify domains of magmatic fabrics and structures. By the onset of D_3 deformation at

greenschist grade, which is dated by Burgess et al. (1995) at 405 Ma, the RBG were completely crystallized sheets, geometrically oriented concordantly to the S_2 schistosity and containing a fairly well-developed solid-state fabric. This demonstrates that the granites intruded prior to the last episode of deformation which affected the thesis area - i.e. pre-D_3 emplacement.

Xenoliths of the HLCG country rocks included in the granite contain D_2 fabrics and structures (see Plates 6 A, 8 A and B). Also, numerous dykes, and many of the larger intrusions, cut across D_2 fabrics (Plates 6 B, 7 B, Figure 12). It is unlikely that D_2 fabrics could have formed in the xenoliths after they have been included in the granite. This demonstrates that the granites could not have been emplaced prior to the formation of D_2 fabrics - i.e. rules out a pre-D_2 emplacement scenario. The RBG suite must have been emplaced syn-D_2.

A number of other factors support syn-D_2 emplacement. The larger laccoliths and sheets are not folded by F_2 (Figure 12). There is close association between anatectic migmatites and RBG intrusions, and close agreement between the

geochronological dates of peak metamorphism and RBG crystallization. A U-Pb zircon age of 420 Ma (van Staal et al., 1994) determined from a sample collected in the Rose Blanche sector agrees with the minimum estimates of peak metamorphic conditions achieved during regional D_2 at 415±2 Ma (U-Pb on titanite, van Staal et al., 1995, Chapter 3).

If the granites were emplaced pre-D_2 then what would be the main factor controlling the level of emplacement of the larger plutons? The RBG would be intruding greenschist-grade, relatively rigid, epizonal rocks. If this was the case, the structural style of the laccoliths would be different. They would tend to be of the punched type (Corry, 1988). A relatively ductile crust, as would be the case during D_2, would favor the Christmas-tree style of emplacement (Corry, 1988) demonstrated for two of the RBG plutons. Syn-D_2 emplacement scenario provides the best explanation for all of the available evidence.

CHAPTER 7 - SUMMARY AND CONCLUSIONS, SUGGESTIONS FOR FURTHER WORK.

7.1 Summary and conclusions.

The Rose Blanche Granites are an example of a syn-tectonic, crustally-derived garnetiferous, two-mica granite suite which intrudes metasedimentary rocks of the Harbour Le Cou Group, Exploits Subzone of the Dunnage Zone - Newfoundland Appalachians. Four episodes of regional deformation have been observed in the HLCG metasediments. Bedding sub-parallel fabrics associated with D_1 have been poorly preserved due to strong transposition and overprinting by D_2, a peak metamorphism event linked to westerly directed overthrusting of the study area as a result of oblique collision between Gondwana and Laurentia. D_2 fabrics have been folded by steeply inclined periclinal southeast-verging F_3 folds developed during a later transpressional D_3 deformation. D_4 is manifested by late steeply-inclined dextral transcurrent shear zones of minor displacement which

cross-cut D_3 folds. Structural history recorded in the wall rocks is very similar to the regional structural and metamorphic histories described by workers studying regional deformation and metamorphism (Burgess et al., 1995; Dubé et al., 1996).

The RBG suite is composed of a multitude of centimeter to kilometer-scale dykes and sills some of which have preserved evidence for the existence of two phases: 1 - garnetiferous, leucocratic RBGrb phase; 2 - ilmenite and hornblende bearing RBGba phase. Field relations indicate that the two phases are cogenetic and have shared identical intrusive and structural histories. Larger plutons examined in the course of the thesis have sheet-like, and laccolithic geometries which are largely concordant with the regional S_2 fabric - the dominant fabric in the field area. Several of the large-scale RBG plutons are demonstrably folded by the regional D_3. The granites contain a weakly to moderately well developed fabric defined by preferential alignment of the micas and flattened quartz grains. AMS fabrics of the RBG are dominated by paramgnetic minerals - primarily biotite. Magnetic lineations (K_1) are sub-horizontal, tightly grouped, and coaxial with the stretching lineation in the

wall rocks - L_2. Poles to magnetic foliation (K_3) are coaxial with the poles to S_2, the main composite foliation in the HLCG. AMS shape fabrics are characterized by primarily oblate ellipsoid shapes and show no systematic spatial variation. Pluton geometries, internal fabrics, and field relations indicate that the RBG were most likely emplaced syn-D_2 during peak metamorphic conditions. Magma generation, segregation, transport and emplacement are consistent with the model of Clements and Mawer (1992).

Although the area examined in the course of this study is not of regional extent, findings of Dubé et al. (1996) Burgess et al. (1995), and Lin et al. (1993) support observations presented in the thesis. The RBG suite, in its entirety, represents a regional domain spanning hundreds of square kilometers. As such it represents a valuable example of generation and emplacement of granitic magma at mid-crustal level.

7.2 Suggestions for further work.

Data presented in the thesis offer two intriguing possibilities for further research:

1. Relationship between crustal anatexis, granite emplacement and movement along major shear zones - the Cape Ray Shear Zone, and the Bay Le Moine Shear Zone.
2. Relationship between quartz petrofabrics and AMS fabrics in folded RBG sheets.

The first avenue of research offers the possibility of obtaining valuable insights into the role of crustal anatexis in the structural evolution of an orogen. Near the northernmost extent of the RBG suite the granites are involved in the movements along the Cape Ray Shear Zone (Dube et al., 1996). A detailed structural and geochronological study of the relations between the RBG and this extremely important tectonic feature could shed considerable insight into the complex movement history along this fault.

The Bay Le Moine Shear Zone is another important tectonic feature which bounds the RBG suite to the east and north of the study area. This shear zone juxtaposes the HLCG with its greenshist-grade lithological and structural equivalent - Bay du Nord Group (Lin et al., 1993). Lin et al. (1993) report that the RBG are strongly sheared by the BLMSZ. A structural study of the granite intrusion in relation to the deformation history of this shear zone could constitute an interesting extension to this study, and provide insights into the relationship between crustal anatexis and the onset of tectonic denudation.

The second avenue of continuation is a more thematic study of the relationship between the two petrofabrics preserved in the deformed RBG - the biotite petrofabric - indirectly estimated using AMS analysis, and the quartz petrofabric - which will have to be studied using a different technique (such as x-ray texture goniometry or intensive universal stage work). The purpose of the investigation would be to establish the possible presence of deformation induced obliquity between AMS and quartz petrofabrics in order to yield a new shear sense indicator. This type of an

investigation would have one inherent difficulty. Because the RBG have been affected by more than one phase of deformation, determination of the episode responsible for the obliquity between the two fabrics (if any is found) will be of critical importance. Data presented in the thesis provide a solid framework for this avenue of research.

The geometry, timing of emplacement and structural history of several RBG intrusions have now been well constrained and it is possible to attempt a comparison between systematic variations in the quartz and biotite petrofabrics preserved in the granites. This will require more sampling in the Burnt Island, the Barasway, and Rose Blanche-Harbour Le Cou sectors in order to obtain a statistically robust sample population. The study should focus on finding a systematic change in the sense of the obliquity (similar to a transition from s-symmetry to w-symmetry to z-symmetry minor folds around the hinge of a larger fold for example) between the AMS fabric and the quartz petrofabric.

Reference List

Aranguen A. and Tubia J.M. (1992) Structural evidence for the relationship between thrusts, extensional faults and granite intrusions in the Variscan belt of Galicia (Spain). *Journal of Structural Geology*, **14**, no. 10, pp. 1229-1237.

Archanjo. and Bouchez J.L. (1994) The Pombal granite pluton: magnetic fabric, emplacement and relationships with the Brasiliano strike-slip setting of NE Brasil (Paraiba State). *Journal of Structural Geology*, **16**, no. 3, pp. 323-335.

Barbarin B. (1990) Granitoids: main petrogenetic classifications in relation to origin and tectonic setting. *Geological Journal*, **25**, pp. 227-238.

Benn K. (1994) Overprinting of magnetic fabrics in granites by small strains: numeric modelling. *Tectonophysics*, **233**, pp. 153-162.

Benn K., Genkin M., van Staal C. R., and Lin S. (1993) Structure and anisotropy of magnetic susceptibility of the Rose Blanch Granite, southwestern Newfoundland: kinematics and relative timing of emplacement. *Current*

Research, Part D; Geological Survey of Canada, **Paper 93-1D**, pp. 73-82.

Blachic J. D. (1975) Plastic-deformation mechanism in quartz: the effect of water. *Tectonophysics*, **27**, pp. 271-294.

Borradaile G.J. (1987) Anisotropy of magnetic susceptibility: rock composition versus strain. *Tectonophysics*, **138**, pp. 327-329.

-----(1991) Correlation of strain with anisotropy on magnetic susceptibility. *Pure and Applied Geophysics.*, **135**, pp. 16-29.

Borradaile G. J. (1988) Magnetic susceptibility, petrofabrics and strain. *Tectonophysics.*, **156**, p. 1.

Borradaile G. J., MacKenzie A., and Jensen Eleanor (1991) A study of colour changes in purple-green slate by petrological and rock-magnetic methods. *Tectonophysics.*, **200**, pp. 157-172.

Borradaile G. J., Puumala M., and Stupavsky M. (1992) Anisotropy of magnetic susceptibility as an indicator of strain and petrofabric in rocks bearing sulphides. *Tectonophysics.*, **202**, p. 309.

Bouchez J.L. and Gleizes G. (1995) Two-stage deformation of the Mont-Louis-Andorra granite pluton (Variscan Pyrenees) inferred from magnetic susceptibility anisotropy. *Journal of the Geological Society, London,* **152**, pp. 669-679.

Brown. M (1993) The generation, segregation, ascent and emplacement of granite magma: the migmatite-to-crustally-derived granite connection in thickened orogens. *Earth Science Reviews,* **36**, pp. 83-130.

Brown P. A. (1974) Basement-cover relationships in southwest Newfoundland., Ph. D. Thesis.: Memorial University of Newfoundland.

---(1977) *Geology of the Port Aux Basques map area (11 O/11).*, Mineral Development Division, Department of Mines and Energy, Government of Newfoundland and Labrador. **Report 77-2.**

---(1976) *Geology of the Rose Blanche map area (11 O/10) Newfoundland.*: St. John's, Newfoundland, Mineral Development Division, Department of Mines and Energy, Government of Newfoundland and Labrador. **Report 76-5.**

Brun J.P., Gapais D., Cogne J.P., Lerdu P., and Vigneresse J.L. (1990) The Flammanville Granite (Northwest

France): an unequivocal example of a syntectonically expanding pluton. *Geological Journal*, **25**, pp. 271-286.

Burgess J. L., Brown M., Dallmeyer R. D., and van Staal C. R. (1995) Microstructure, metamorphism, thermochronology and P-T-t deformation history of the Port aux Basques gneisses, south-west Newfoundland, Canada. *Journal of Metamorphic Geology*, **13**, pp. 751-776.

Cadman A. C., Graham Park R., Tarney J., and Halls H. C. (1992) Significance of anisotropy of magnetic susceptibility fabrics in Proterozoic mafic dykes, Hopedale Block, Labrador. *Tectonophysics.*, **207**, pp. 303-314.

Carmichael R. S. (1982) Magnetic properties of minerals and rocks. in *CRC Handbook of Physical Constants for Rocks.* (Editors. Weast R. C. and Ashe M. J.), Roca Baton, Fla., CRC Press, p. pp. 229-287.

Carter N. L., Christie J. M., and Griggs D. T. (1964) Experimental deformation and recrystallization of quartz. *Journal of Geology*, **72**, pp. 687-733.

Chen R. T. and Oertel G. (1991) Determination o March strain from phyllosilicate preferred orientation: a semi-numerical method. *Tectonophysics.*, **200**, pp. 173-185.

Chorlton L. B. (1983) Geological development of the southern Long Range mountains, southwest Newfoundland: a regional synthesis, Ph. D. Thesis: Memorial University of Newfoundland.

Clemens J.D. and Mawer C.K. (1992) Granitic magma transport by fracture propagation. *Tectonophysics*, **204**, pp. 339-360.

Corry C. E. (1988) Laccoliths; Mechanics of emplacement and growth. Geological Society of America Special Paper 220.

Evans J. P. (1988) Deformation mechanisms in granitic rocks at shallow crustal levels. *Journal of Structural Geology*, **10**, pp. 437-443.

Fryer B. J., Kerr A., Jenner G. A., and Longstaffe F. J. (1992) Probing the crust with plutons: Regional isotopic geochemistry of granitoid intrusions across insular Newfoundland. *Current Research Newfoundland Department of Mines and Energy, Geological Survey Branch*, **Report 92-1**, pp. 119-139.

Genkin M. B., Benn K., and van Staal C. R. (1993) Structure, microstructure and AMS of the Rose Blanche Granites, southwestern Newfoundland., GAC/MAC Joint Annual Meeting, Edmonton.

Gugielmo G. (1993) Interference between pluton expansion and non-coaxial tectonic deformation: three-dimentional computer model and field implications. *Journal of Structural Geology*, **15**, no. 3-5, pp. 593-608.

Guglielmo G. (1993) Magmatic strains and foliation triple points of the Merrimac plutons, northern Sierra Nevada, California: implications for pluton emplacement and timing of subduction. *Journal of Structural Geology*, **15**, no. 2, pp. 177-189.

Henry B. (1989) Magnetic fabric and orientation tensor of minerals in rocks. *Tectonophysics.*, **165**, pp. 21-27.

Hibbard J. (1979) Myrmekite as a marker between preaqueous and postaqueous phase saturation in granitic systems. *Geological Society of America Bulletin.*, **90**, pp. 1047-1062.

Hirt A.M., Evans K.F., and Engelder T. (1995) Correlation between magnetic anisotropy and fabric for Devonian

shales on the Appalachian Plateau. *Tectonophysics*, **247**, pp. 121-132.

Hrouda F. (1987) Mathematical model relationship between the paramagnetic anisotropy and strain in slates. *Tectonophysics*, **142**, pp. 323-327.

Hrouda F. and Janak F. (1971) A study of some red sediments on the basis of their magnetic susceptibility anisotropy. *Sedimentary Geology.*, **6**, pp. 187-199.

Jeffrey G.B. (1922) The motion of ellipsoidal particles immersed in a viscous fluid. *Proceedings of the Royal Society of London*, **Ser. A, 102**, pp. 161-179.

Jover O., Rochette P., Lorand J.P., Maeder M., and Bouchez J.L. (1989) Magnetic mineralogy of some granites from the French Massif Central: origin of their low-field susceptibility. *Physics of the Earth and Planetary Interiors*, **55**, pp. 79-92.

Karlstrom K.E., Miller C.F., Kingsbury J.A., and Wooden J.L. (1993) Pluton emplacement along an active ductile thrust zone, Piute Mountains, southeastern California: Interaction between deformational and solidification

processes. *Geological Society of America Bulletin*, **105**, pp. 213-230.

Lafrance B. and Williams P. F. (1992) Silurian deformation in eastern Notre Dame Bay, Newfoundland. *Canadian Journal of Earth Sciences.*, **29**, pp. 1899-1914.

Lagarde J. L., Omar S. A., and Roddaz R. (1990) Structural characteristics of granitic plutons emplaced during weak regional deformation: examples from late Carboniferous plutons, Morocco. *Journal of Structural Geology.*, **12**, no. 7, pp. 805-821.

Lin S., van Staal C. R., and Lee C. (1993) The Harbour le Cou Group and its correlation with the Bay du Nord Group, southwestern Newfoundland. *Current Research, Part D; Geological Survey of Canada*, **Paper 93-1D**, pp. 57-64.

March A. (1932) Mathematische theorie der reglung nach der korngestalt bei affiner deformation. *Z. Krist.*, **81**, pp. 285-297.

Melka R., Schulmann K., Schlmannova B., Hrouda F., and Lobkowicz M. (1992) The evolution of perpendicular linear fabrics in synkinematically emplaced tourmaline

granite (central Moravia-Bohemian Massif). *Journal of Structural Geology*, **14**, no. 5, pp. 605-620.

Nicolas A. and Poirier J. P. (1976) Crystalline plasticity and solid state flow in metamorphic rocks. Toronto, John Wiles & Sons.

Olivier Ph. and Archanjo C.J. (1994) Magnetic and magmatic structures of the Emmas granodioritic pluton (Cachoeirinha belt, NE Brazil). Relationships with Pan-African strike-slip fault systems. *Tectonophysics*, **229**, pp. 239-250.

Owens W.H. (1974) Mathematical model studies on factors affecting the magnetic anisotropy of deformed rocks. *Tectonophysics*, **24**, pp. 115-131.

Paterson S.R., Vernon R.H., and Tobisch O.T. (1989) A review of criteria for the identification of magmatic and tectonic foliations in granitoids. *Journal of Structural Geology*, **11**, no. 3, pp. 349-363.

Patterson S. R. and Fowler T. K. Jr. (1993) Re-examining the pluton emplacement processes. *Journal on Structural Geology*, **15**, no. 2, pp. 191-206.

Potter D. K. and Stephenson A. (1990) Field-impressed anisotropies of magnetic susceptibility and remanence in minerals. *Journal of Geophysical Research*, **95**, no. B10, pp. 15,573-15,588.

Pryer L. L. (1993) Microstructures in feldspars from a major crustal thrust zone: the Grenville Front, Ontario, Canada. *Journal of Structural Geology.*, **15**, pp. 21-36.

Quinlan G. M., Hall J., Williams H., Wright J. A., Colman-Sadd S. P., O'Brien S., Stockmal G. S., and Marillier F. (1992) Lithoprobe onshore seismic reflection transects across the Newfoundland Appalachians. *Canadian Journal of Earth Sciences*, **29**, pp. 1865-1877.

Richter C., Frisch W., Ratschbacher L., and Schwartz H. (1991) The magnetic fabrics of experimentally deformed artificial clay-water dispersions. *Tectonophysics*, **200**, pp. 143-155.

Rochette P. (1987) Magnetic susceptibility of the rock matrix related to magnetic fabric studies. *Journal of Structural Geology*, **9**, no. 8, pp. 1015-1020.

-----(1988) Mathematical model relationship between the paramagnetic anisotropy and strain in slates-discussion. *Tectonophysics*, **156**, pp. 313-315.

Rochette P. and Fillion G. (1988) Identification of multicomponent anisotropies in rocks using various field and temperature values in a cryogenic magnetometer. *Physics of the Earth and Planetary Interiors*, **51**, pp. 379-386.

Rochette P., Scaillet B., Guillot S., Le Fort P., and Pecher A. (1994) Magnetic properties of the High Himalayan leucogranites: Structural implications. *Earth and Planetary Science Letters*, **126**, pp. 217-234.

Schofield D. I., Winchester J. A., and van Staal C. R. (1993) The Isle aux Morts metabasalt, southwest Newfoundland. *Current Research, Part D, Geological Survey of Canada*, **Paper 93-1D**, pp. 39-46.

Simpson C. and Wintsch R. P. (1989) Evidence for deformation-induced K-feldspar replacement by myrmekite. *Journal of Metamorphic Geology*, **12**, pp. 261-275.

Stel H. and Breedveld M. (1990) Crystallographic orientation patterns of myrmekitic quartz: a fabric memory in quartz ribbon-bearing gneisses. *Journal of Structural Geology.*, **12**, pp. 19-28.

Strong D. F. and Dickson W. L. (1978) Geochemistry of Paleozoic granitoid plutons from contrasting tectonic zones of northeast Newfoundland. *Canadian Journal of Earth Sciences*, **15**, pp. 145-156.

Sun W., Hudleston P.J., and Jackson M. (1995) Magnetic and petrofabric studies in the multiply deformed Thompson Formation, east-central Minnesota. *Tectonophysics*, **249**, pp. 109-124.

Tobisch O.T., Renne P.R., and Saleeby J.B. (1993) Deformation resulting from regional extension during pluton ascent and emplacement, central Sierra Nevada, California. *Journal of Structural Geology*, **15**, no. 3-5, pp. 609-628.

Tullis J., Christie J. M., and Griggs D. T. (1973) Microstructures and preferred orientations of experimentally deformed quartzites. *Geological Society of America Bulletin*, **84**, pp. 297-314.

Urai J. L., Means W. D., and Lister G. S. (1986) Mineral and rock deformation: laboratory studies. The Paterson Volume. (editors. Hobbs B. E. and Heard H.C.), Washington D. C., American Geophysical Union, p. 324 p.p.

van Staal C. R., Hall L., Schofield D., and Valverde P. (1996) Geology, Port aux Basques, Newfoundland (part of NTS 11-O/11). *Geological Survey of Canada, Open File 3165, scale 1:25000.*

van Staal C. R. (1994) Brunswick subduction complex in the Canadian Appalachians: Record of the Late Ordovician to Late Silurian collision between Laurentia and the Gander margin of Avalon. *Tectonics*, **13**, no. 4, pp. 946-962.

van Staal C. R., Dunning G., Valverde P., Burgess J., and Brown M. (1994) Arenig and younger evolution of the Gander margin: a comparison of the New Brunswick and Newfoundland segments. *Atlantic Geology*, **30**, no. 2, pp. 178-179.

van Staal C. R. and Williams P. F. (1988) Collision along an irregular margin: a regional plate tectonic interpretation of the Canadian Appalachians: Discussion. *Canadian Journal of Earth Sciences.*, **25**, pp. 1912-1916.

van Staal C. R., Winchester J. A., Brown M., and Burgess J. L. (1992) A reconnaissance geotraverse through southwestern Newfoundland. *Current Research, Part D, Geological Survey of Canada*, **Paper 92-1D**, pp. 133-143.

van Staal C. R. (1988) Collision along an irregular margin: a regional plate tectonic interpretation of the Canadian Appalachians: Discussion. *Canadian Journal of Earth Sciences.*, **25**, pp. 1912-1916.

Vigneresse J.L. (1995) Control of granite emplacement by regional deformation. *Tectonophysics*, **249**, pp. 173-186.

Whalen J. B. (1989) The Topsails igneous suite, western Newfoundland: an Early Silurian subduction-related magmatic suite? *Canadian Journal of Earth Sciences*, **26**, pp. 2421-2434.

Whalen J. B., van Staal C. R., Jenner G. A., and Longstaffe F. J. (1995) Tectonostratigraphic zone correlation after promontory-promontory collision: geochemical and isotopic insights from southwestern Newfoundland. *(in press)*.

White S. (1977) Geological significance of recovery and recrystallization in quartz. *Tectonophysics*, **39**, pp. 143-170.

Whitney J.A. (1988) The origin of granite: The role and source of water in the evolution of granitic magmas. *Geological Society of America Bulletin*, **100**, pp. 1886-1897.

Williams H. (1979) Appalachian Orogen in Canada. *Canadian Journal of Earth Sciences*, **16**, pp. 792-807.

Williams H., Colman-Sadd S. P., and Swinden H. S. (1988) Tectonic-stratigraphic subdivisions of central Newfoundland. *in Current Research, Part B, Geological Survey of Canada.*, **Paper 88-1B**, pp. 91-98.

Wilson, J. T. (1966). Did the Atlantic close and then re-open? *Nature*. 211, pp.676-681.

Zavoyskiy V.N. (1982) Use of magnetic susceptibility tensor for solving problems in structural geology. *Izvestiya, Earth Physics*, **18**, no. 3, pp. 217-223.

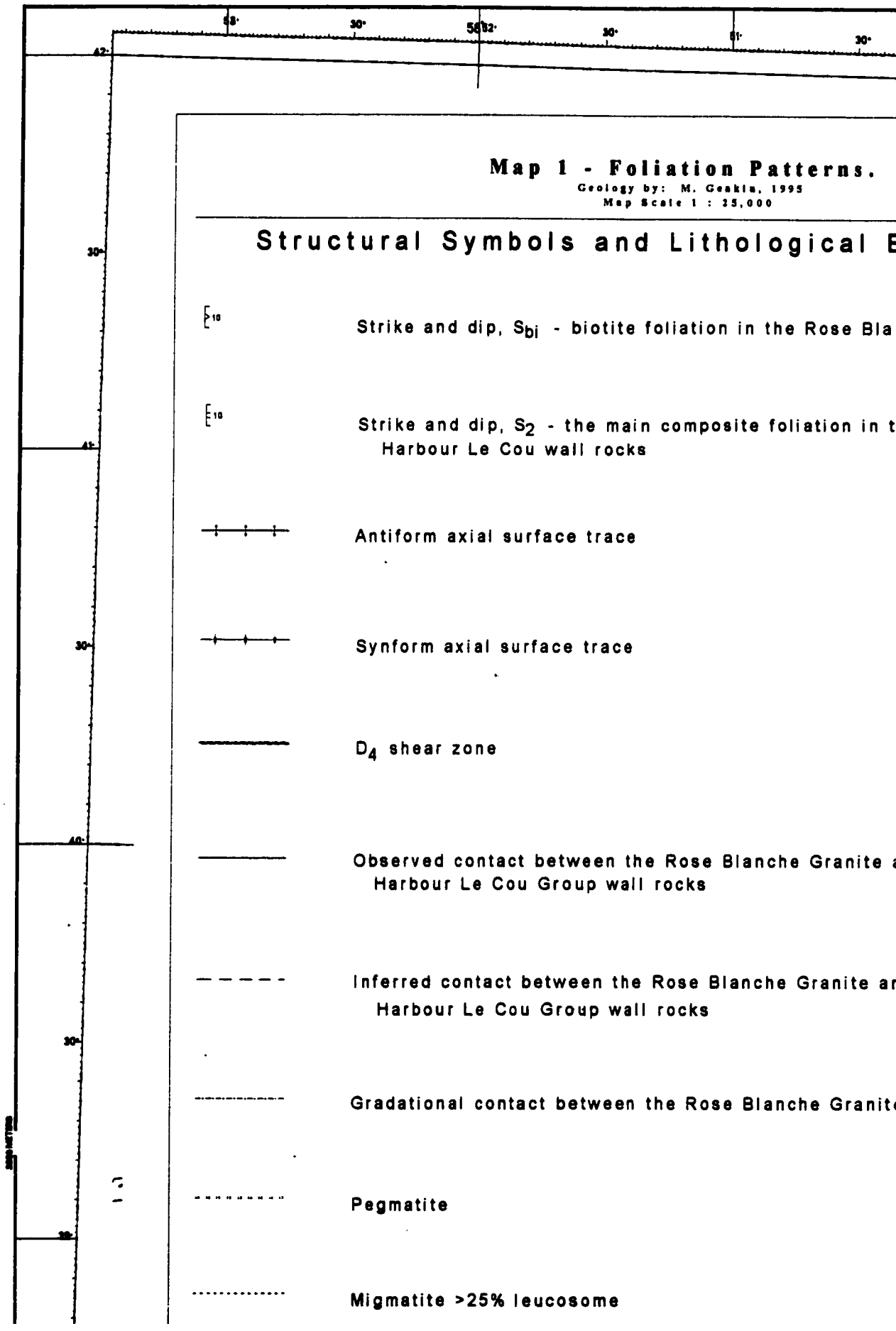

Map 1 - Foliation Patterns.

Geology by: M. Geskin, 1995
Map Scale 1 : 25,000

Structural Symbols and Lithological E

Strike and dip, S_{bi} - biotite foliation in the Rose Bla

Strike and dip, S_2 - the main composite foliation in t
Harbour Le Cou wall rocks

Antiform axial surface trace

Synform axial surface trace

D_4 shear zone

Observed contact between the Rose Blanche Granite a
Harbour Le Cou Group wall rocks

Inferred contact between the Rose Blanche Granite ar
Harbour Le Cou Group wall rocks

Gradational contact between the Rose Blanche Granit

Pegmatite

Migmatite >25% leucosome

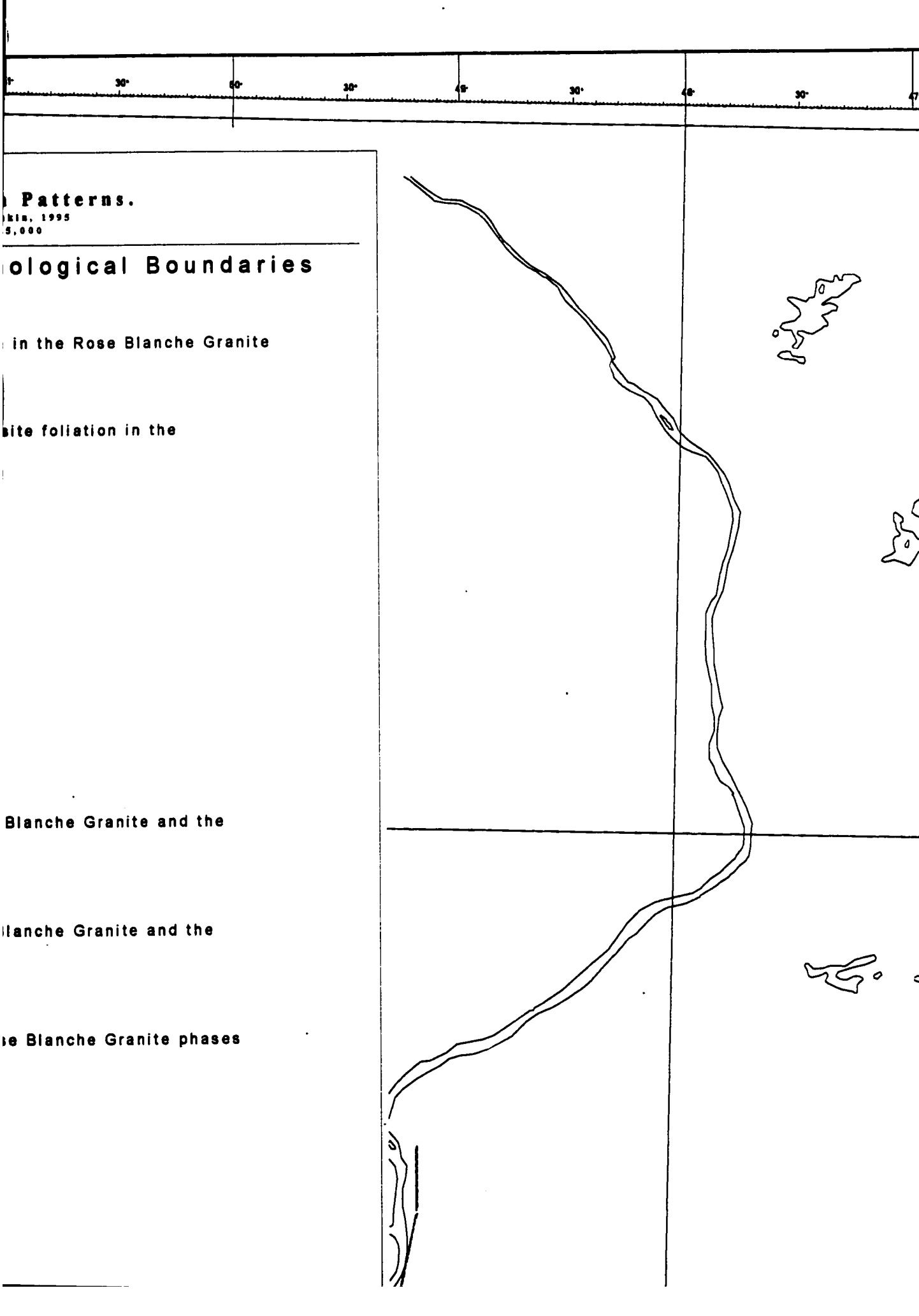

Patterns.

ological Boundaries

in the Rose Blanche Granite

ite foliation in the

Blanche Granite and the

lanche Granite and the

e Blanche Granite phases


30'
47°
30'
46°
30'
45°
30'
44°

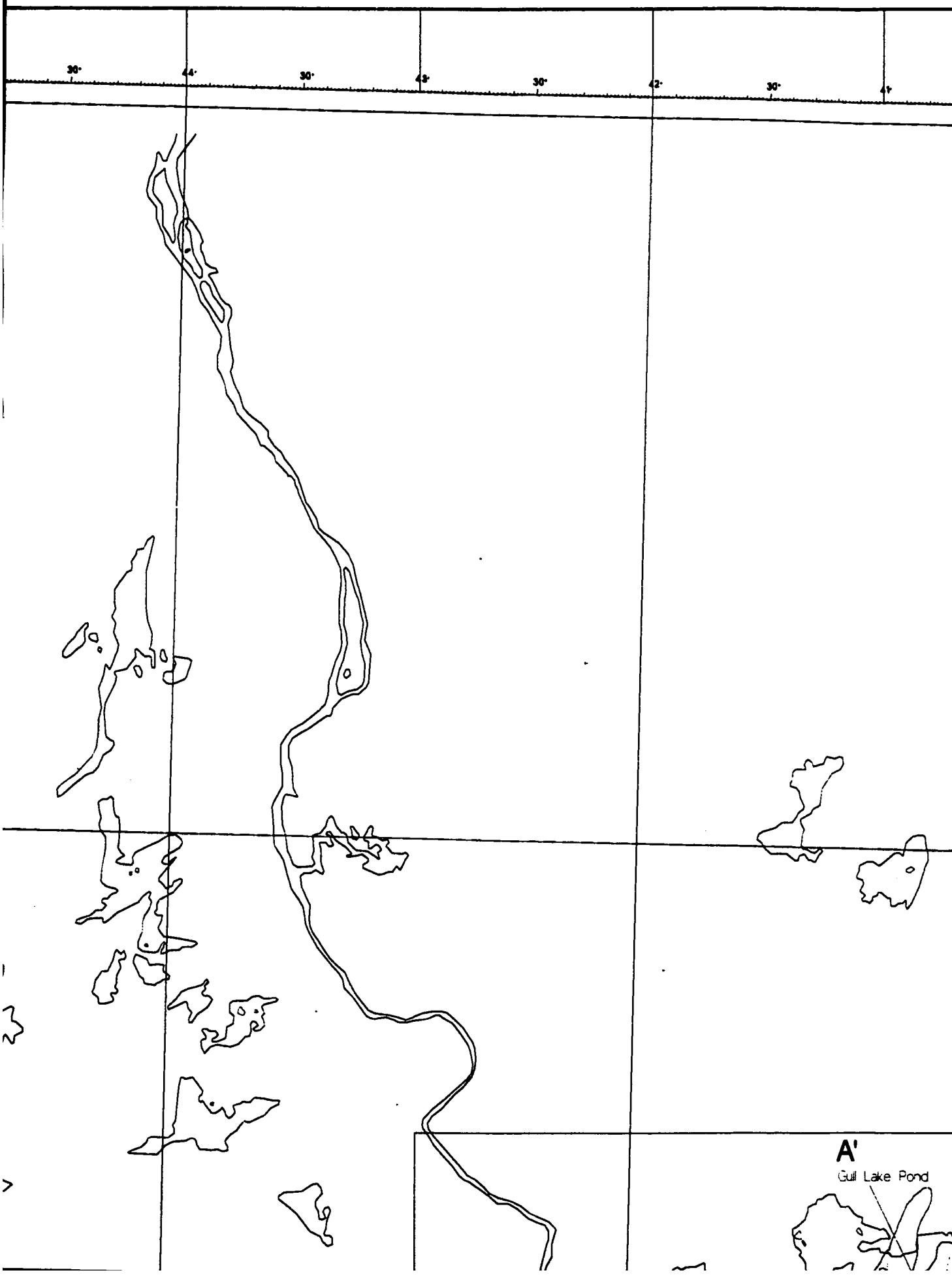
30'
44'
30'
43'
30'
42'
30'
41'
A'
Gull Lake Pond

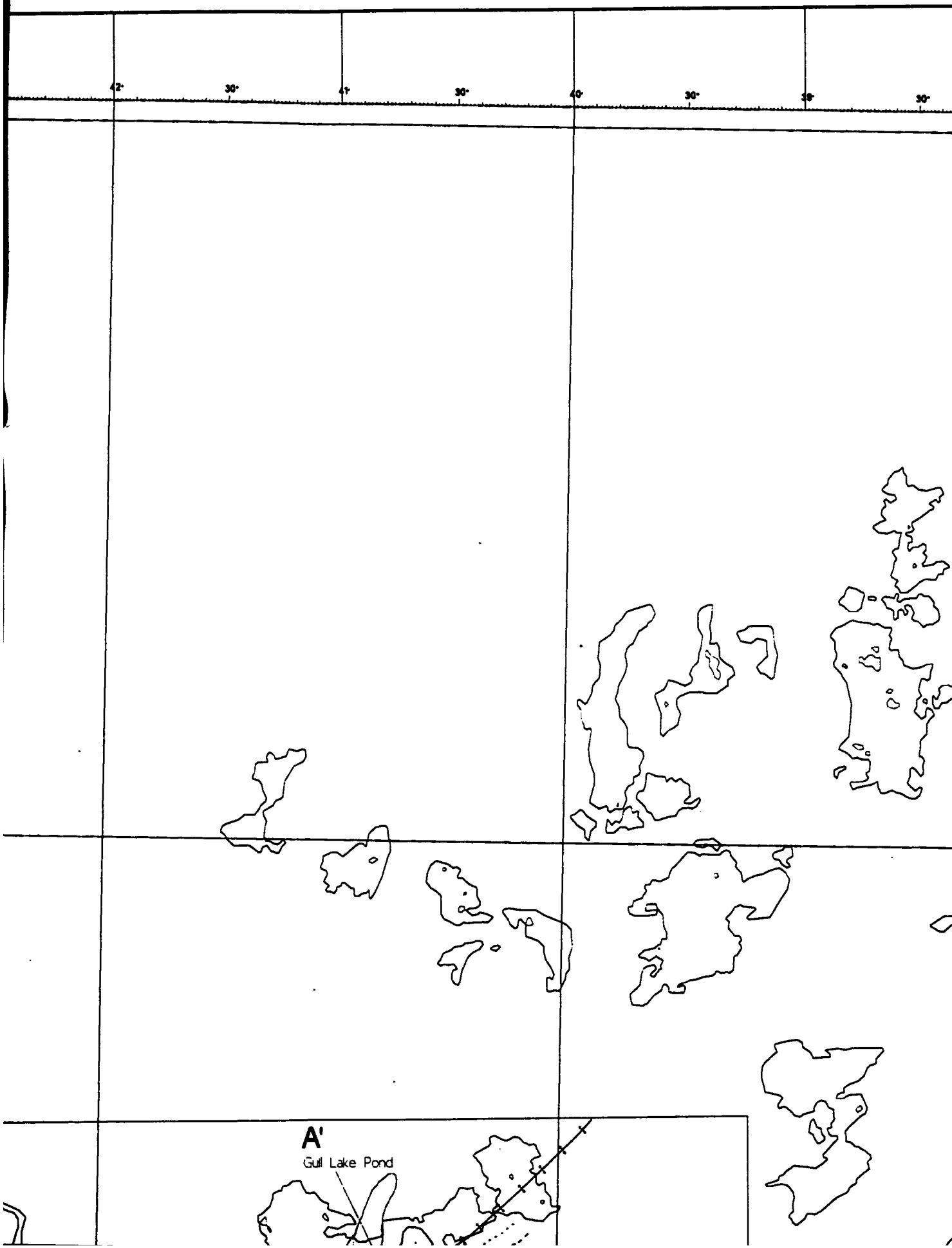
42°
30'
41°
30'
40°
30'
39°
30'
A'
Gull Lake Pond

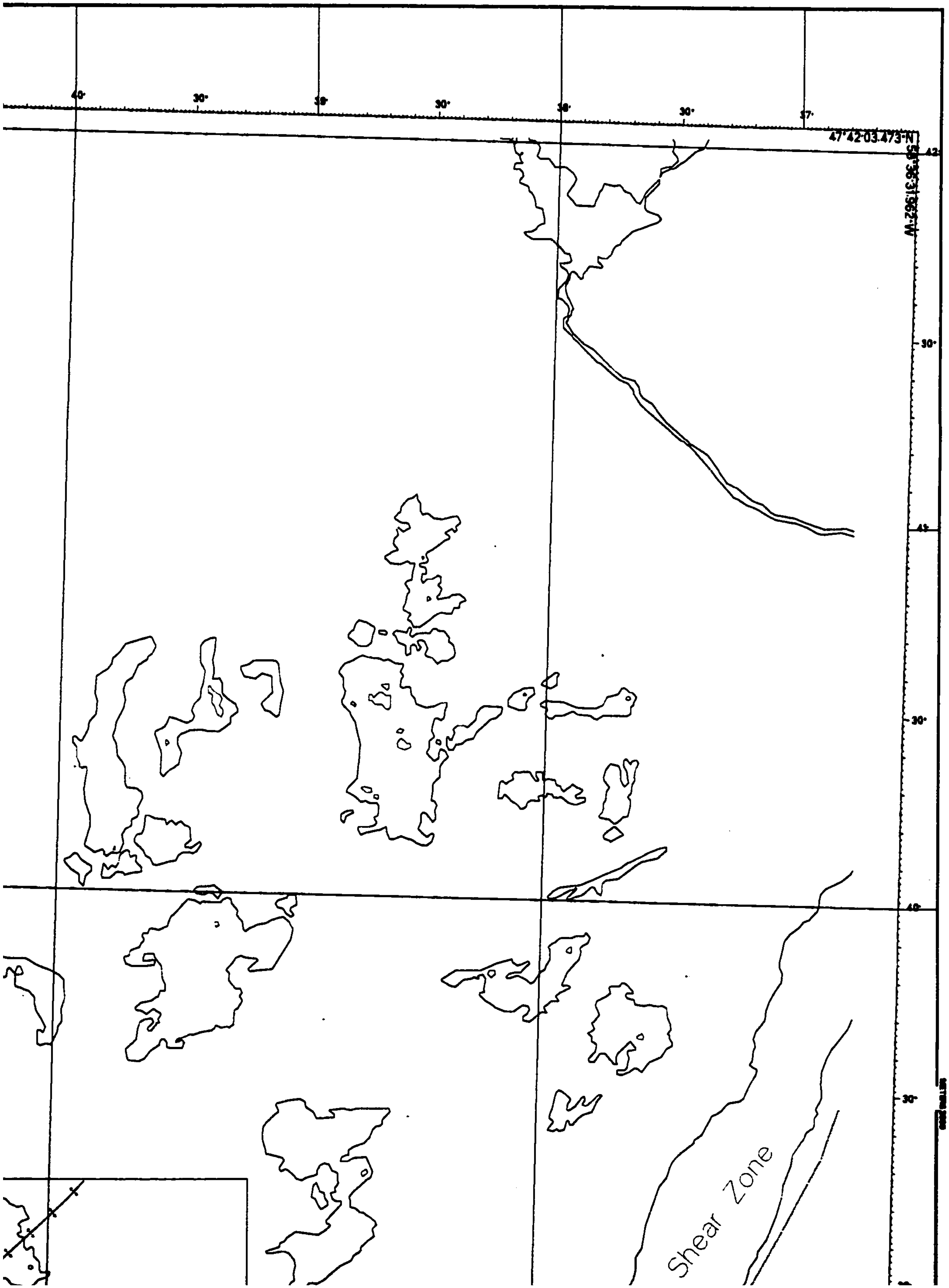
40'
30"
39'
30"
38'
30"
37'
47°42'03.473"N
36'31.962"W
42'
30"
41'
30"
40'
30"
Shear Zone

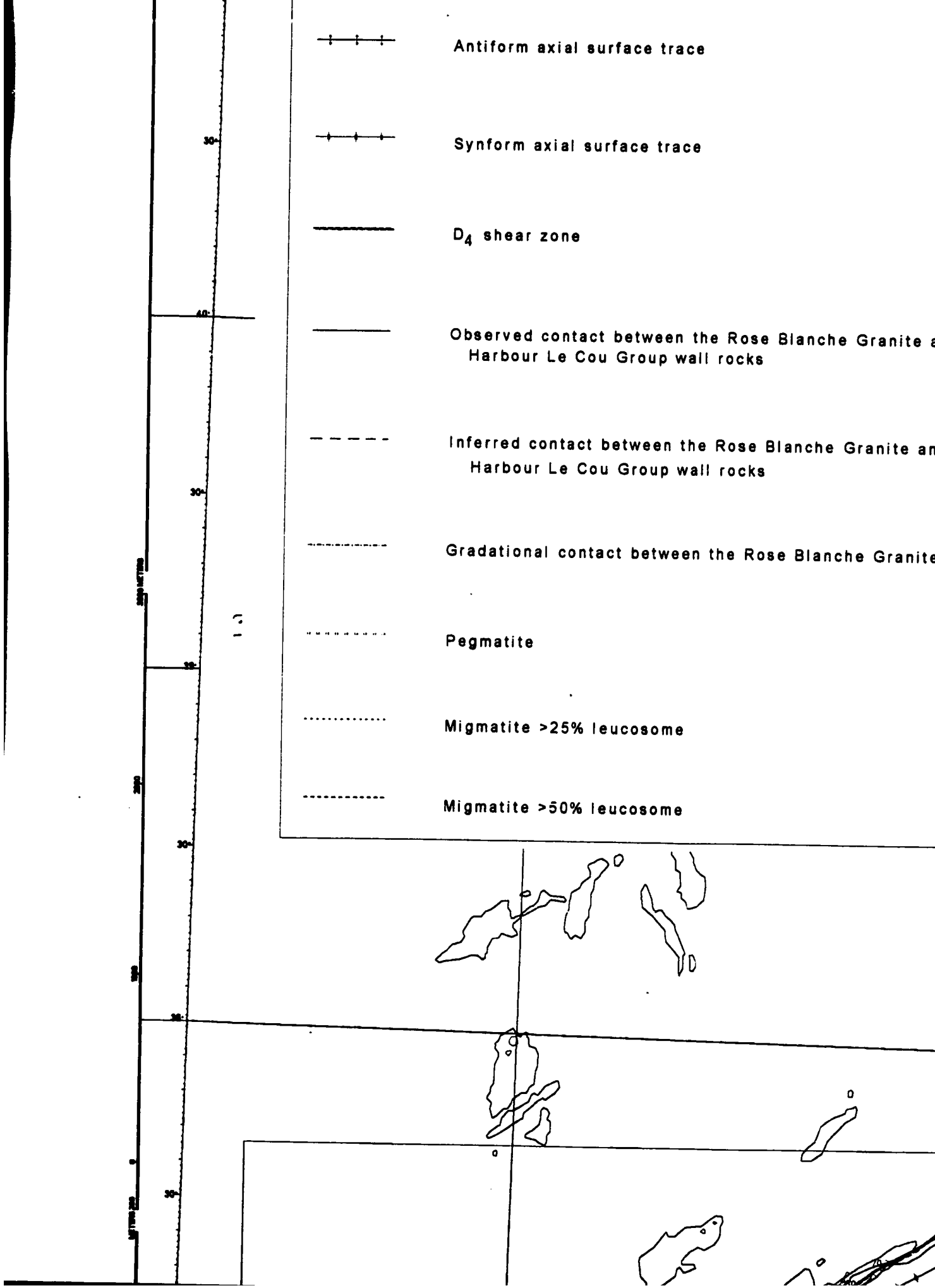
Antiform axial surface trace
Synform axial surface trace
D_4 shear zone
Observed contact between the Rose Blanche Granite a
Harbour Le Cou Group wall rocks
Inferred contact between the Rose Blanche Granite an
Harbour Le Cou Group wall rocks
Gradational contact between the Rose Blanche Granite
Pegmatite
Migmatite >25% leucosome
Migmatite >50% leucosome

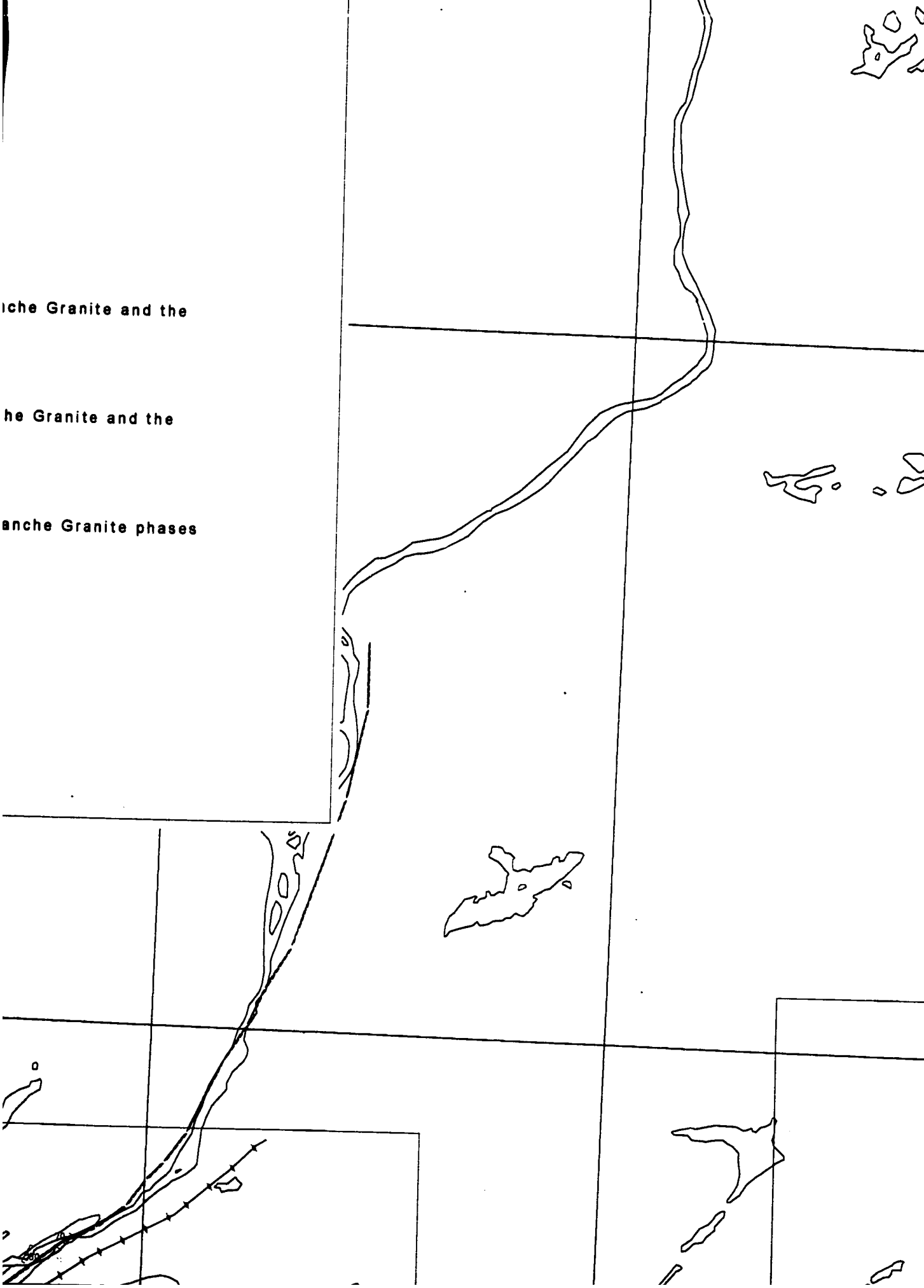

ıche Granite and the

he Granite and the

anche Granite phases

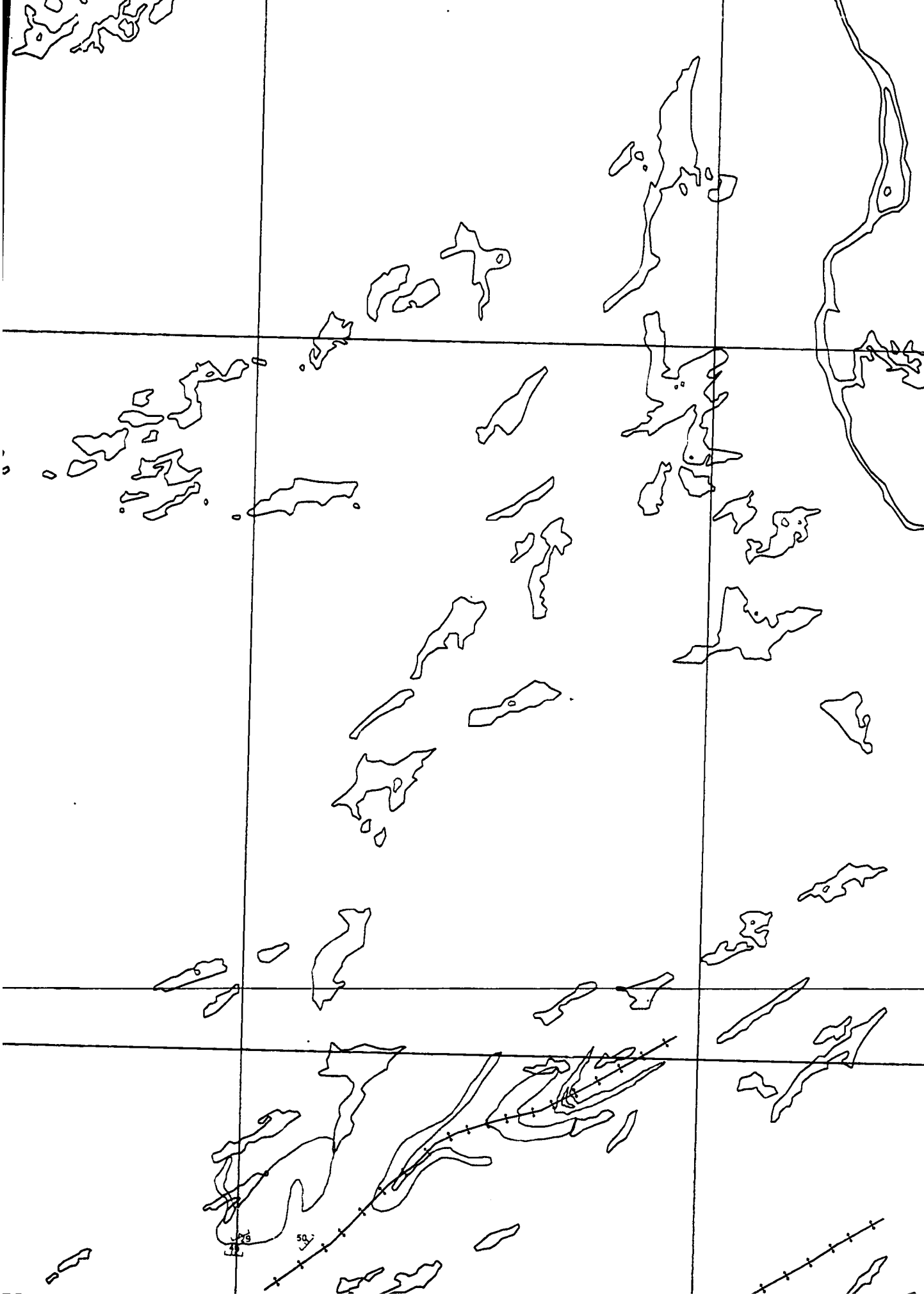

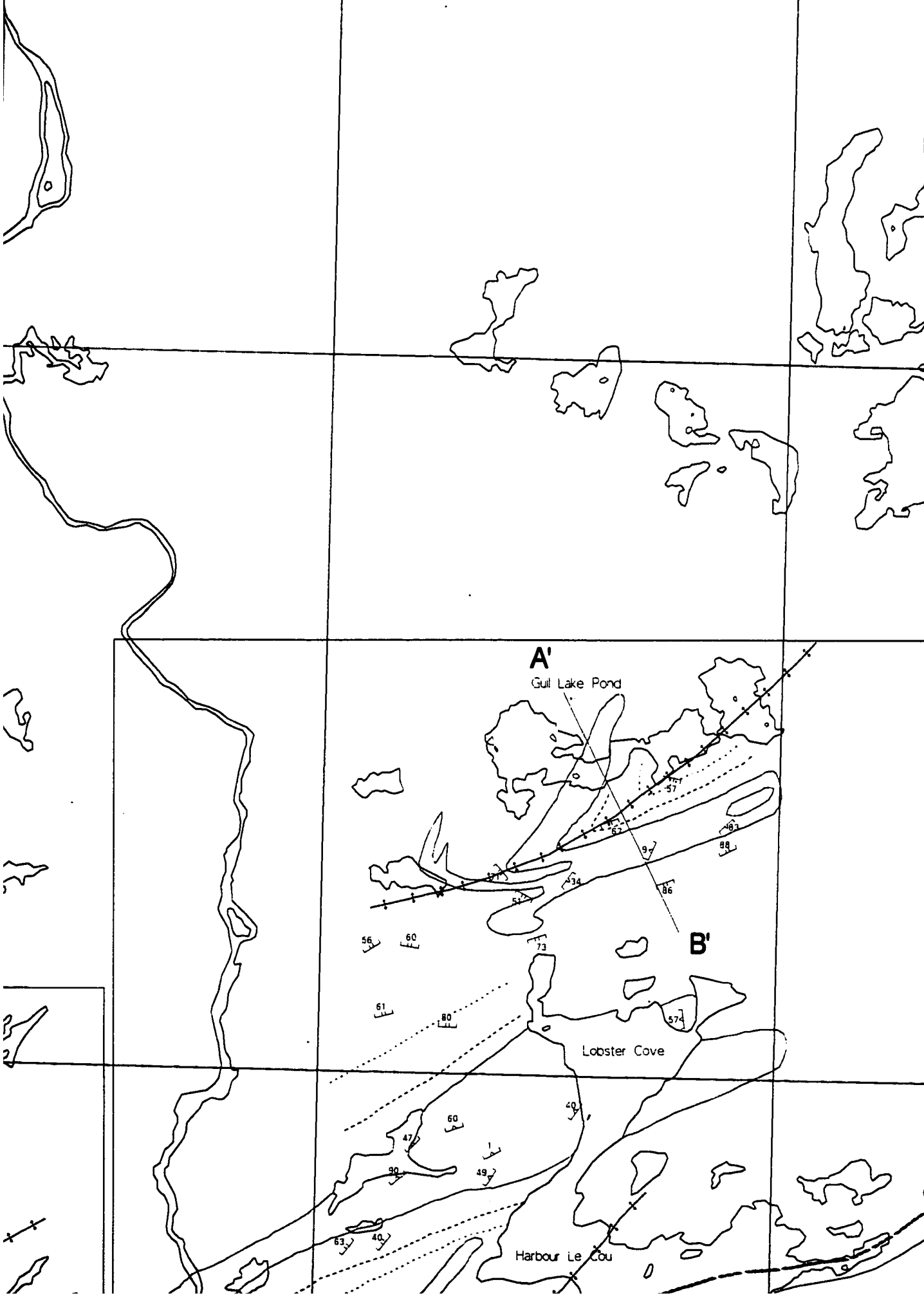
A'
Gull Lake Pond
B'
Lobster Cove
Harbour Le Cou

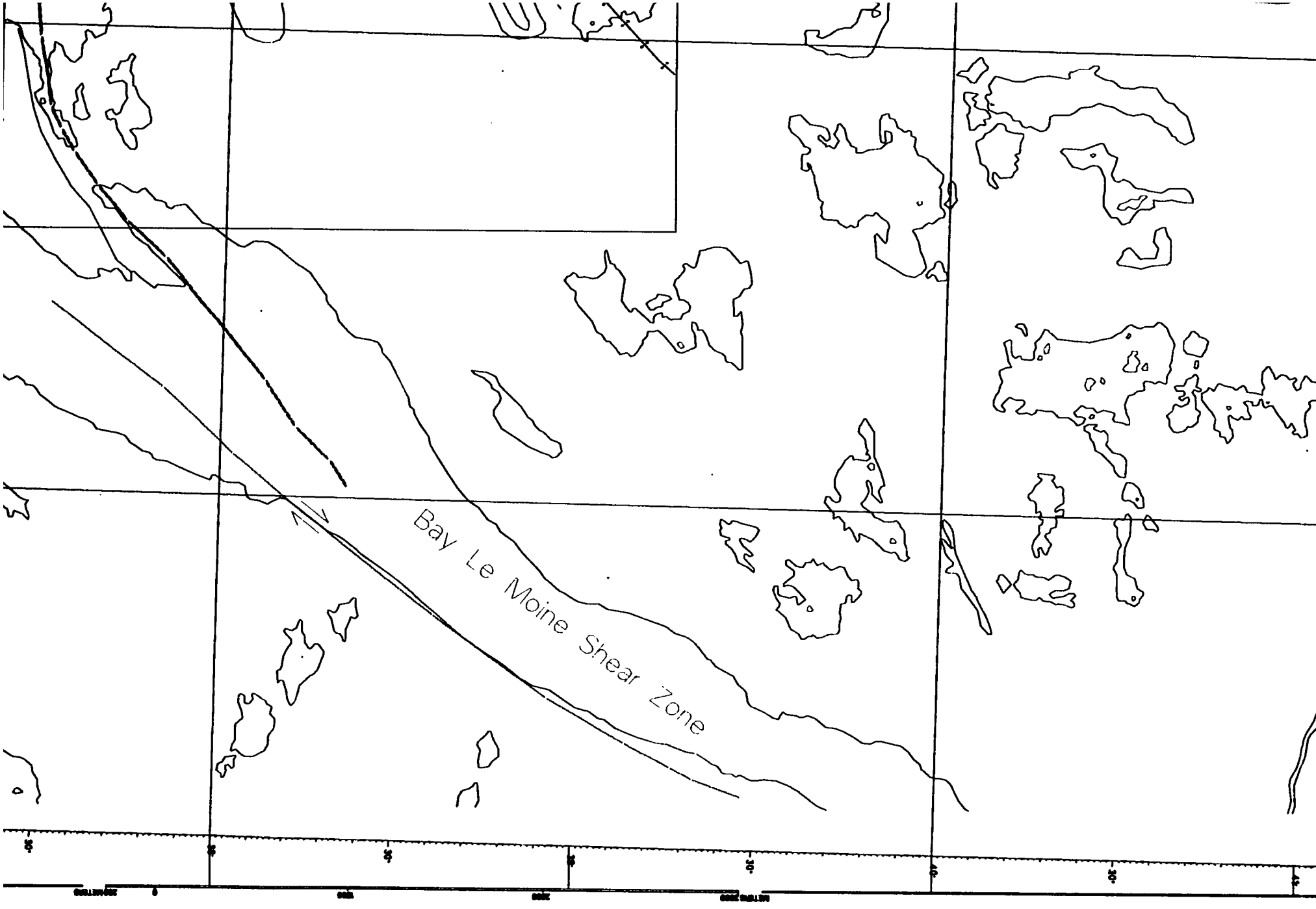
Bay Le Moine Shear Zone

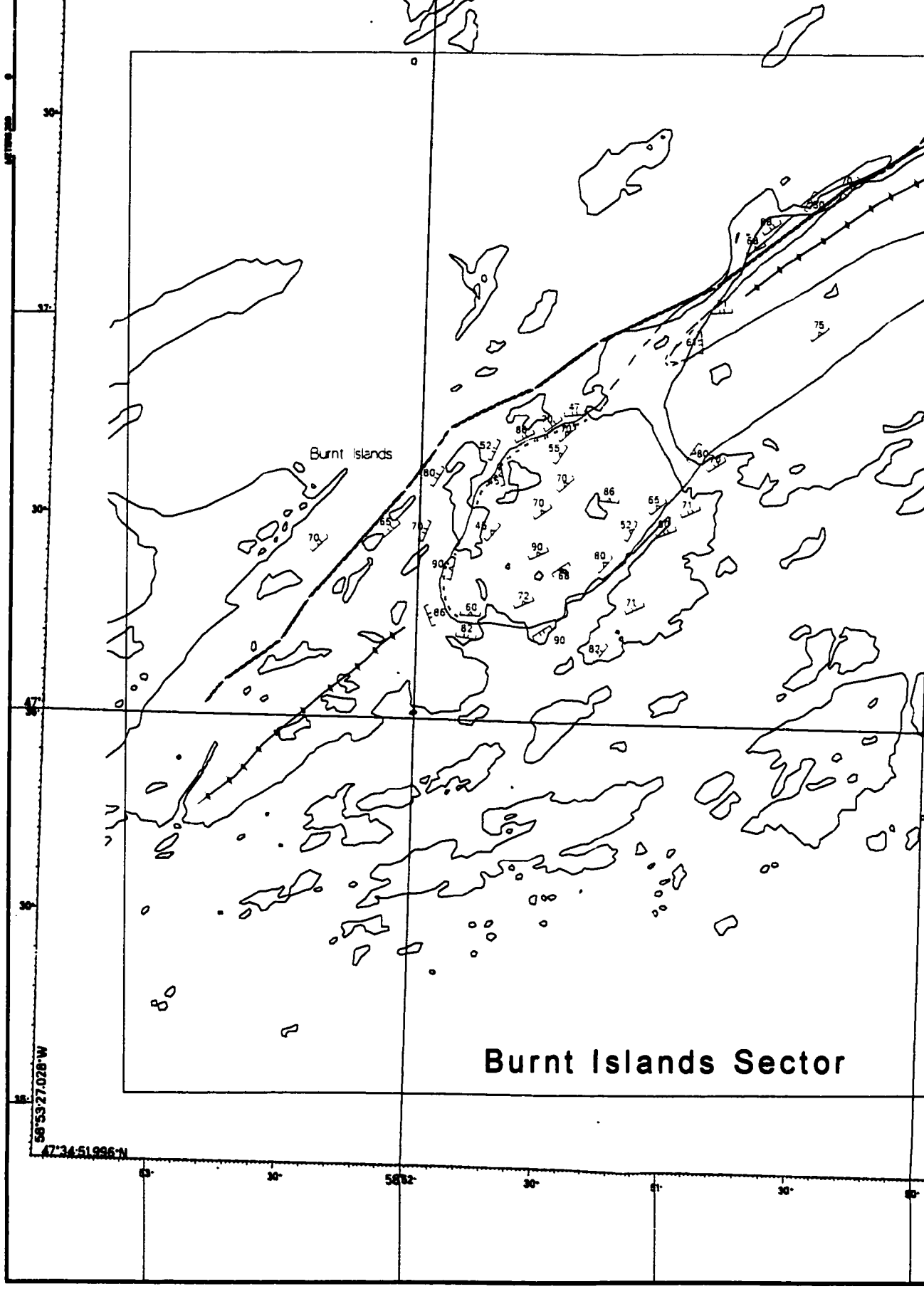
Burnt Islands
Burnt Islands Sector
58°53'27.028"W
47°34'51.996"N

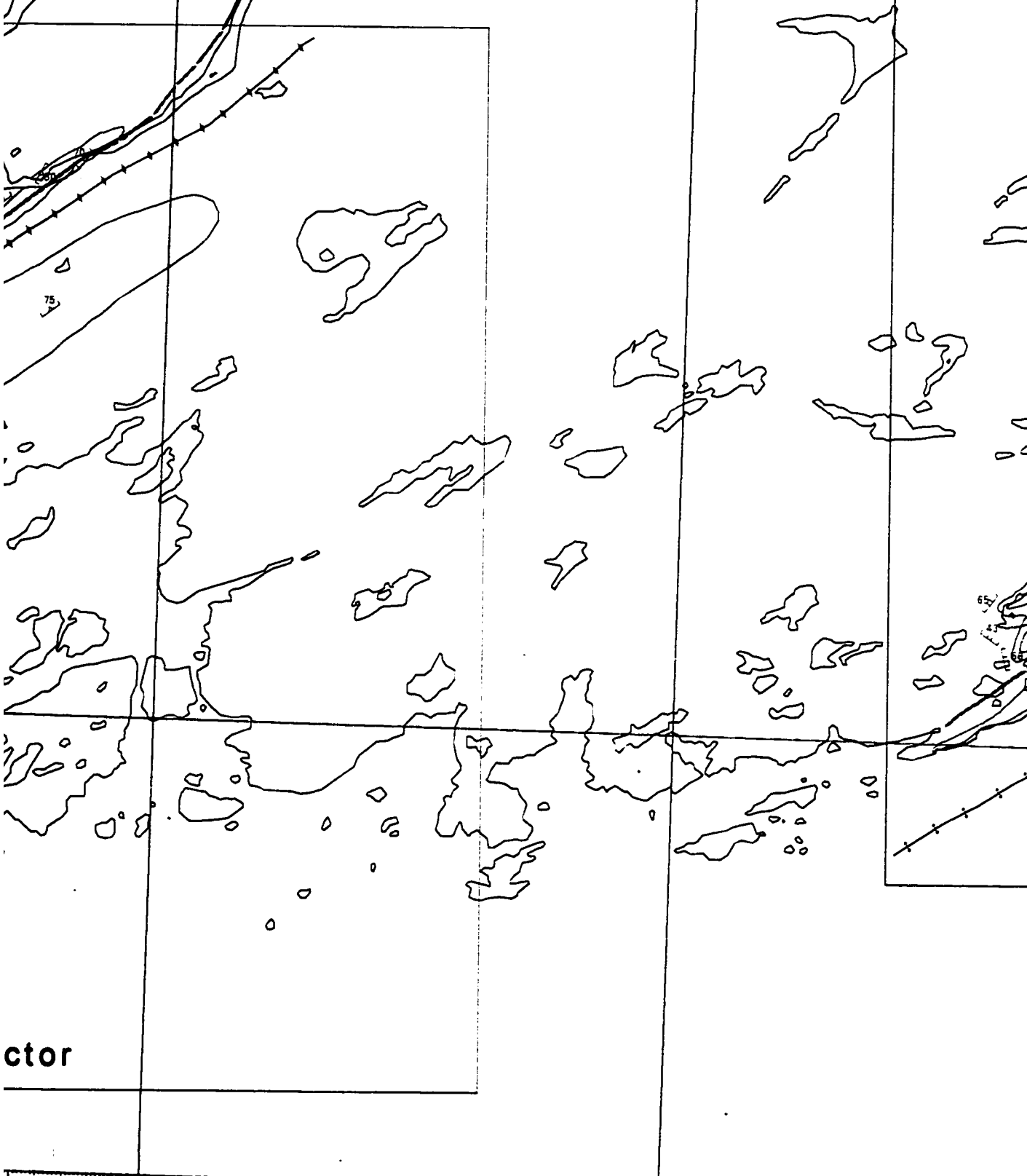
ctor

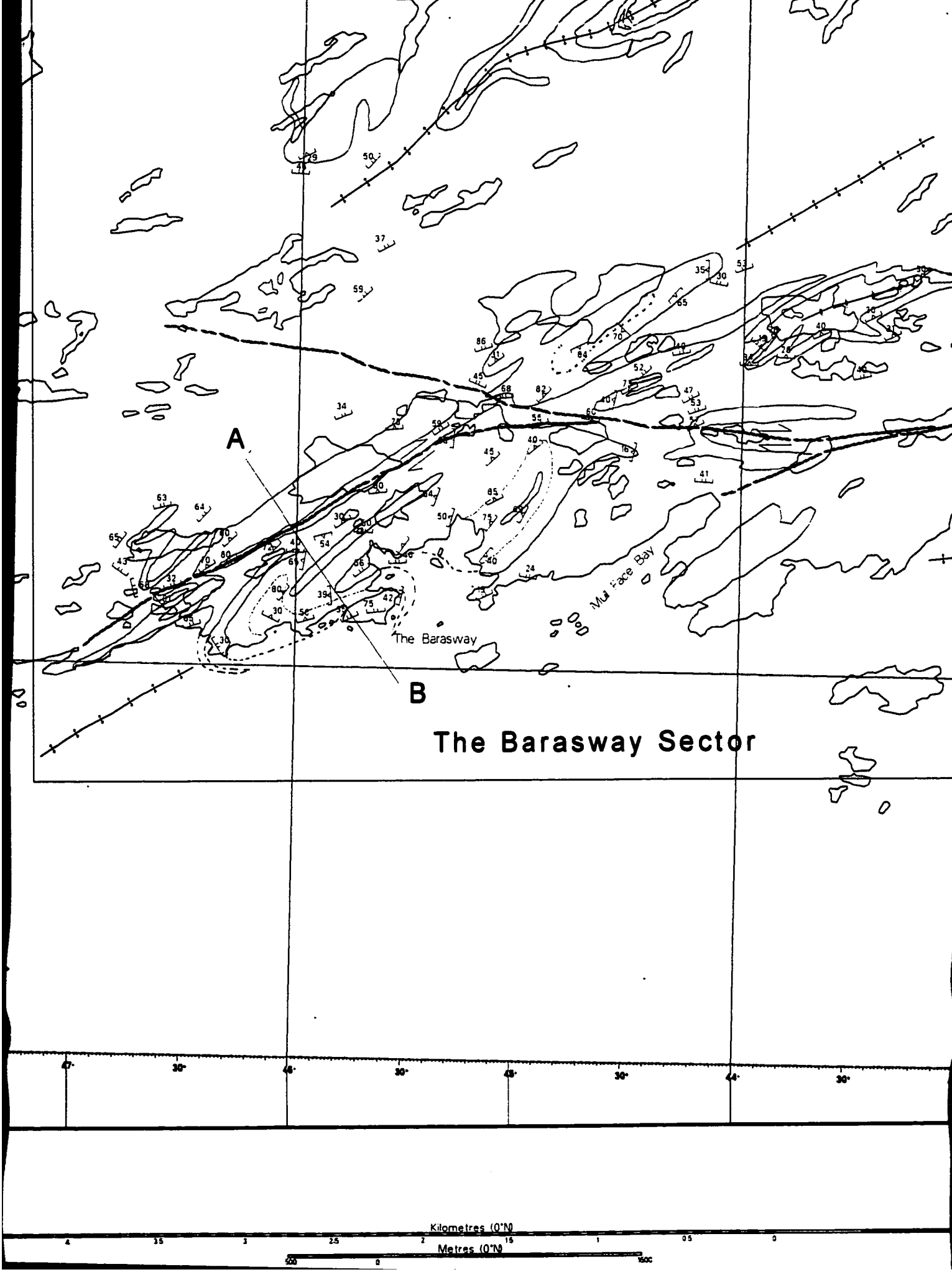

The Barasway Sector

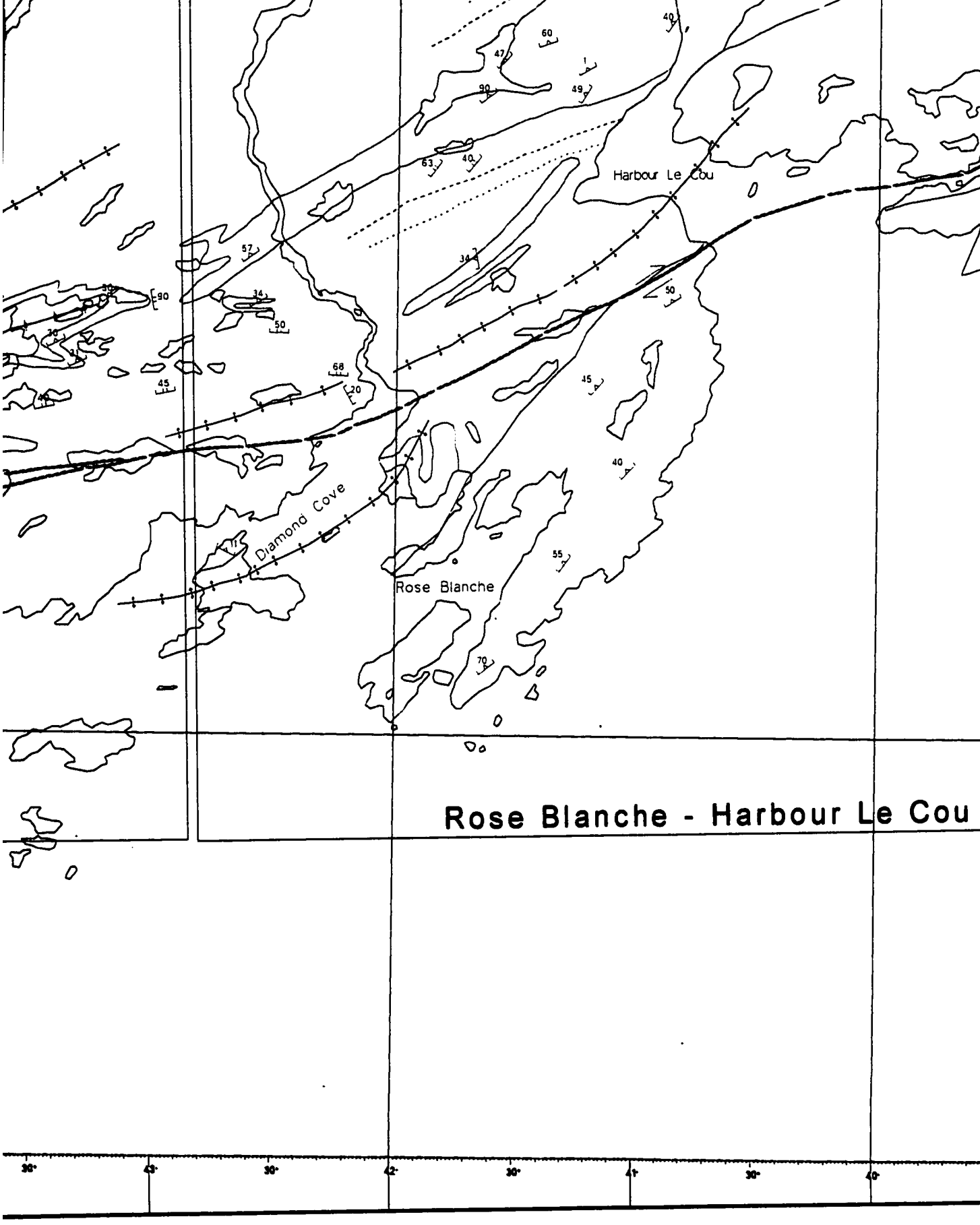
Harbour Le Cou
Diamond Cove
Rose Blanche
Rose Blanche - Harbour Le Cou
57°30'
57°
56°30'
56°
55°30'
55°
54°30'
54°

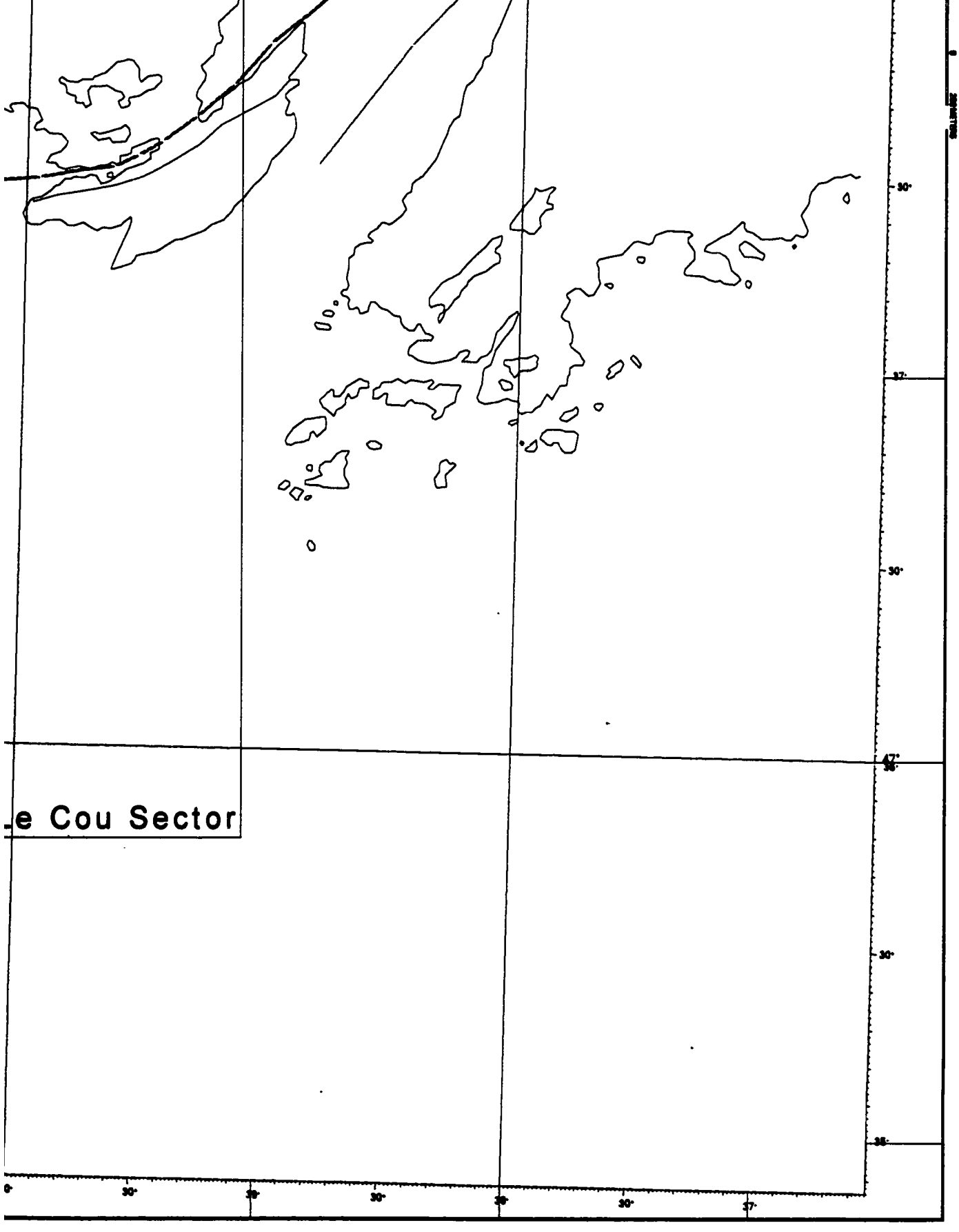
e Cou Sector

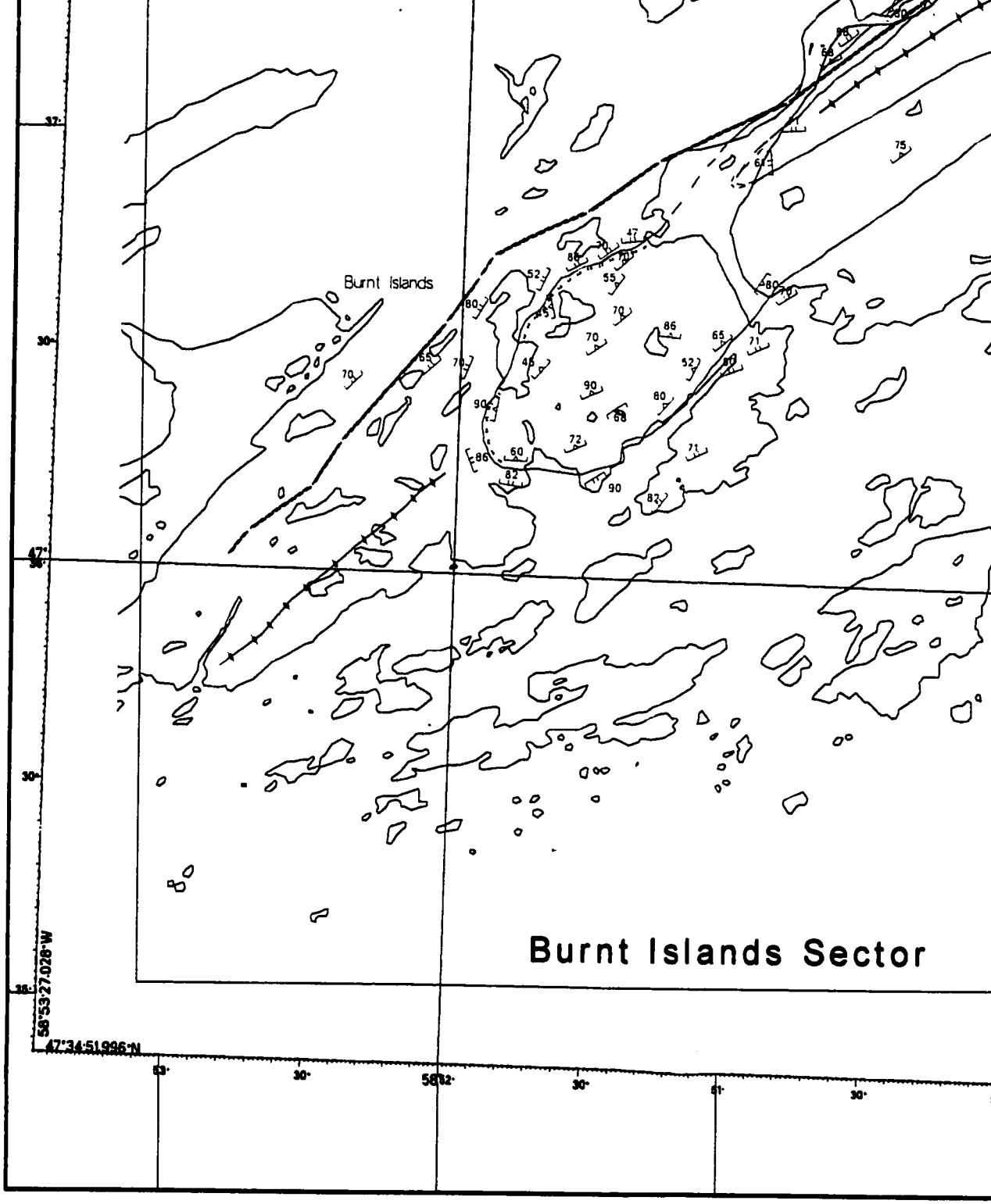
Burnt Islands
Burnt Islands Sector
58°53'27.028"W
47°34'51.996"N

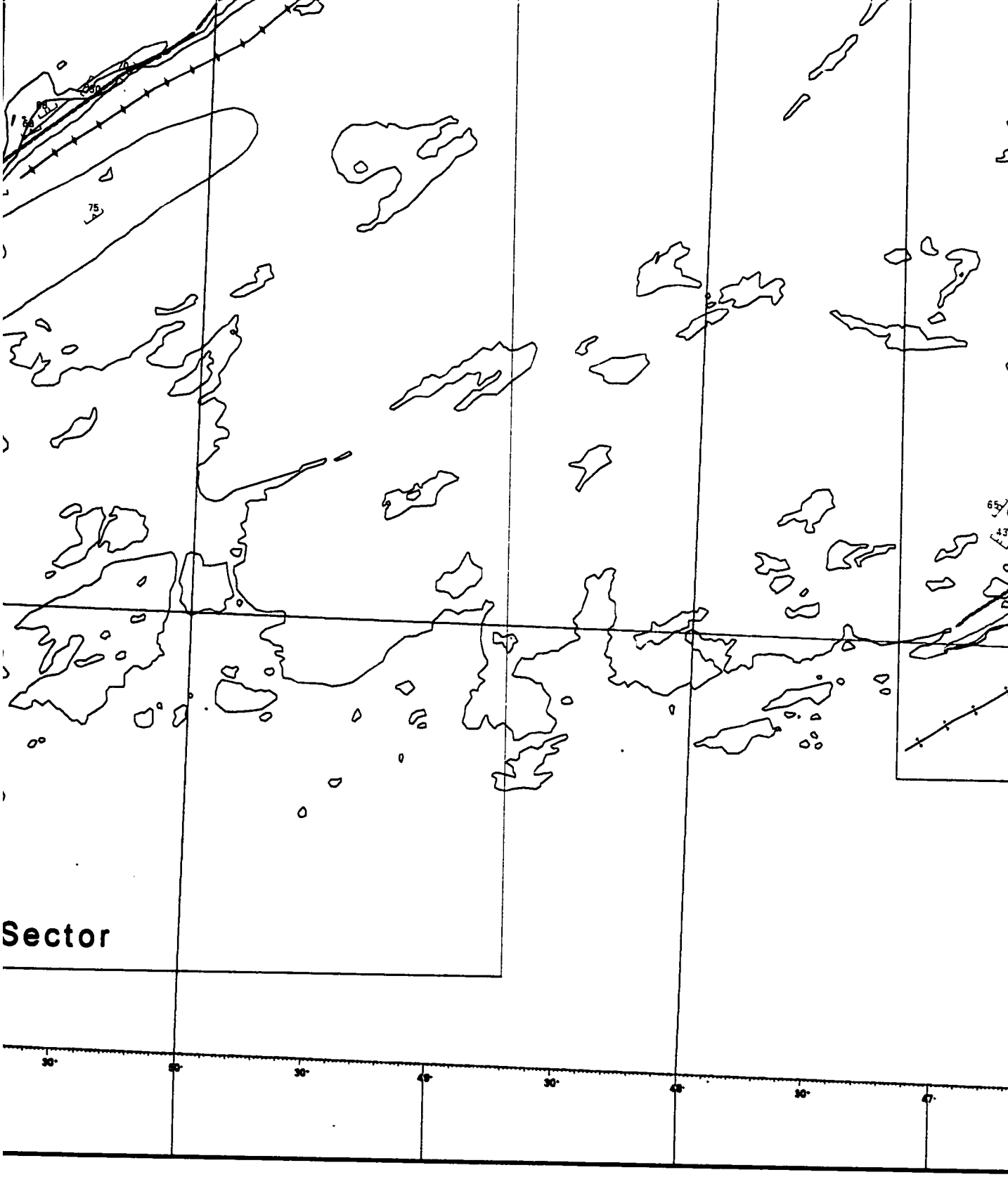
Sector

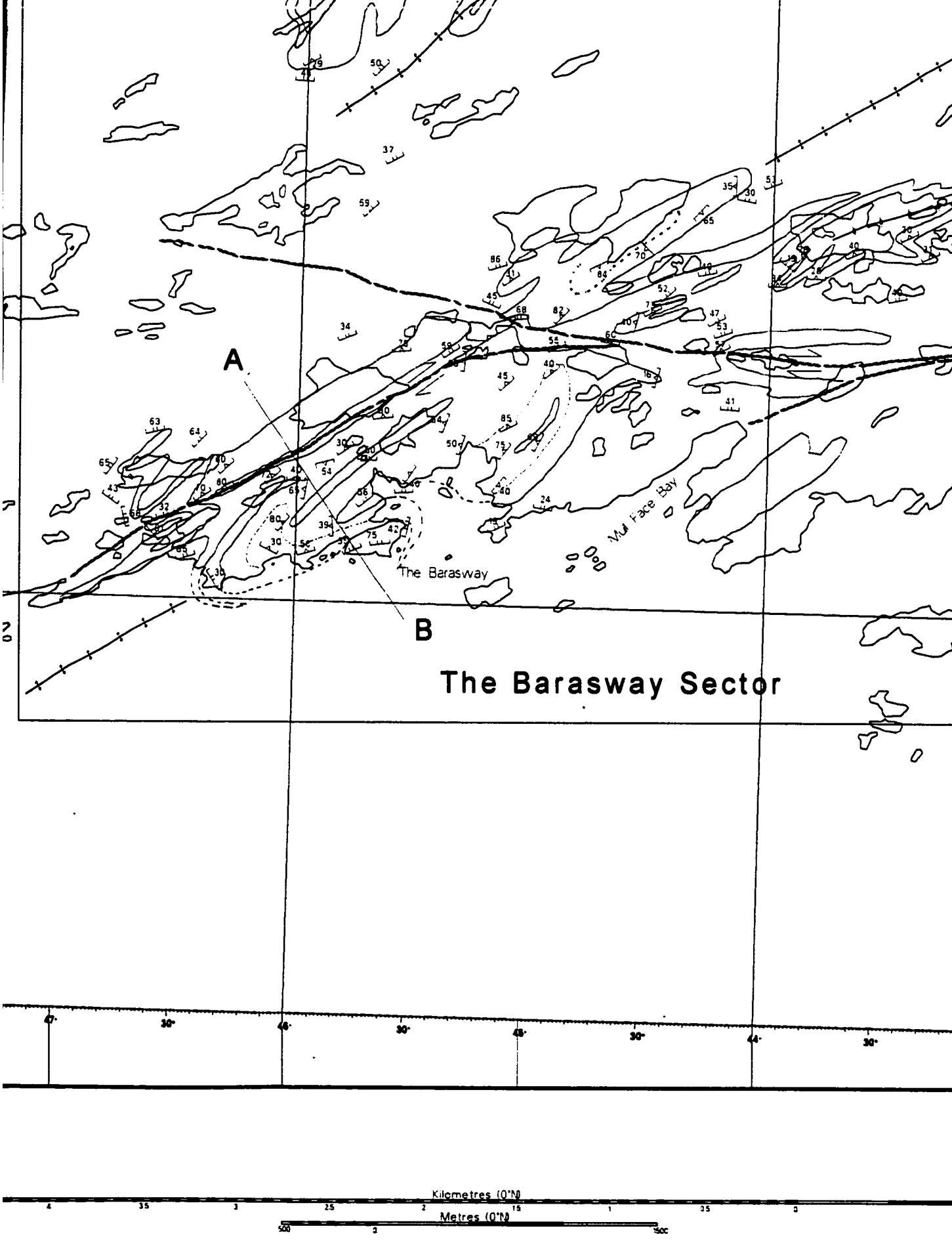
A
B
The Barasway
Mud Face Bay
The Barasway Sector
47°
30'
46°
30'
45°
30'
44°
30'
Kilometres (0°N)
Metres (0°N)

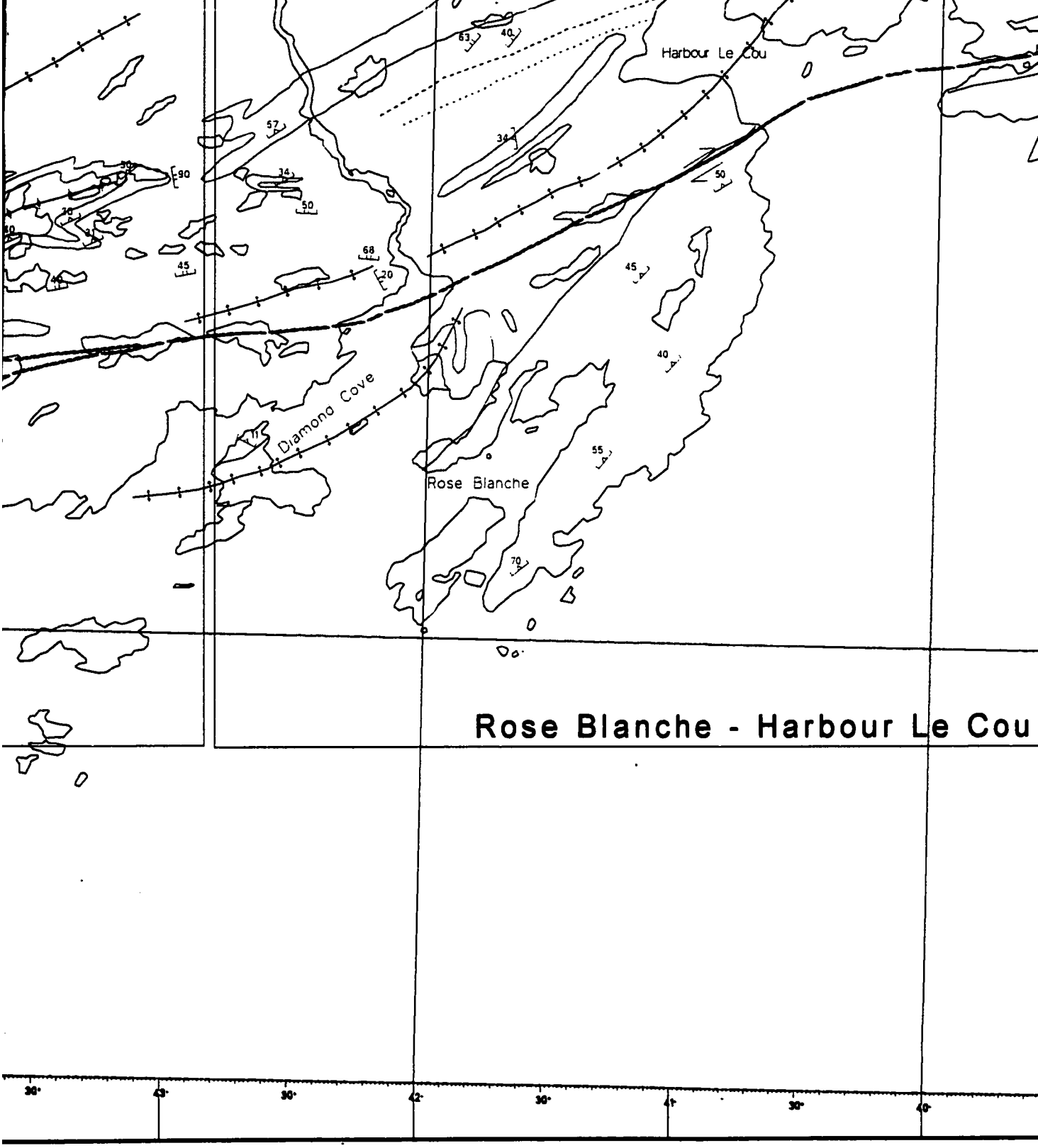
Harbour Le Cou
Diamond Cove
Rose Blanche
Rose Blanche - Harbour Le Cou

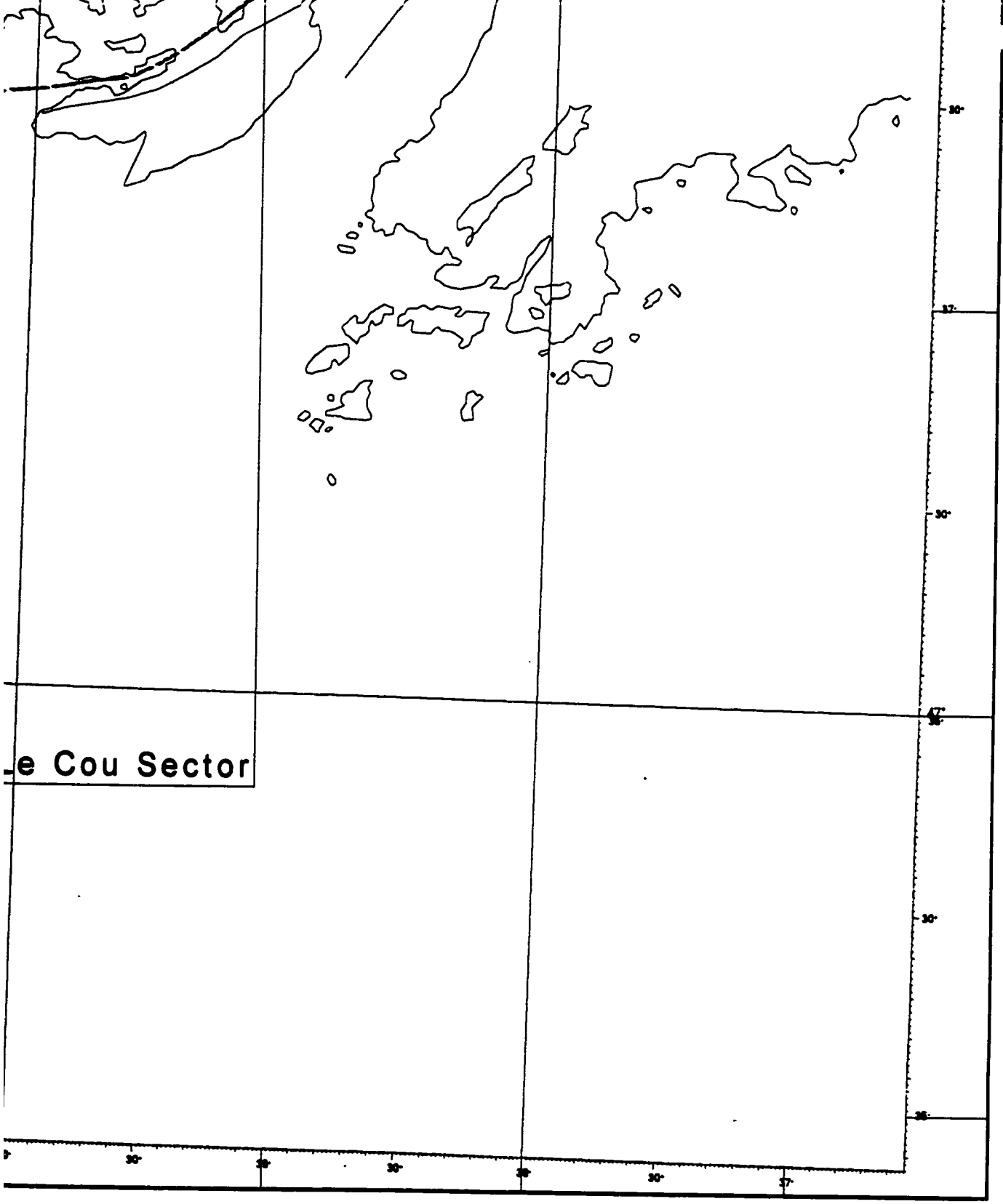
e Cou Sector

Map 2 - Lineation Patterns

Geology By: M. Genkin, 1995

Map Scale 1 : 25,000

Structural Symbols and Lithological Boun

Trend and plunge, L_2 - stretching lineation, Harbour Le Co

Trend and plunge, F_2 - hinge, Harbour Le Cou Group with s

Trend and plunge, F_3 - hinge, Harbour Le Cou Group, with

Trend and plunge, L_4 - quartz stretching lineation, D_4 shea

Trend and plunge, L_{qtz} - quartz stretching lineation, Rose B

Antiform axial surface trace

Synform axial surface trace

D_4 shear zone

Observed contact between the Rose Blanche Granite and the Harbour Le Cou Group wall rocks

Inferred contact between the Rose Blanche Granite and the Harbour Le Cou Group wall rocks

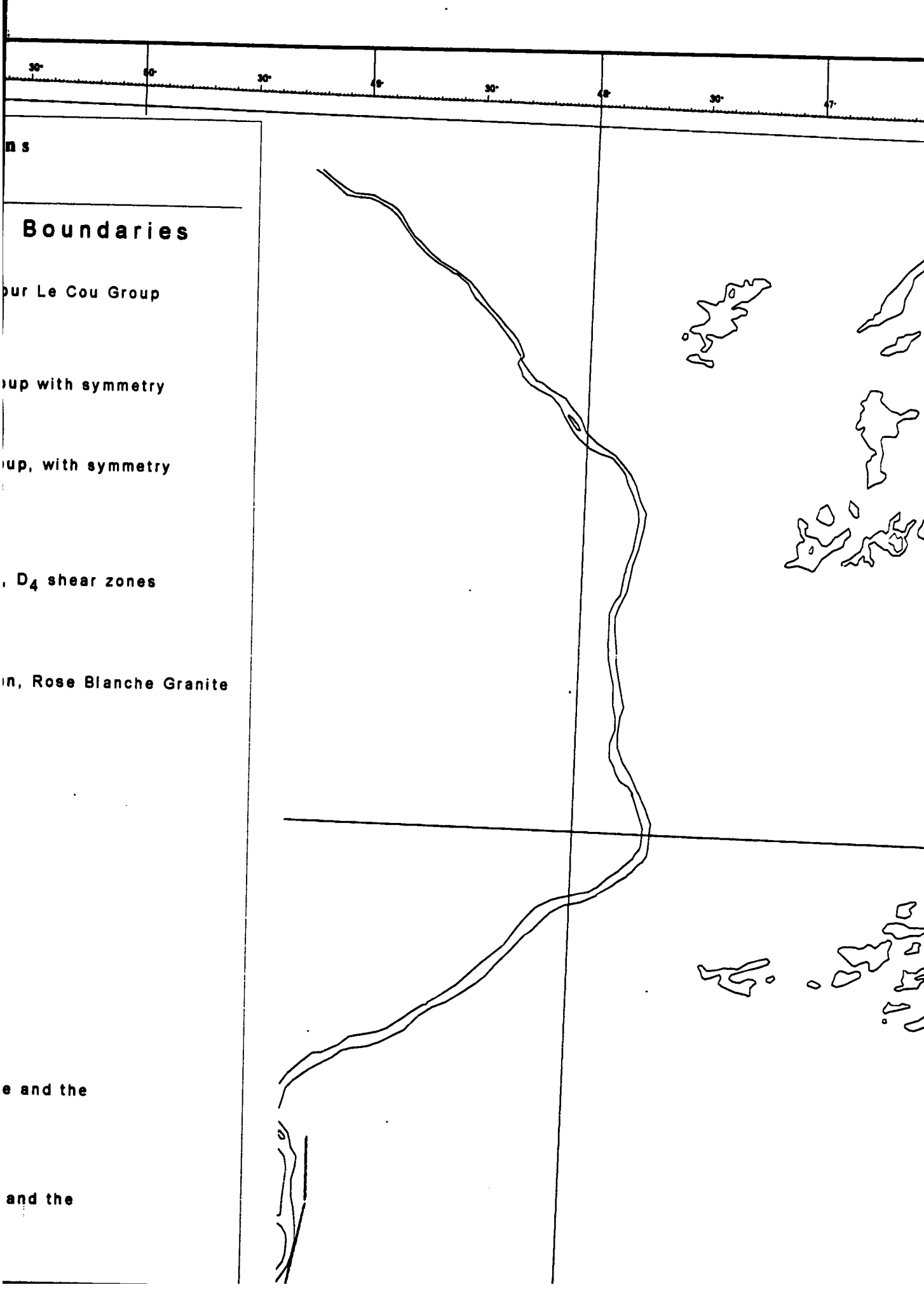
Boundaries
our Le Cou Group
up with symmetry
up, with symmetry
, D_4 shear zones
n, Rose Blanche Granite
e and the
and the

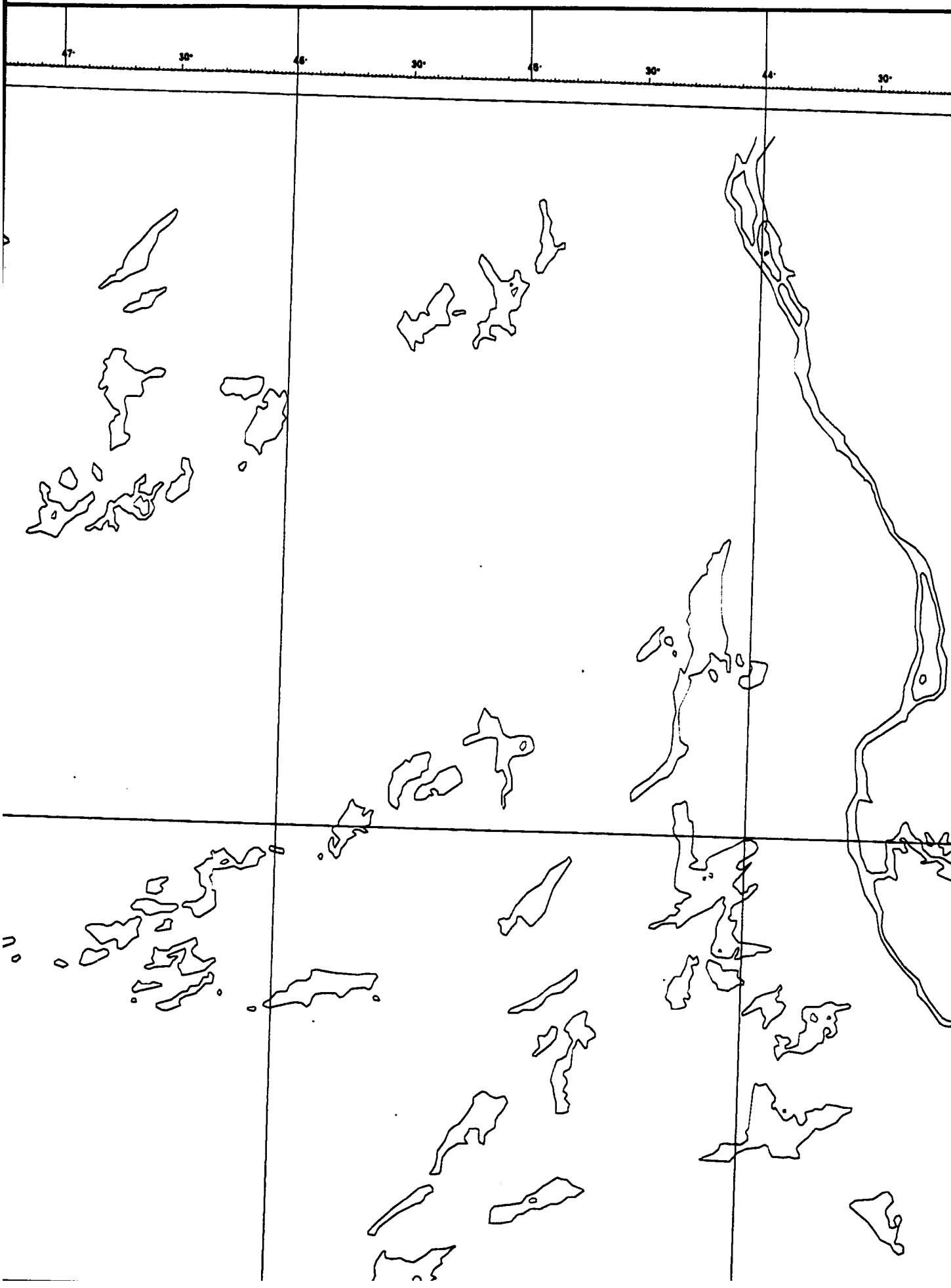
47°
30'
46°
30'
45°
30'
44°
30'

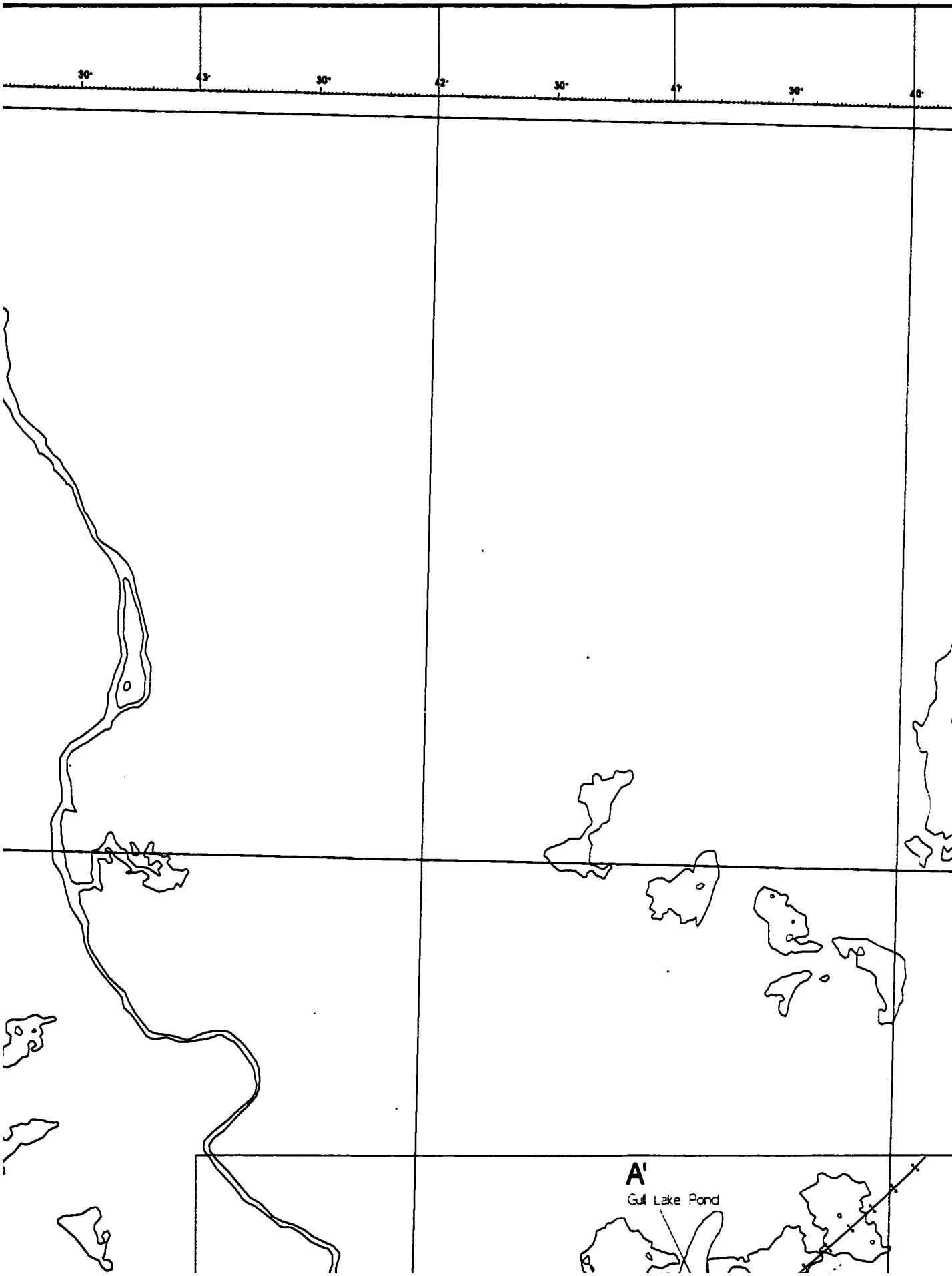
30'
43°
30'
42°
30'
41°
30'
40°
A'
Gull Lake Pond

40°
30'
39°
30'
38°
30'
37°
47°42'03.473"N
89°36'31.562"W
42°
30'
41°
30'
40°
30'
39°
Shear Zone

Trend and plunge, L_4 - quartz stretching lineation, D_4 sh

Trend and plunge, L_{qtz} - quartz stretching lineation, Rose

Antiform axial surface trace

Synform axial surface trace

D_4 shear zone

Observed contact between the Rose Blanche Granite and t
Harbour Le Cou Group wall rocks

Inferred contact between the Rose Blanche Granite and th
Harbour Le Cou Group wall rocks

Gradational contact between Rose Blanche Granite phases

Pegmatite

Migmatite >25% leucosome

Migmatite >50% leucosome

ching lineation, D_4 shear zones

etching lineation, Rose Blanche Granite

Blanche Granite and the

Blanche Granite and the

lanche Granite phases

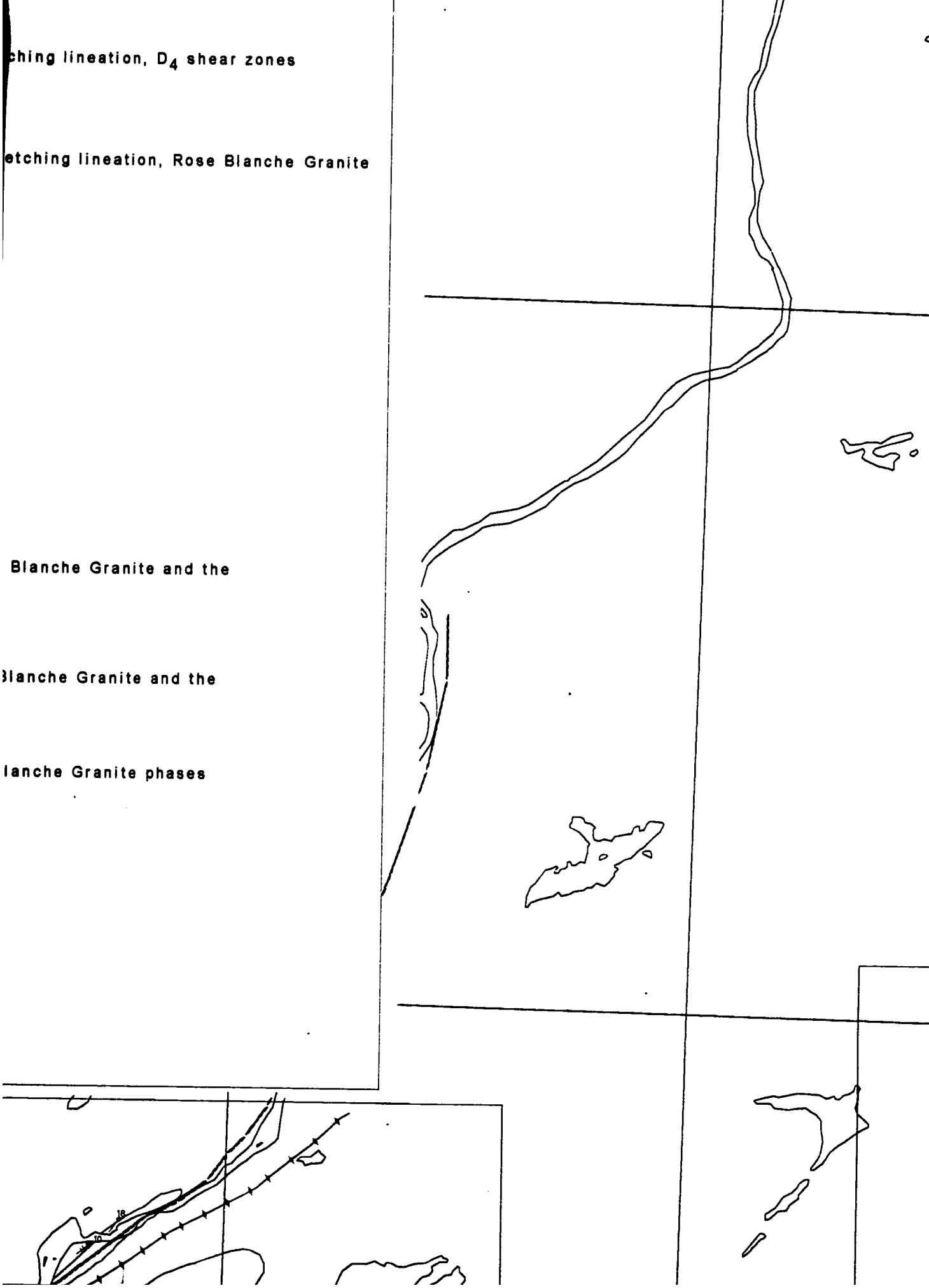

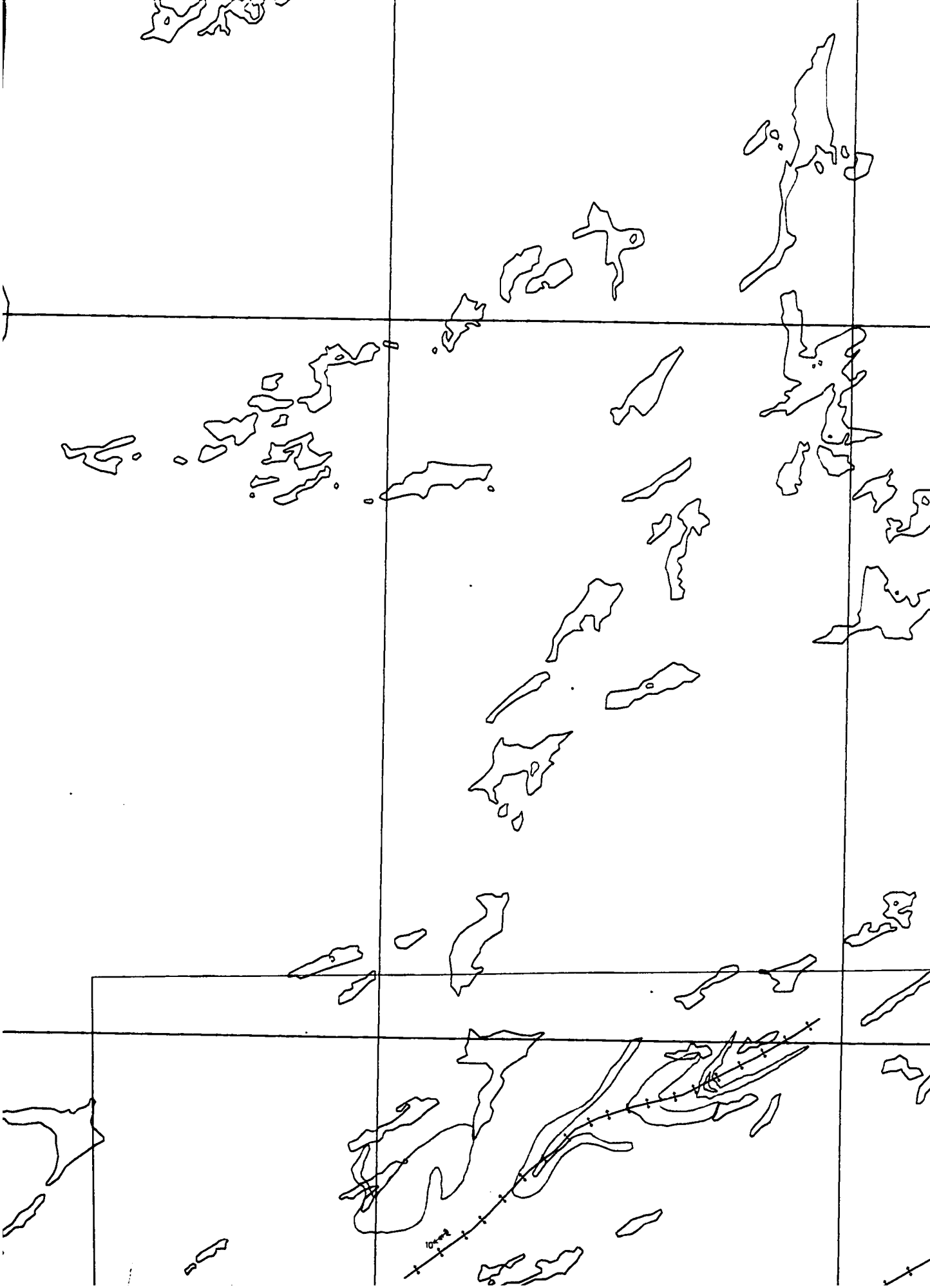


A'
Gull Lake Pond
Lobster Cove
Harbour Le Cou

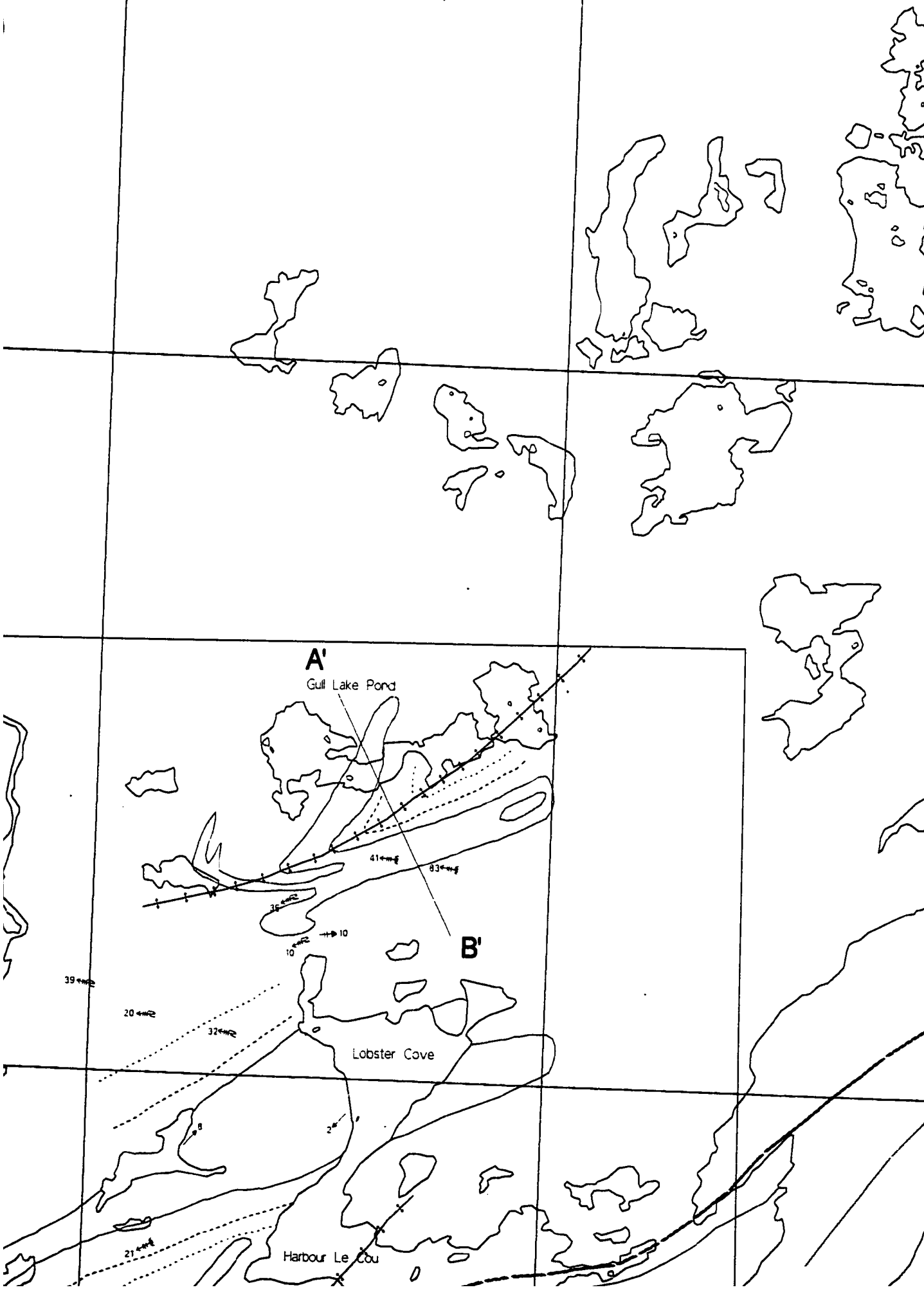
A'
Gull Lake Pond
B'
Lobster Cove
Harbour Le Cou

Bay Le Moine Shear Zone

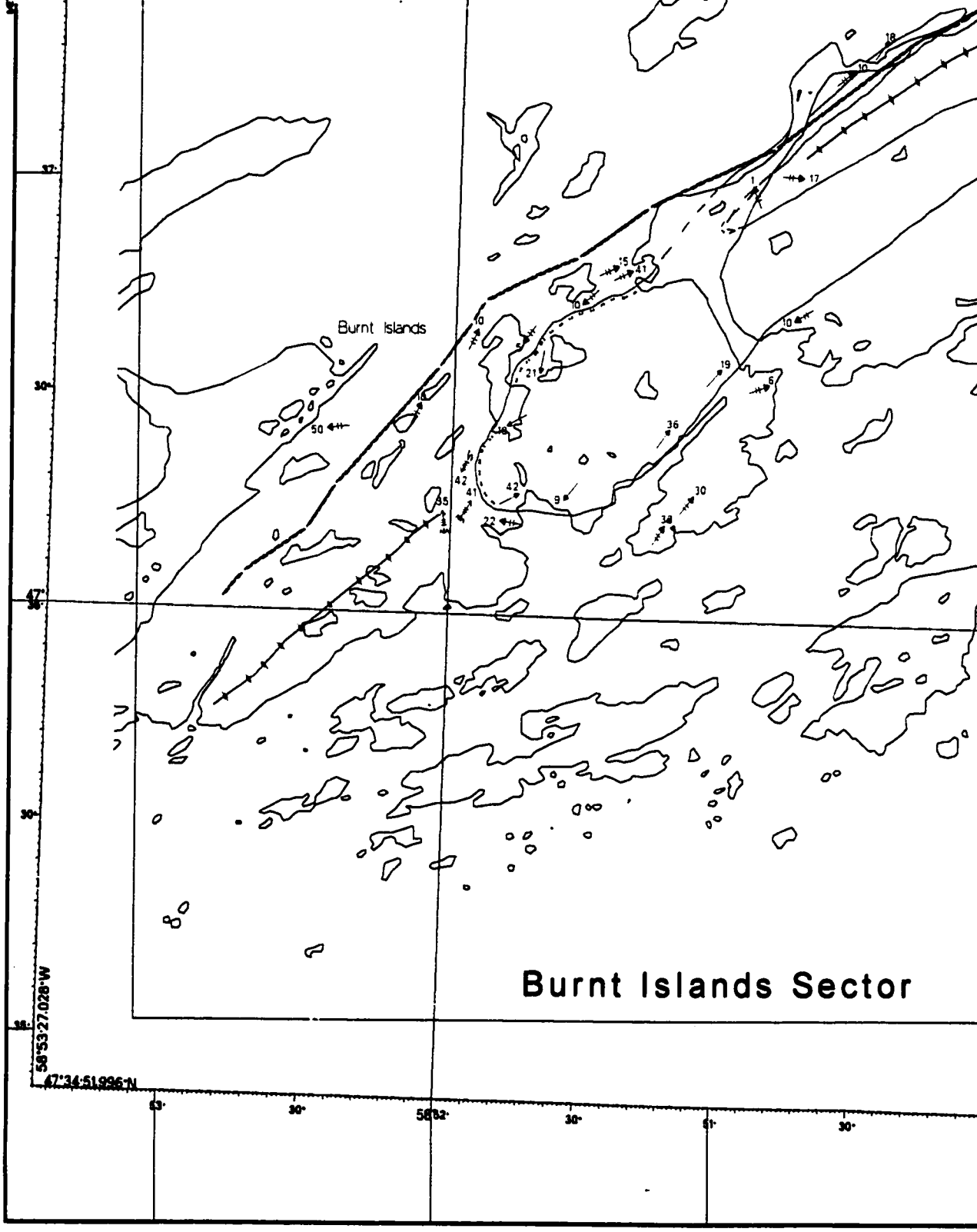
Burnt Islands
Burnt Islands Sector
58°53'27.028"W
47°34'51.996"N

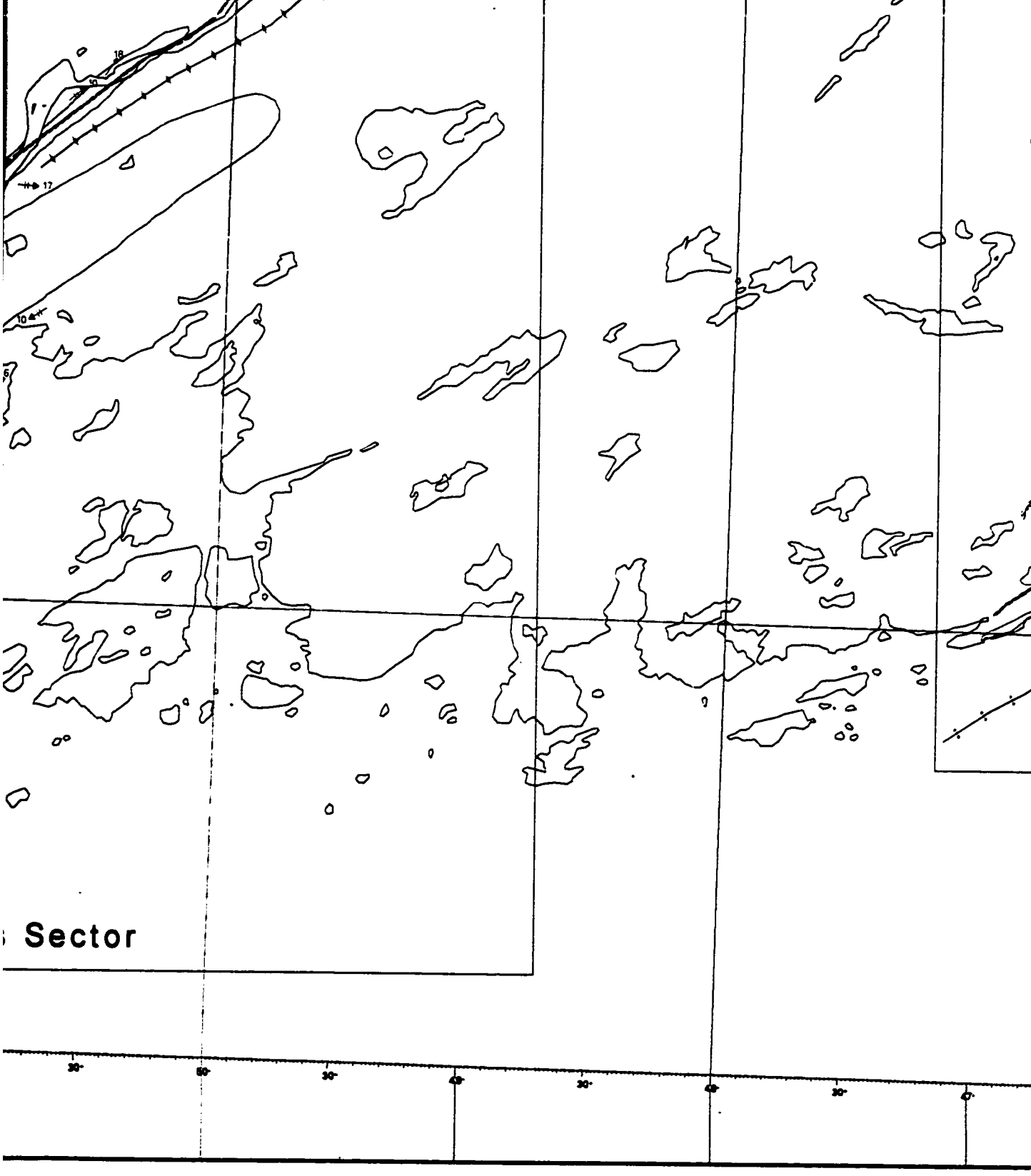
Sector

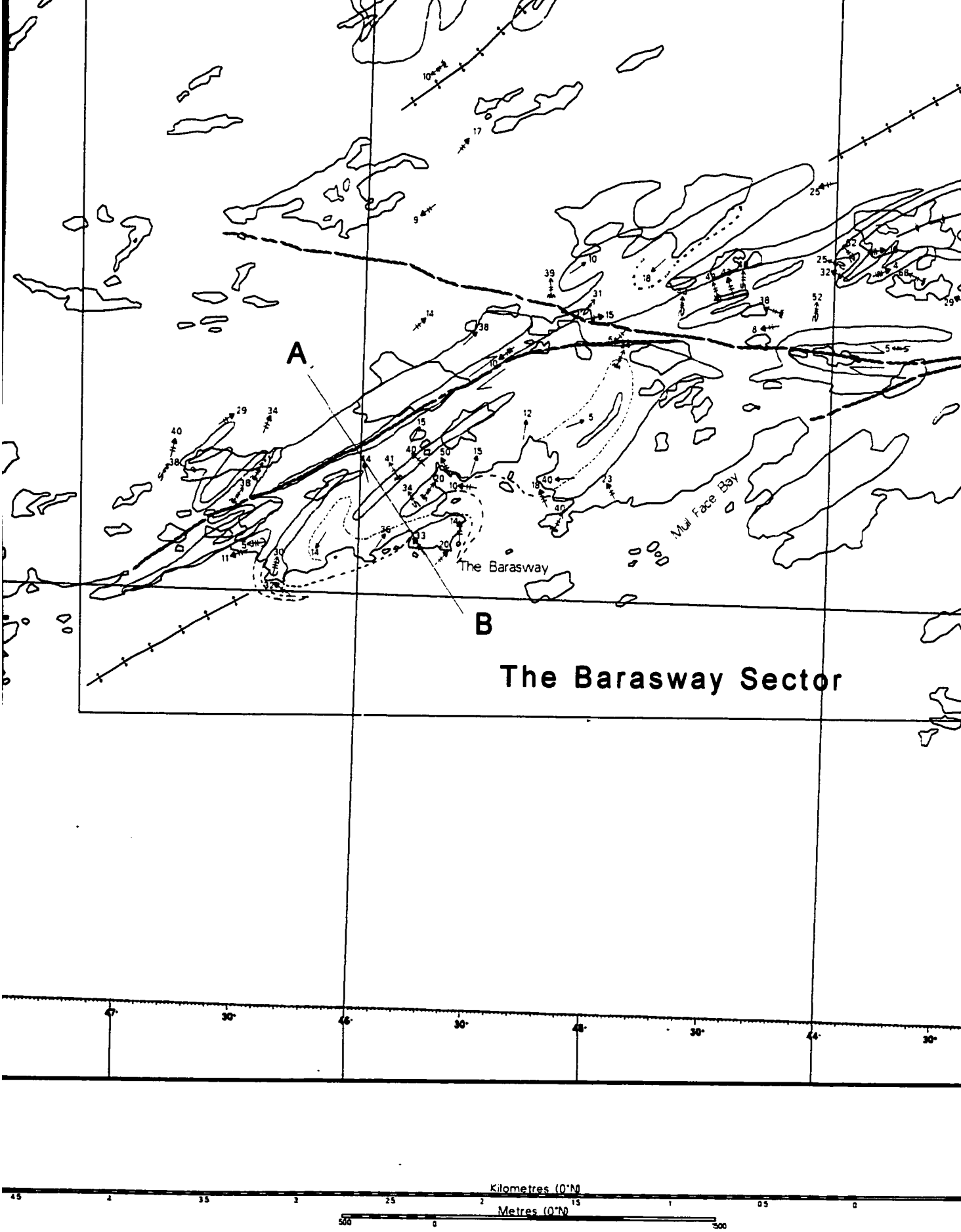
A
B
The Barasway
Mud Face Bay
The Barasway Sector
47°
30'
46°
30'
45°
30'
44°
30'
Kilometres (0°N)
4.5
4
3.5
3
2.5
2
1.5
1
0.5
0
Metres (0°N)
500
0
500

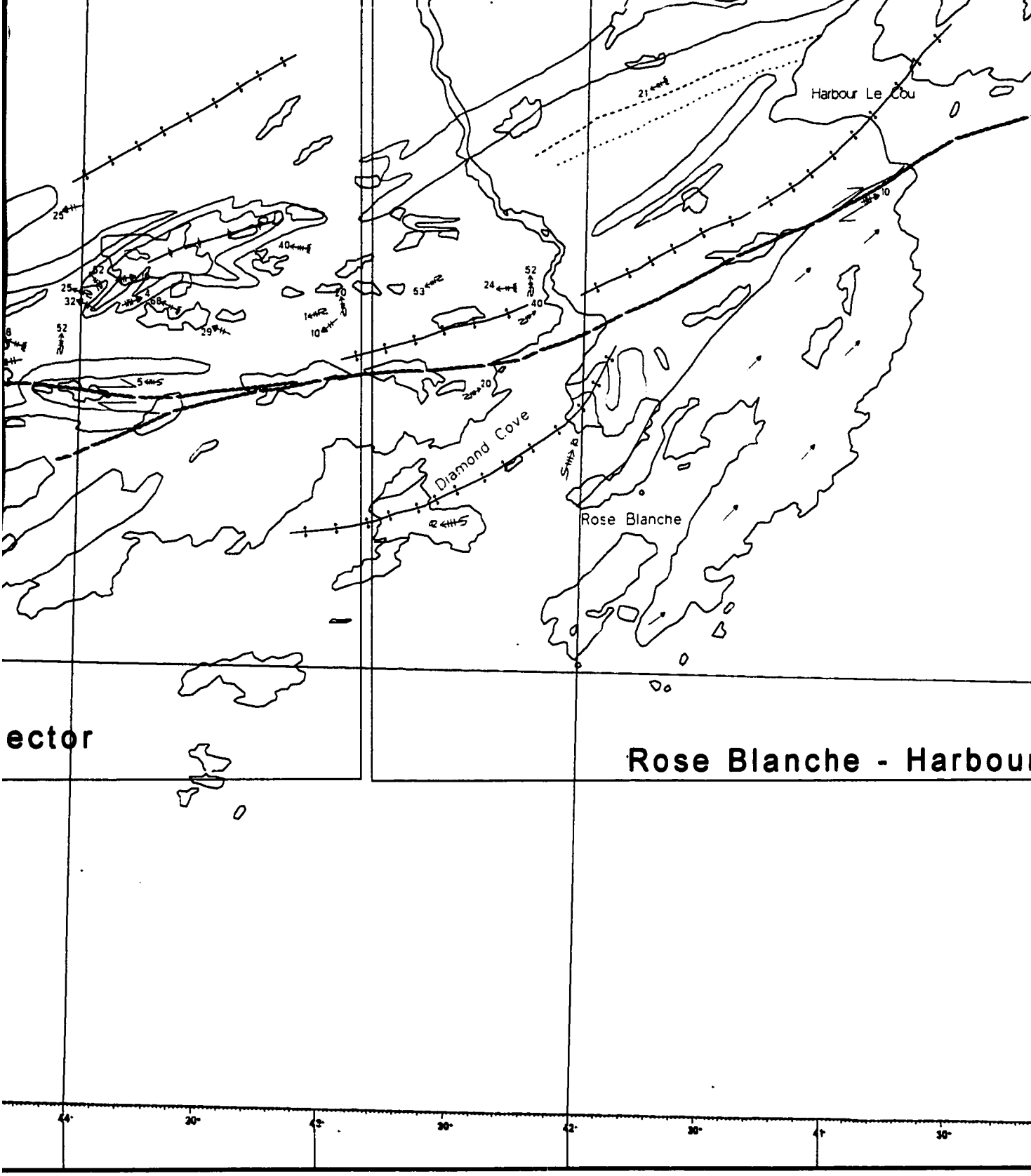

ector

Rose Blanche - Harbou

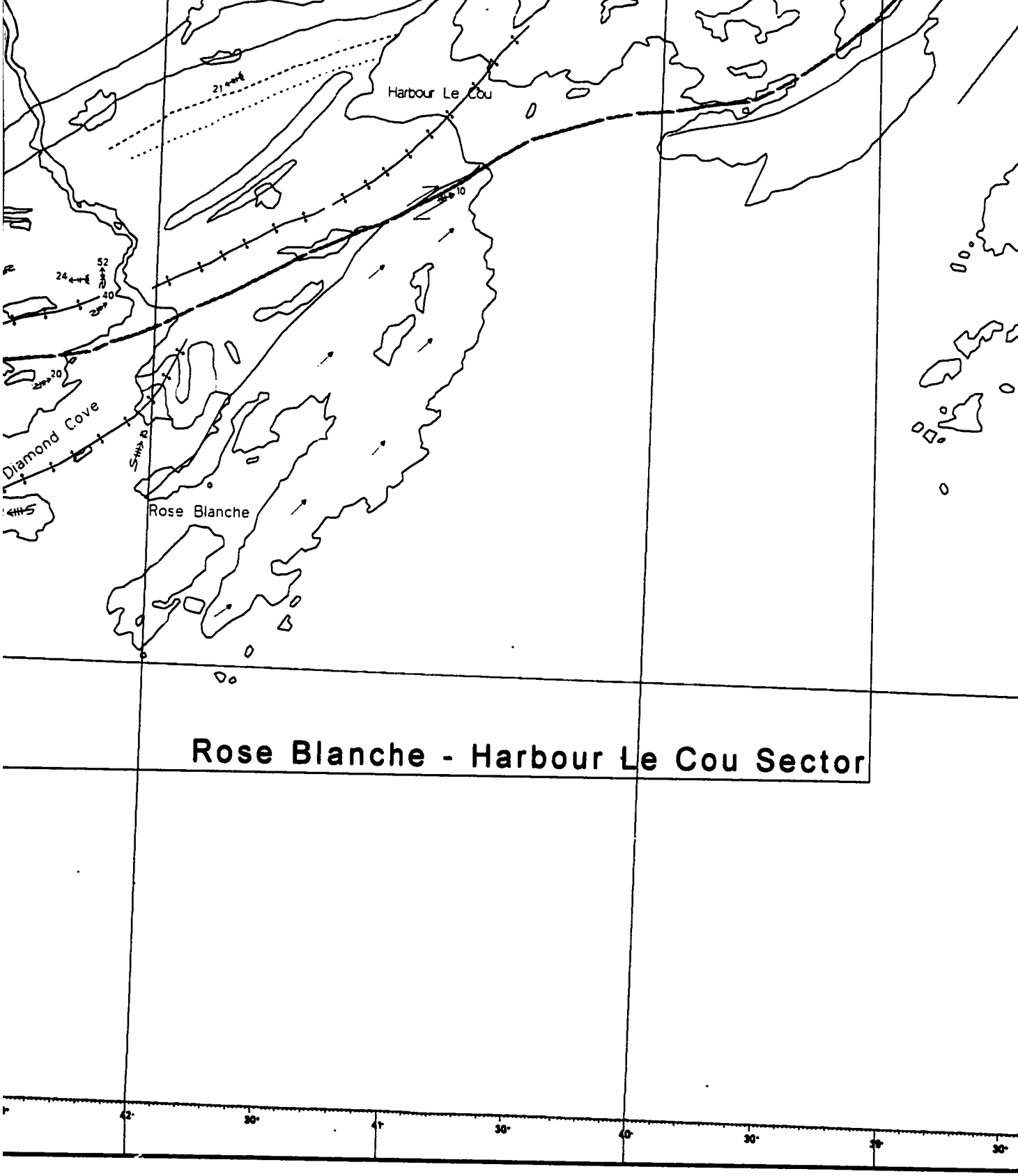

Rose Blanche - Harbour Le Cou Sector

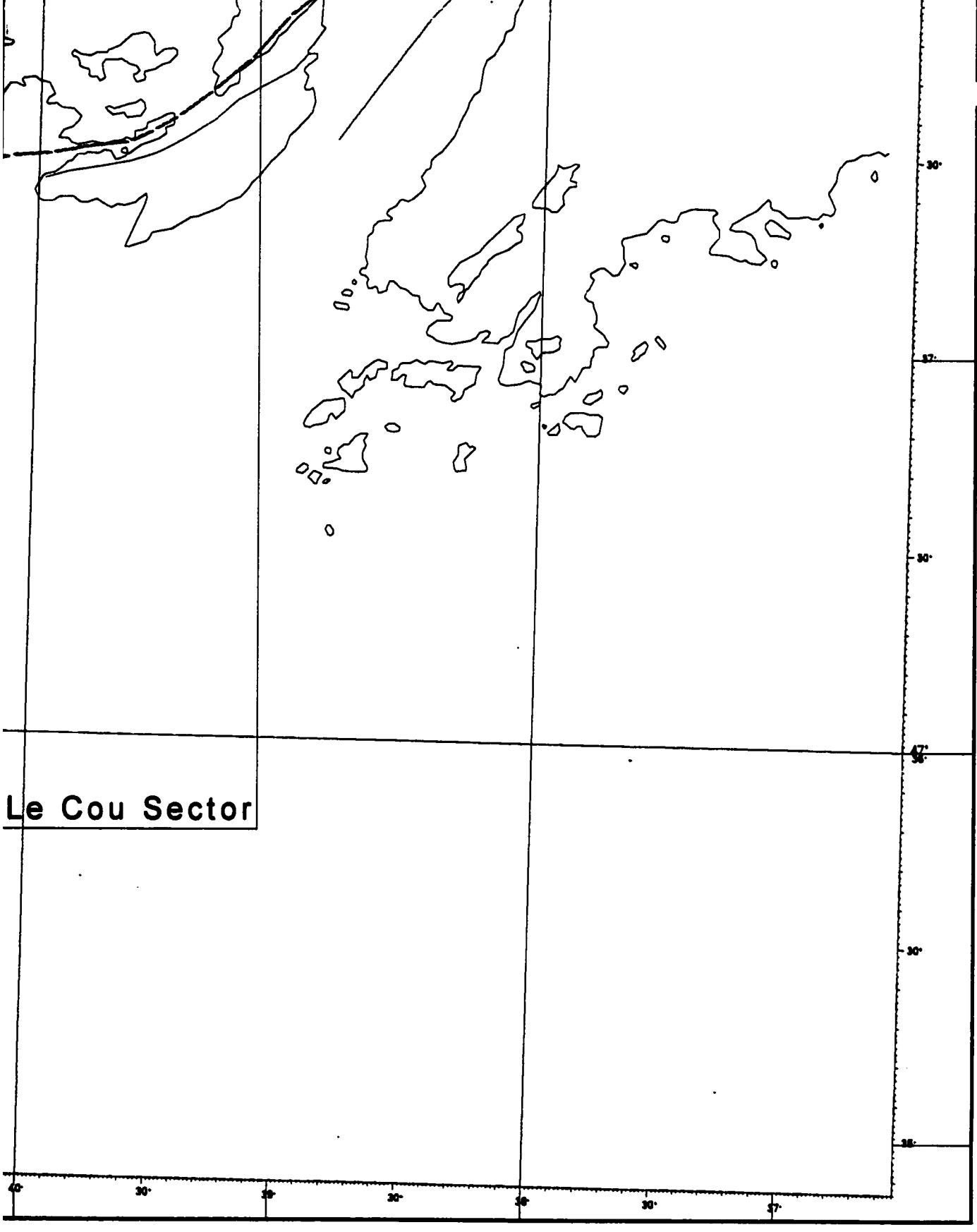
Le Cou Sector

TEST TARGET (QA-3)

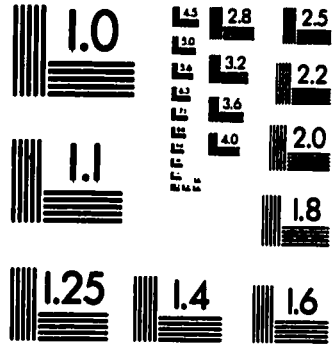

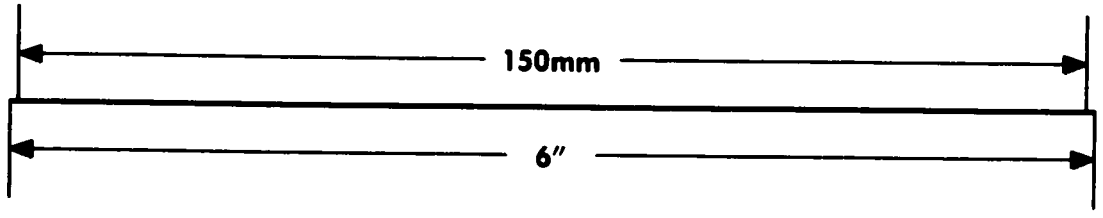

APPLIED IMAGE, Inc
1653 East Main Street
Rochester, NY 14609 USA
Phone: 716/482-0300
Fax: 716/288-5989